BACTERIAL AMYLOID CURLI INFLUENCES AGGREGATION OF AMYLOID BETA PEPTIDES ASSOCIATED WITH ALZHEIMER´S DISEASE

A Thesis Submitted to the
College of Graduate and Postdoctoral Studies
In Partial Fulfillment of the Requirements
For the Degree of Master of Science
In the Department of Biochemistry, Microbiology, and Immunology
University of Saskatchewan
Saskatoon, Saskatchewan

By
NANCY PAMELA ABOYTES FLORES

PERMISSION TO USE

In presenting this thesis/dissertation in partial fulfillment of the requirements for a Postgraduate degree from the University of Saskatchewan, I agree that the Libraries of this University may make it freely available for inspection. I further agree that permission for copying of this thesis/dissertation in any manner, in whole or in part, for scholarly purposes may be granted by the professor or professors who supervised my thesis/dissertation work or, in their absence, by the Head of the Department or the Dean of the College in which my thesis work was done. It is understood that any copying or publication or use of this thesis/dissertation or parts thereof for financial gain shall not be allowed without my written permission. It is also understood that due recognition shall be given to me and to the University of Saskatchewan in any scholarly use which may be made of any material in my thesis/dissertation.

DISCLAIMER

This document was exclusively created to meet the thesis and/or exhibition requirements for the degree of Master of Science at the University of Saskatchewan. Reference in this thesis/dissertation to any specific commercial products, process, or service by trade name, trademark, manufacturer, or otherwise, does not constitute or imply its endorsement, recommendation, or favoring by the University of Saskatchewan. The views and opinions of the author expressed herein do not state or reflect those of the University of Saskatchewan and shall not be used for advertising or product endorsement purposes.

Requests for permission to copy or to make other uses of materials in this thesis/dissertation in whole or part should be addressed to:

Head of the Department of Biochemistry, Microbiology, and Immunology
GA20, Health Sciences, 107 Wiggins Rd
University of Saskatchewan
Saskatoon, Saskatchewan S7N 5E5 Canada

OR

Dean
College of Graduate and Postdoctoral Studies
University of Saskatchewan
116 Thorvaldson Building, 110 Science Place
Saskatoon, Saskatchewan S7N 5C9 Canada

ABSTRACT

Amyloid proteins are associated with various disorders such as Alzheimer's, Parkinson's, prion diseases, and type 2 diabetes. Each of these illnesses involves a specific amyloid protein or peptide that misfolds and forms fibrils. Apart from pathological amyloids, there are amyloids that are considered functional amyloids. Functional amyloids are produced by different organisms, and in contrast to pathological amyloids, they serve various biological functions. For my MSc. project I focus on the pathological amyloid-β (Aβ) associated with Alzheimer's disease and the functional amyloid curli. Curli is produced by the foodborne pathogen *Salmonella* and the commensal bacteria *Escherichia coli*. Curli is classified as a functional amyloid because it provides a structural role in the biofilm extracellular matrix. CsgA and CsgB are the curli structural components. When CsgA and CsgB reach the cell surface, they change from an unstructured state as secreted proteins to β-rich structures that assemble into amyloid fibrils at the cell surface. Despite being encoded by distinct protein sequences, curli fibrils share a common 3D structure with Aβ. The mechanism of how Aβ peptides convert from soluble functional proteins into insoluble amyloid fibrils is not fully understood. Given that both proteins are naturally amyloidogenic and share a similar structural fold, the subject of my M.Sc. research is to investigate if *Salmonella* curli can cross-react with Aβ peptides. The effects of curli on aggregation and aggregate cytotoxicity of Aβ(1-42) and Aβ(1-40) peptides were investigated by a combination of biophysical (Western blot analysis and kinetic studies with thioflavin T fluorescence) and cellular assays (cell viability in male and female human fibroblasts). I demonstrate that curli can physically interact with both Aβ peptides *in vitro*. The biophysical data shows that curli promotes Aβ(1-42) fibrillization and accelerate the overall aggregation of Aβ(1-40) (i.e., oligomers + fibrils). The data with cultured cells shows that Aβ(1-42)/curli aggregates are less cytotoxic that Aβ(1-42) aggregates. Our results support mounting evidence that oligomers—as opposed to mature fibrils— are probably the more toxic species of the peptides. Although we cannot correlate our results to the complex pathology of AD yet, our findings contribute to evidence that exogenous (sometimes bacterial) amyloids may influence and cross-react with host amyloids. Moreover, the interactions shown in my work may provide new insights into the molecular mechanisms of interactions between bacterial amyloids and human amyloids.

ACKNOWLEDGEMENTS

I would like to express my deepest gratitude to my supervisor, Dr. Aaron P. White, for his mentorship during this journey.

I would like to thank my committee members, Drs. Scot Stone, Mirek Cygler and Scott Napper for your invaluable suggestions and feedback.

Words cannot express my gratitude to Dr. Darrell D. Mousseau and his lab, Dr. Tyler Wenzel, Ryan Heistad, and Justin Lukan. This endeavor would not have been possible without your expertise and support.

Dr. Darrell, thank you for always being there to chat and discuss new ideas, for giving me quick lectures about stats, for taking special interest in my work and for all your supportive and encouraging words.

Many thanks to the White lab and colleagues at VIDO for supporting me during my graduate studies. Dr. Sivaranjani Murugesan, thank you for every piece of advice and for training me. Special thanks to Bonita McCuaig, for all your proofreading, boxing and trivia nights.

Last for not least, I am thankful to my parents, Silvia and Sergio; my sister, Sam, and the love of my life, Nick. I would never make it here without having your emotional support and your constant belief in me. You all kept my spirits and motivation high during this process.

DEDICATION

To my family

For all your support along the way.

To Nick

For not letting me give up. You make me see the light when everything is dark. I can´t wait to see what life will bring for us.

TABLE OF CONTENTS

LIST OF TABLES

LIST OF FIGURES

LIST OF ABBREVIATIONS

AD	Alzheimer's disease
AFM	Atomic force microscopy
ALS	Amyotrophic lateral sclerosis
ANOVA	Analysis of variance
APP	Amyloid precursor protein
Aβ	Amyloid beta
α-syn	Alpha-synuclein
CD	Circular dichroism spectroscopy
CR	Congo Red
Cryo-EM	Cryogenic electron microscopy
csg	Curli-specific genes
DLS	Dynamic light scattering
DMEM	Dulbecco's modified eagle's medium
DMSO	Dimethyl sulfoxide
ECM	Extracellular matrix
EOAD	Early-onset Alzheimer's disease
HFIP	1,1,1,3,3,3-hexafluoroisopropanol
kDa	Kilodaltons
LB	Luria Bertani
LOAD	Late-onset Alzheimer's disease
MD	Molecular dynamic
MES	2-(N-morpholino)ethanesulfonic acid
MTT	3-(4,5-Dimethylthiazol-2-yl)-2,5-di-phenyltetrazolium bromide
ND	Neurodegenerative disease
PBS	Phosphate buffered saline
PD	Parkinson's disease
PrP^{C}	Cellular prion protein
PrP^{Sc}	Infectious prion protein

QLS	Quasielastic light scattering
rdar	Red, dry, amd rough
RFU	Relative fluorescence unit
SDS-PAGE	Sodium dodecyl sulfate polyacrylamide gel electrophoresis
ssNMR	Solid-state nuclear magnetic resonance
T agar	Tryptone agar
$t_{1/2}$	Half-time
T8SS	Type VIII secretion system
TBS	Tris-buffered saline
TEM	Transmission electron microscopy
ThT	Thioflavin T
TLR	Toll-like receptor
TSE	Transmissible spongiform encephalopathies

CHAPTER I. LITERATURE REVIEW AND INTRODUCTION

1.1. AMYLOID PROTEINS

Amyloid proteins are subjects of interest because of their link to several disorders such as Alzheimer's (AD), Parkinson's (PD), prion diseases and type 2 diabetes (T2D) where a particular amyloid protein or peptide that misfolds and forms fibrils is directly tied to each illness (Barron, 2017; Benson, 2023). Pathological amyloids are not the only type of amyloids that exist. Artificial amyloids, which were discovered in the 1990s, are globular proteins that under certain conditions can form fibrils that are similar to amyloid fibrils (Gustavsson *et al.*, 1991). The latest type of amyloids discovered are functional amyloids. Functional amyloids are produced by different organisms and contrary to pathological amyloids, functional amyloids perform diverse biological functions (Fowler *et al.*, 2007). Although amyloid proteins from different types are encoded by different sequences, all amyloids have a have a common fibril scaffold (structure), which unites them all. Therefore, it is critical to comprehend how these proteins aggregate to form fibrils and what factors are important in defining their function.

1.1.1 Amyloid structure

Pathological and functional amyloids are proteins that form elongated β-sheet-rich fibrils (**Figure 1.1**) (Rambaran and Serpell, 2008; Greenwald *et al.*, 2018). The β-sheets made of aligned β-strands (arrows in **Figure 1.1**) are highly organized and constitute the so-called cross-β structure. Observation of the cross-β structure by x-ray diffraction has elucidated a characteristic diffraction pattern (Sunde *et al.*, 1997). The β-strands are perpendicular to the fibril axis and are 4.7 Å apart. The β-sheets run parallel to the fibril axis and the stacking distance is approximately 10 Å (Sunde *et al.*, 1997; Greenwald *et al.*, 2018).This cross-β structure allows amyloid proteins to bind specific dyes like Congo Red (CR), Thioflavin T (ThT), and ProteoStat® (Reinke and Gestwicki, 2011; Navarro and Ventura, 2014; Yakupova *et al.*, 2019). Amyloid fibrils are typically made up of two to eight filamentous subunits called protofibrils (Cohen *et al.*, 1982). These protofibrils interact laterally along the fibril axis. Each protofibril has the cross-β structure and can be built up from two to six β-sheets (**Figure 1.1** depicts a protofibril with two β-sheets) (Cohen *et al.*, 1982). The cross-β structure is strongly ordered and presents an extraordinary stability and resistance to denaturation and digestion (Rambaran and Serpell, 2008). This stability is due to the interactions

between mated β-sheets that face each other. The tight interface between β-sheets is known as the "steric zipper" (Sawaya *et al.*, 2021). The steric zipper favours amyloid assembly and formation of β-sheet hydrogen bonds (Sawaya *et al.*, 2021).

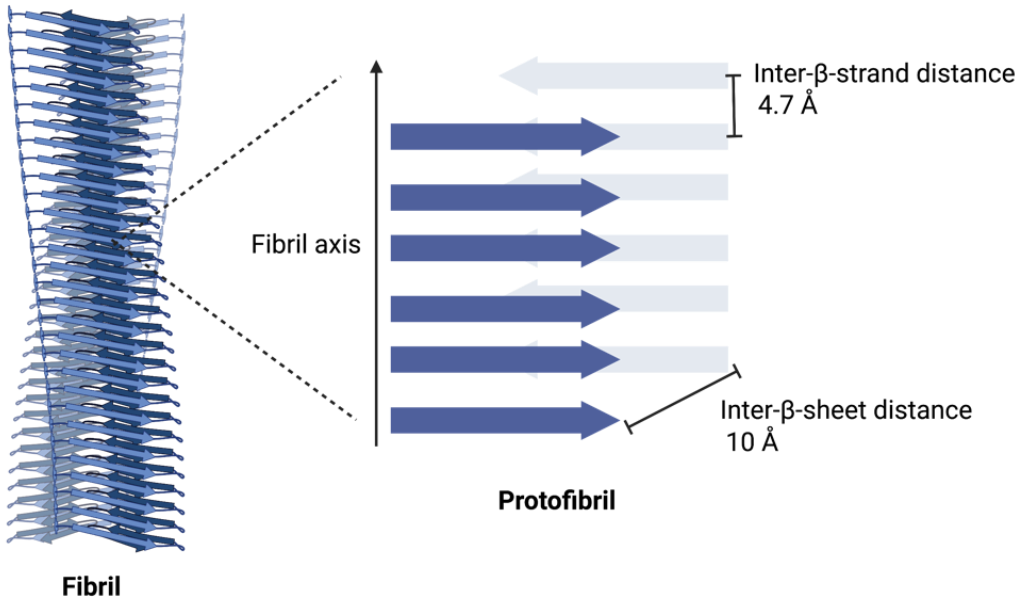

Figure 1.1. Characteristic cross-β structure in amyloid protein fibrils. The β-strands in each β-sheets are separated by 4.7 Å. The cross-β-sheet structure is arranged by β-sheets running parallel to the fibril axis and associated at a distance of 10 Å. Adapted from(Harada *et al.*, 2018). Created with BioRender.com.

The large variety of protein sequences capable of producing amyloid fibrils at first looked incompatible with the uniform morphology of the fibrils. Recent developments have made it possible to obtain amyloid structures with great resolution and provide some answers. Experimental techniques including cryogenic electron microscopy (cryo-EM) and solid-state nuclear magnetic resonance (ssNMR) spectroscopy have provided the first comprehensive structural models of amyloid assembly *in vitro* from peptide fragments or full-length polypeptides (Benzinger *et al.*, 1998; Balbach *et al.*, 2000; Balbach *et al.*, 2002; Jaroniec *et al.*, 2002; Nelson *et al.*, 2005). Studies highlighted the significance of β-stacking, amide ladders, and salt bridges in maintaining the cross-β structure. For example, amyloids almost always assemble under the same architecture called parallel in-register intermolecular β-sheet (PIRIBS) scaffold, although they have no amino acid homology (Sawaya *et al.*, 2021).

The PIRIBS-based core is characterized by a stack of β-loop-β motifs with identical groups of amino acids aligned along the fibril axis with narrow 4.7 Å intervals (Groveman *et al.*, 2014; Sawaya *et al.*, 2021). As a result, a particular residue of the amyloid can most frequently interact with an identical residue in the neighbouring layers. This structural aspect may highlight the unique properties of each residue and how they influence the amyloid fibril assembly (Groveman *et al.*, 2014; Sawaya *et al.*, 2021). For instance, hydrophobic residues form extensive hydrophobic patches that run along the fibril axis, whereas charged residues may disturb local structures by disrupting the attraction between the intermolecular β-sheets and being preferentially exposed to the solvent. This characteristic also explains why a single mutation has a significant impact on the amyloid structure and its characteristics (Groveman *et al.*, 2014; Sawaya *et al.*, 2021). It is hypothesized that the in-register amyloids have lower free energies than native conformations (Baldwin *et al.*, 2011). The in-register alignment is thermodynamically favoured by the hydrogen bonds that connect the amyloid backbones (Baldwin *et al.*, 2011; Sawaya *et al.*, 2021). Roterman *et al.* (2017) described the in-register amyloids as "ribbon-like micelles" with exposed hydrophobicity at the stacked ends which allows for limitless extension. Proteins are more prone to aggregation when their hydrophobic β-sheets are exposed on the molecular surface (Richardson and Richardson, 2002). Proteins that are physiologically soluble and rich in β-sheets have structural characteristics that prevent their solvent-facing β-sheets from unwanted interactions and aggregation with other molecules (Richardson and Richardson, 2002).

Although most amyloid fibrils are confined to the same PIRIBS scaffold newer studies have exhibited the diversity of amyloid conformations, including the occurrence of polymorphism (which will be discussed later), wherein a single polypeptide chain may fold into numerous unique amyloid structures (Heise *et al.*, 2005; Paravastu *et al.*, 2008b; Fitzpatrick *et al.*, 2017; Sawaya *et al.*, 2021; Caughey *et al.*, 2022; Li and Liu, 2022). As a result, differences in structural conformations may characterize the function or pathogenesis of an amyloid protein.

1.1.2 Amyloid polymerization

Amyloids polymerize into fibrils through a self-assembly process from soluble monomers/oligomers to insoluble amyloid fibrils (Iadanza *et al.*, 2018). The nucleation-dependent polymerization model is the most widely recognized amyloid aggregation model (Jarrett and Lansbury, 1993). In this model, the fibrillation process generates a sigmoidal kinetic curve with

three stages. The first stage is the lag phase. This stage is followed by the growth phase, also known as elongation phase. Finally, the last stage is the stationary or plateau phase (**Figure 1.2**) (Arosio *et al.*, 2015).

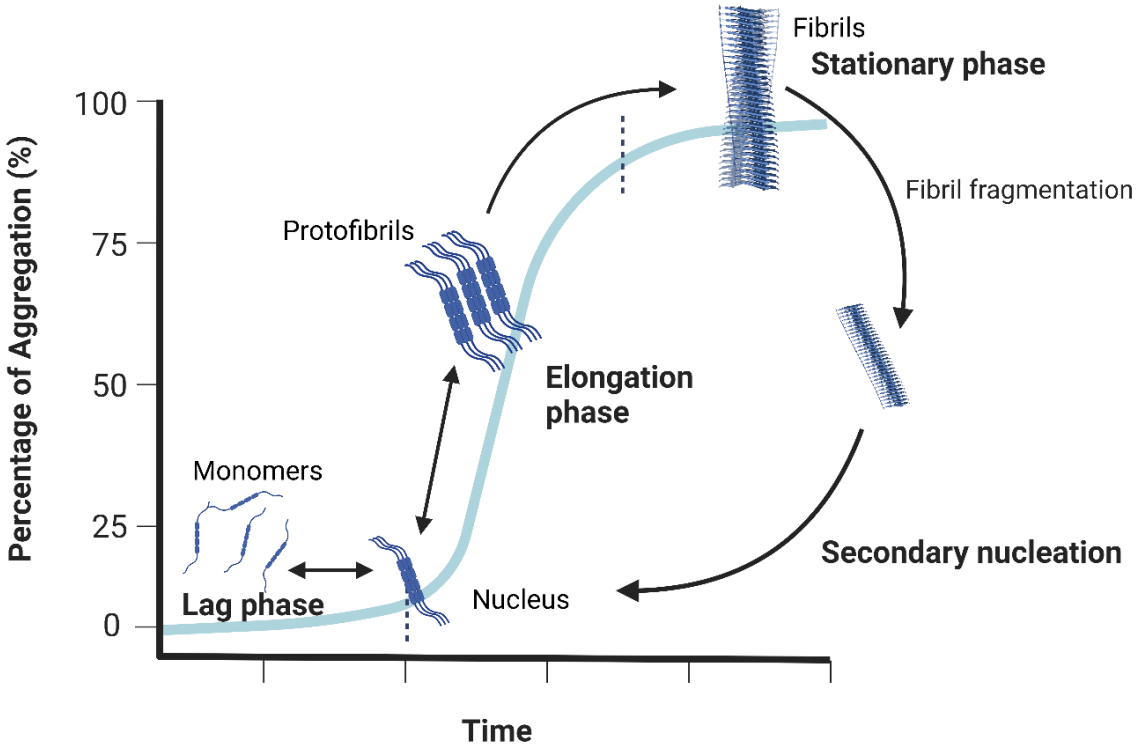

Figure 1.2. Nucleation-dependent polymerization model of amyloid fibril formation. In the lag phase monomers form the critical nucleus and primary nucleation occurs. In the elongation phase, the nucleus interacts with monomers and oligomers to create prefibrillar structures that will later become protofibrils. In the stationary phase, protofibrils assemble into mature amyloid fibrils. Finally, secondary nucleation occurs when preformed fibrils fragmentate and autocatalyze nucleation. Created with BioRender.com.

During the lag phase, a phenomenon known as primary nucleation occurs (Auer, 2014; Arosio *et al.*, 2015). During this stage a critical nucleus consisting of monomeric subunits is created. This small aggregate is sufficiently stable for growth, adding more monomers in a monomer aggregation process that prevails over monomer dissociation (Arosio *et al.*, 2015; Lee and Terentjev, 2017). This results in the elongation phase, where interactions between nucleus, monomers and oligomers lead to the formation of pre-fibrillar structures that will grow and form protofibrils. Protofibrils are more stable and make the assembly process more favorable, resulting into an exponential growth. Finally, in the plateau or stationary phase, monomer concentration

reaches the equilibrium and the protofibrils assemble into mature amyloid fibrils. Mature amyloid fibrils can fragment and produce several catalytic subunits (new nucleus). This fibril assisted nucleation is the so-called "secondary nucleation" (Almeida and Brito, 2020).

1.1.3 Experimental approaches to study amyloids

Since amyloid fibrils are insoluble and non-crystallizable it is difficult to understand their structure and folding process. When studying amyloid proteins, the most common probe for observing amyloid fibril formation is thioflavin T (ThT). This benzothiazole dye has been used since 1959 (Vassar and Culling, 1959) and notwithstanding current concerns over its usage as an amyloid-specific probe, it is still considered one of the "gold standards" for identifying and analyzing amyloid fibril formation *in vivo* and *in vitro*.

ThT emits a strong fluorescence signal at around 482 nm when excited at 450 nm when applied to molecules containing β-sheet-rich deposits, such as the cross-β sheet quaternary structure of amyloid fibrils (**Figure 1.1**) (LeVine, 1993; Nilsson, 2004). While the exact mechanism of interaction between ThT and amyloid fibrils is still unknown, the most accepted theory proposes that ThT intercalates within the exposed side-chain grooves that are parallel to the fibril axis (**Figure 1.3**) (Krebs *et al.*, 2005; Hawe *et al.*, 2008; Biancalana *et al.*, 2009). It has been proposed that the smallest binding location for ThT on the fibril surface is four consecutive β-strands (**Figure 1.3**) (Biancalana *et al.*, 2009; Wu *et al.*, 2009).

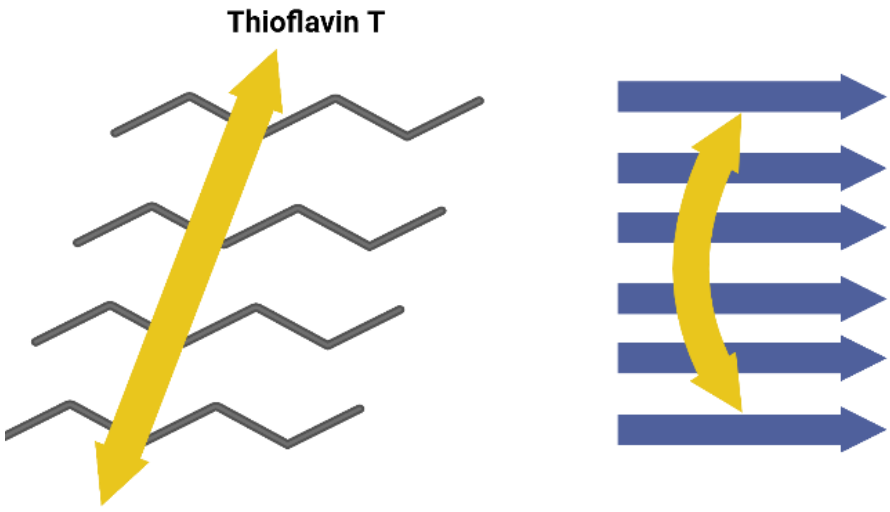

Figure 1.3. ThT-amyloid fibril binding. Proposed ThT-amyloid fibril biding mechanism. ThT binds the side-chain grooves that are parallel to the fibril axis. The minimal binding site is four β-strands. Adapated from (Biancalana and Koide, 2010). Created with BioRender.com.

Fluorescence from the amyloid-ThT complex allows assessment of amyloid fibril production as a function of amyloid fibril length and quantity since there is a stoichiometric and saturable interaction between ThT and amyloid fibrils (Bolder *et al.*, 2007). Thus, ThT is simply added to samples containing fibril structures at a concentration greater than the number of possible ThT-fibril binding sites, and ThT fluorescence emission is measured at ~490 nm with excitation at ~440 nm (Naiki *et al.*, 1989). The ThT fluorescence assay has two variations: the *in situ* real-time ThT assay, in which fibril formation is performed in the presence of ThT, allowing for real-time monitoring of fibrillation kinetics; and the single time-point dilution ThT assay, in which samples of a fibril-forming polypeptide are diluted into buffered solutions of ThT, allowing for simpler single time-point readings (Gade Malmos *et al.*, 2017).

An *in situ* ThT assay is the most appealing option when experimental conditions to examine the fibrillization of a specific amyloid protein have been properly selected. This allows for real-time monitoring of several samples in 96 or 386 well plates throughout the incubation time. However, many practical issues need to be addressed to lessen the chance of being deceived by findings from a subpar ThT assay.

1.2 FUNCTIONAL AMYLOIDS

There are amyloids that possess physiological roles for the cells, these amyloids are called "functional amyloids" and can be found in fungi, mammals, and bacteria (**Table 1.1**) (Otzen and Riek, 2019). There are many functional amyloids, including those listed in Table 1.1. Here, we will focus on curli, which is produced by *Salmonella enterica* and *Escherichia coli*.

Table 1.1. Some functional amyloids.

Organism	Amyloid protein	Function	Reference
Mammals	Pmel17	Pigmentation of skin	(Maji *et al.*, 2009)
Mammals	Peptide hormones	Hormone storage and release	(Maji *et al.*, 2009)
Drosophila	Orb2	Long-term memory	(White-Grindley *et al.*, 2014)
Fungi	Class I hydrophobins	Surface adherence, spore development and invasion	(Piscitelli *et al.*, 2017)

Candida albicans	Als5p	Cell-cell aggregation and cell-substrate adhesion	(Chan and Lipke, 2014)
Saccharomyces cerevisiae	Flocculins Flo11p and Flo1p	Cellular aggregation and biofilm-like mat formation	(Chan *et al.*, 2016)
E. coli / S. enterica	curli	Biofilm formation, main component of extracellular matrix	(Chapman *et al.*, 2002)
Bacillus subtilis / B. cereus	TasA	Antibacterial activity. Formation of hydrophobic biofilms. Spore component	(Romero *et al.*, 2010)
Streptomyces spp.	chaplins/rodlins	Formation of aerial hyphae and surface tension	(Willey *et al.*, 2006; Di Berardo *et al.*, 2008)
Pseudomonas spp.	FapC	Biofilm formation and surface hydrophobicity	(Dueholm *et al.*, 2010; Dueholm *et al.*, 2013)
Staphylococcus aureus and *S. epidermidis*	Phenol-Soluble Modulins (PSMs)	Biofilm formation and regulation	(Schwartz *et al.*, 2012; Wu *et al.*, 2018)
Streptococcus mutans	P1	Found in dental plaque and involved in biofilm formation	(Oli *et al.*, 2012)

1.2.1 Curli

Enteric bacteria, like non-pathogenic and human and animal pathogenic *E. coli* and *Salmonella enterica* serovars produce the fibrillar amyloid protein curli. Since its discovery in the late 1980s, curli has been linked to several physiological and pathogenic functions (Collinson *et al.*, 1996; Römling *et al.*, 1998; Chapman *et al.*, 2002; Tursi and Tükel, 2018). These extracellular fibrils participate in surface and cell-cell interactions that promote host colonization and biofilm formation to shield bacteria from physical and chemical stressors (Collinson *et al.*, 1996; Römling

et al., 1998; Chapman *et al.*, 2002; Tursi and Tükel, 2018). Cell aggregation and bacterial adhesion to surfaces are both facilitated by curli fibrils, which are also a crucial component of the extracellular matrix (ECM) needed to create mature biofilms (Collinson *et al.*, 1996; Römling *et al.*, 1998; Chapman *et al.*, 2002; Solomon *et al.*, 2005; Tursi and Tükel, 2018). In a biofilm, bacterial cells represent only 10% of the components. The other 90% is constituted by the ECM which contains lipids, polysaccharides, DNA and proteins (Flemming and Wingender, 2010). Curli fibrils constitute 85% of the ECM in biofilms (McCrate *et al.*, 2013). Due to their interactions with a variety of host proteins, including contact-phase and extracellular matrix proteins, which are thought to help bacteria spread through the host, curli fibrils are recognized as key virulence factors (Sjöbring *et al.*, 1994; Ben Nasr *et al.*, 1996; Herwald *et al.*, 1998; Olseán *et al.*, 2002; Dueholm *et al.*, 2012; Nhu *et al.*, 2018). Curli fibrils are considered as pathogen-associated molecular patterns (PAMPs) because they are recognized by toll-like receptors which activate the innate immune system is activated (Tursi and Tükel, 2018; Miller *et al.*, 2021).

1.2.1.1 Curli biogenesis

Curli-specific genes (*csg*) clustered in the operons *csgBAC* and *csgDEFG*, are responsible for encoding the accessory proteins involved in the structure and assembly of curli in both bacterial species, *E. coli* and *Salmonella* (**Figure 1.4**) (Römling *et al.*, 1998; Bhoite *et al.*, 2019). Indeed, curli genes in *E. coli* and *Salmonella* are highly conserved and can be complemented (Römling *et al.*, 1998). The sequence similarities at the amino acid level are higher than the homologies for most functionally and sequentially related fimbrial genes, with 86% for the major subunit CsgA, 100% for the nucleator CsgB, 96% for the transcriptional regulator CsgD and 99% for the secretion pore CsgG (Römling *et al.*, 1998). Curli biogenesis has been termed the Type VIII secretion system (T8SS) (Bhoite *et al.*, 2019), here CsgD promotes the transcription of the *csgBAC* operon (Römling *et al.*, 1998; Evans *et al.*, 2015).

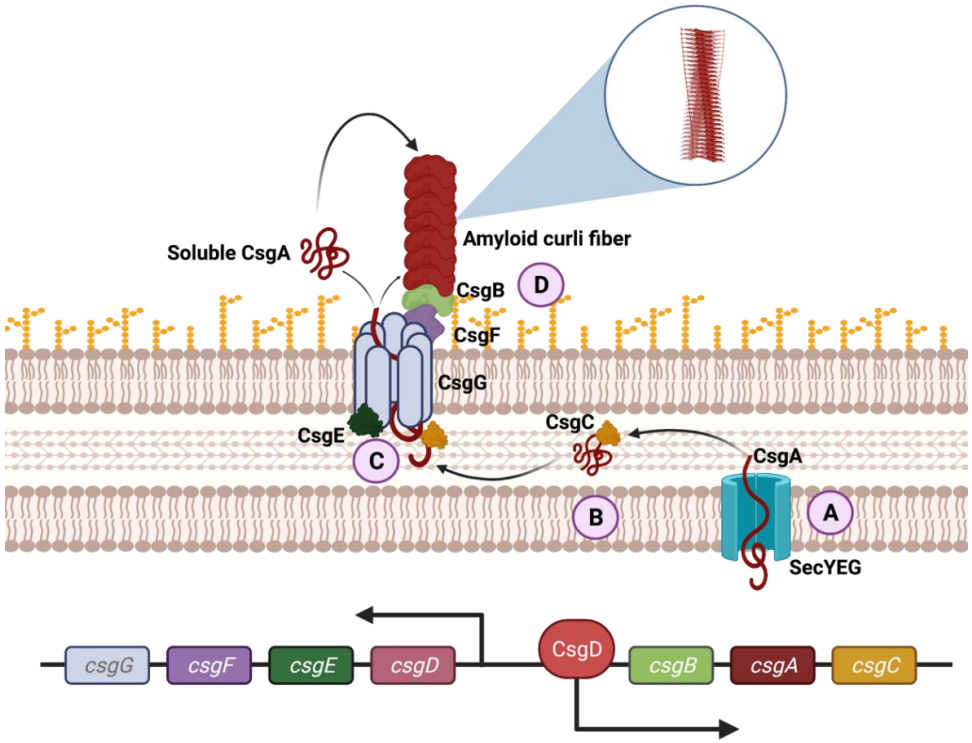

Figure 1.4. Curli biogenesis by the Type VIII Secretion System. CsgD promotes transcription of the csgBAC operon. (A) CsgA is translocated into the periplasm where it interacts with (B) the chaperone, CsgC, to keep its soluble, not polymerized state. (C) CsgE, will eventually help transport CsgA to the CsgG secretion channel. (D) Outside the cell, CsgA begins fibril formation due to the nucleation action of CsgB. A diagram of the two curli operons, csgBAC and csgDEFG, is shown in the bottom. Adapted from (Blanco *et al.*, 2012). Created with BioRender.com.

CsgA, the major curli subunit, is translocated to the periplasm by the SecYEG complex (**Figure 1.4 A**) (Van Gerven *et al.*, 2015). Once there, CsgA stays in a soluble, unstructured, depolymerized form because of the chaperone protein CsgC (**Figure 1.4 B**) (Evans *et al.*, 2015). In the periplasm, this unfolded CsgA interacts with CsgE that eventually helps to transport it to the CsgG secretion channel (**Figure 1.4 C**) (Van Gerven *et al.*, 2015; Klein *et al.*, 2018). CsgE is also thought to play an important role in the prevention of non-specific substrate secretion after capping the CsgG translocation pore (Klein *et al.*, 2018). In the extracellular space, CsgA begins fibril formation and elongation due to the nucleation action of the CsgB protein (**Figure 1.4 D**) (Van Gerven *et al.*, 2015; Klein *et al.*, 2018). The fibrilization process also depends on the CsgF protein that forms a complex with CsgG and constitutes a bridge between the pore and the growing curli fibers. CsgF is also thought to coordinate the nucleating role of CsgB (Van Gerven *et al.*,

2015; Klein *et al.*, 2018; Bhoite *et al.*, 2019). Outside of the cell, the subunits that composed curli self-assemble and form amyloid fibers (Sunde and Blake, 1997).

Curli gene expression regulation is incredibly intricate and responsive to a variety of environmental factors (Gerstel and Römling, 2003). Growth at temperatures below 30°C was one of the first circumstances identified as promoting curli gene expression (Römling *et al.*, 1998; Bordeau and Felden, 2014). Indeed, curli expression works best at temperatures below 30°C for most of the *E. coli* and *Salmonella* strains. However, the ability of numerous clinical *E. coli* bacteria, particularly sepsis isolates, to express curli at 37°C has been reported (Bian *et al.*, 2000).

1.2.1.2 Curli structure

Curli fibrils are unbranched, abundant in β-sheets, and resistant to protease digestion (Collinson *et al.*, 1991; Collinson *et al.*, 1993). Curli induces a red shift when combined with CR (Klunk *et al.*, 1999) and a 10- to 20-fold increase in fluorescence when combined with ThT (LeVine, 1999). These two dyes are known to bind amyloids. The preserved cross-strand structure, in which condensed β-sheets are stacked parallel to the fibrils axis and individual β-strands are perpendicular to the fibre axis, is the distinguishing feature of amyloid fibrils (Sunde *et al.*, 1997).

CsgA is the primary curli subunit. An N-terminal of 22 amino acids (N22) needed for secretion and a C-terminal amyloid core domain make up the mature CsgA protein (**Figure 1.5**) (Collinson *et al.*, 1999; Robinson *et al.*, 2006; Shewmaker *et al.*, 2009). The CsgA sequence contains five imperfect repeats (R1 through R5) (**Figure 1.5 A** and **B**) (Cherny *et al.*, 2005; Wang *et al.*, 2007). Each repeating unit consists of a Ser-X5-Gln-X-Gly-X-Gly-Asn-X-Ala-X3-Gln (**Figure 1.5 A**) (Cherny *et al.*, 2005; Wang *et al.*, 2007; Sleutel *et al.*, 2023). These repeat components create strands 1 and 2 as well as the connecting loop, or arc (**Figure 1.5**) (Cherny *et al.*, 2005; Wang *et al.*, 2007; Sleutel *et al.*, 2023). As a result, the residues indicated as Arc 1 and Arc 2 in **Figure 1.5 A** map onto the outward facing surface residues of the strand-arc-strand motif that constitutes a single curli repeat, whereas the residues of motif a and motif b (**Figure 1.5 A**) map onto the inward facing steric zipper residues. After motif b, the last four to five residues, X-G-X-X-(X), create a second arc that links motif b to motif a from the next repeat resulting in what is called a "β-solenoid" structure (**Figure 1.5 B**) (Sleutel *et al.*, 2023). In this structure the repeating units align their Ser and Gln and, Gln and Asn residues in stacks that help stabilize the amyloid fold, thorough polar zippers which are ladders of sidechain hydrogen bonds (**Figure 1.5**

C) (Cherny *et al.*, 2005; Wang *et al.*, 2007; Sleutel *et al.*, 2023). Curli presents a PIRIBS fibril scaffold where repeats align in parallel and residues in a repeat register (hydrogen-bonds) with identical sidechain residues stacked along the length of the fibril (Sawaya *et al.*, 2021). As previously discussed, PIRIBS geometry is known to be abundant in several eukaryotic and pathological amyloids (Michelitsch and Weissman, 2000).

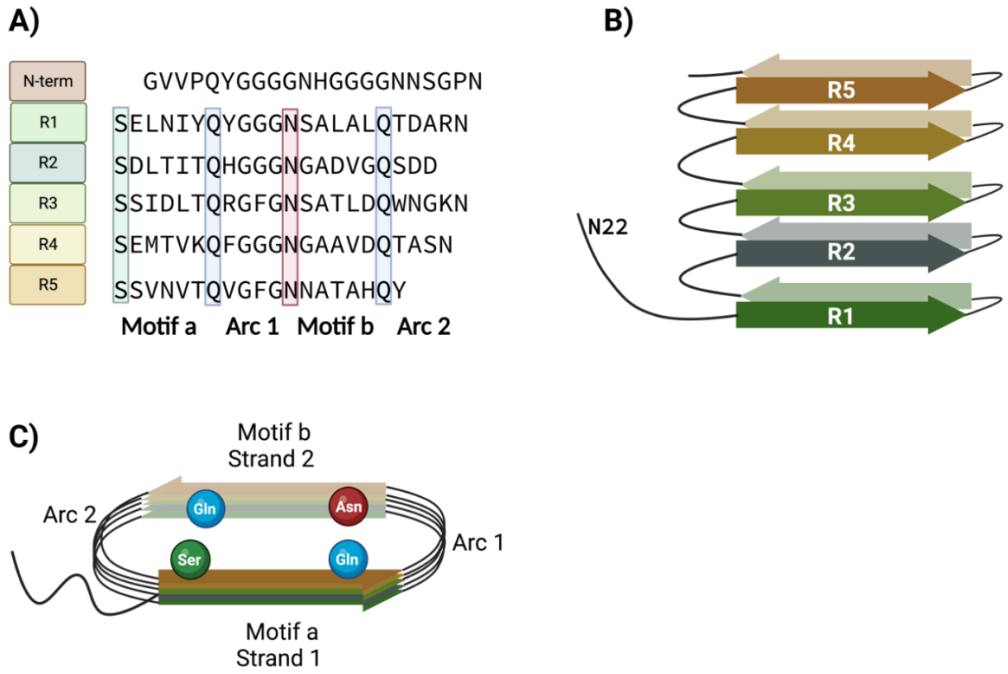

Figure 1.5. CsgA sequence and predicted structure. A) CsgA has an N-terminal of 22 amino acids (N22) and five repeat units each with a proposed β strand-arc-β strand-arc fold. B. The five repeating units come together to form a "β solenoid" fold (side view). C) Ser, Gln, and Asn residues (boxes in A) line up in stacks that maintain the amyloid structure. Created with BioRender.com.

1.2.1.3 Curli production inside the host

Curli fibrils are a major component of biofilms (Solomon *et al.*, 2005). Biofilms are a collection of bacteria that is enclosed in a self-produced, three-dimensional extracellular matrix and attached to a biotic or abiotic surface (Hall-Stoodley *et al.*, 2004). When resources are low and conditions such as temperature, osmolarity, and oxygen availability are unstable, bacteria are protected by the biofilm (Hall-Stoodley *et al.*, 2004). Additionally, the biofilm hinders the host's immune system and harmful substances like antibiotics from entering (Sharma *et al.*, 2019).

Several researchers first questioned whether curli/biofilm formation was feasible *in vivo* due to the lack of substantial csgD expression at 37°C (Normark *et al.*, 1998; Römling *et al.*, 2003;

White *et al.*, 2008). Biofilms are essential for microbial survival in the environment (Fazeli-Nasab *et al.*, 2022). Biofilms create a stable habitat for bacteria. Several studies have hypothesized that the ability to form a biofilm is a conserved trait that allows bacteria like *Salmonella* or *E. coli* to persistently colonize sites both inside and outside of the host, ultimately conferring them an evolutionary advantage during the cycle of infection and transmission(**Figure 1.6**) (Römling *et al.*, 2003; MacKenzie *et al.*, 2017; MacKenzie *et al.*, 2019). For instance, variations in temperature, shifts in the availability of nutrients, and exposure to harsh or harmful substances are just a few of the triggers that can cause planktonic *Salmonella* to enter a biofilm state (**Figure 1.6**) (De Oliveira *et al.*, 2014; Paytubi *et al.*, 2017; González *et al.*, 2019).

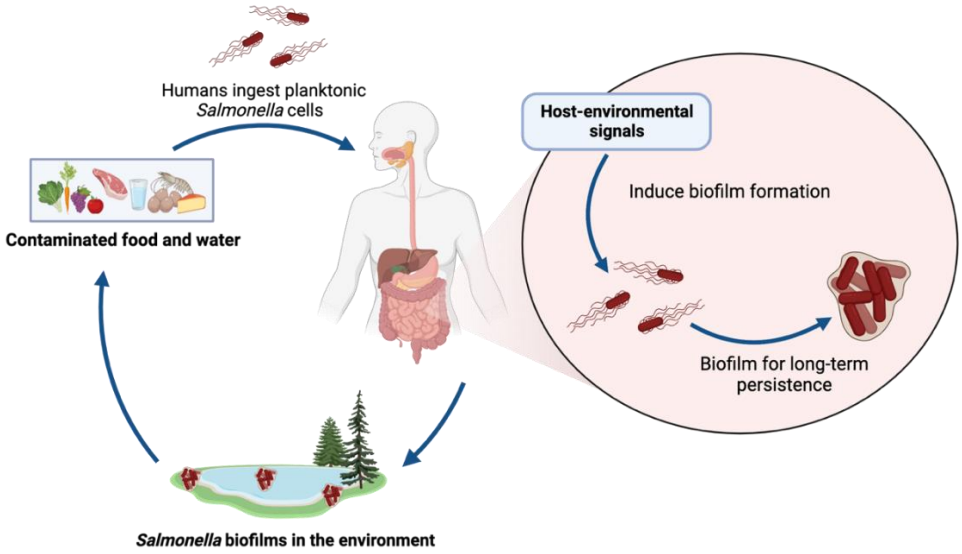

Figure 1.6. Suggested transition of planktonic *Salmonella* into a biofilm as an evolutionary advantage during the cycle of infection and transmission. Created with BioRender.com.

Increasing evidence suggest that curli is expressed *in vivo*. *Salmonella* biofilm formation containing curli was observed within the cecum of chickens (Sheffield *et al.*, 2009; El Hag *et al.*, 2017). For *S.* Typhimurium and *S. Pullorum*, the ability to build biofilms helps the bacteria overcome colonization resistance and establish long-lasting asymptomatic infection in chickens (Sheffield *et al.*, 2009; El Hag *et al.*, 2017). Formation of biofilms and detection of CsgA (the major curli subunit) in the *Caenorhabditis elegans* (*C. elegans*) gut colonized by *S.* Typhimurium were associated with increased bacterial persistence (Desai *et al.*, 2019). Similarly, *S.* Typhimurium orally infected mice exhibit curli expression in the cecum and colon (Miller *et al.*,

2020). In humans, anti-CsgA antibodies have been detected in blood cultures from sepsis patients (Bian *et al.*, 2000). *E. coli* is usually engaged in sepsis pathogenesis (Ananias and Yano, 2008). All these finding suggest that curli genes may be expressed to some extent during human infection.

Additionally, systemic exposure to curli is thought to be facilitated by its innate capacity to bind fibronectin, plasminogen, and tissue type plasminogen activator (Sjöbring *et al.*, 1994; Hammar *et al.*, 1995). Tissue breakage occurs when plasminogen is activated (Castellino and Ploplis, 2005). This raises the possibility of a mechanism promoting bacterial spread. Curli also binds to host fibrinogen and bradykinin (Ben Nasr *et al.*, 1996; Olseán *et al.*, 2002). Bradykinin leads to a variety of biological effects such as decreasing blood pressure, reducing oxidative stress, and enhancing permeability of the blood-brain barrier (BBB) (Raymond *et al.*, 1986; Rodríguez-Massó *et al.*, 2021).

1.3 AMYLOID PROTEINS AND NEURODEGENERATIVE DISEASES

Neurodegenerative diseases (NDs) are illnesses involving degeneration of the brain. Commonly, they begin with a loss of mental or physical function and steadily intensify until disablement or death. Even while it is not well understood how these diseases develop and how they spread, amyloid proteins have been linked to several NDs (Soto, 2003; Soto and Pritzkow, 2018). The common pattern that appears in all these NDs is an aberrant propensity for specific amyloid proteins unique to each disorder to aggregate because of misfolding (**Table 1.2**) (Soto, 2003; Soto and Pritzkow, 2018). In 2021, over 55 million people in the world were suffering from an ND and 10 million new cases are reported each year, with Alzheimer's disease representing the majority of them (60-70%) (Greenblat, 2021).

Table 1.2 Some amyloid proteins and their associated neurodegenerative disease.

DISEASE	AMYLOID PROTEIN
Alzheimer's disease	Amyloid beta (Aβ)
Parkinson's disease	Alpha-synuclein (α-syn)
Amyotrophic lateral sclerosis (ALS)	Superoxide dismutase
Transmissible spongiform encephalopathies (TSE), a.k.a. Prion diseases	Cellular prion protein (PrP^{C}) imprinted by the infectious prion protein (PrP^{Sc})

1.3.1 Alzheimer's disease

Alzheimer's disease is the most prevalent neurodegenerative condition associated with aging, which has a complicated, multiple, irreversible aetiology (Thies and Bleiler, 2012). AD is manifested as a pronounced amnestic cognitive impairment. Non-amnestic cognitive impairment can also occur but it less frequent. Short-term memory issues are the most typical way that AD manifests, although other symptoms include trouble with speaking, visuospatial processing, and executive skills (Knopman *et al.*, 2021).

Most AD patients (95%) have the disease's late-onset (LOAD) variant, in which symptoms first appear in their mid-60s or later. On the other hand, when symptoms start showing before age 65, patients are diagnosed as having early-onset AD (EOAD) (Mendez, 2017). While LOAD is sporadic, EOAD can be either familial or sporadic (Knopman *et al.*, 2021).

1.3.1.1 Risk factors

AD has been associated with a complex interplay of age, genetics, conditions, and lifestyle risk factors. The major risk factor for AD is age. Studies have shown that the percentage of people with AD dramatically increases with age (Harman, 2006; Hebert *et al.*, 2010; Knopman *et al.*, 2021). Ages between 65-74 represent only 5%, whereas those between ages of 75 and 84, account for 13.1%. At age 85 or more, the prevalence is between 30% and 40% (Jeremic *et al.*, 2021; Rajan *et al.*, 2021).

Additionally, numerous genes that raise the risk of Alzheimer's disease have been reported (Tanzi, 2012; Van Cauwenberghe *et al.*, 2016; Knopman *et al.*, 2021; Bellenguez *et al.*, 2022). Particularly, the influence of the *APOE* gen on the risk of developing LOAD. Apolipoprotein E is a protein that carries cholesterol in the bloodstream and is created according to the *APOE* blueprint. There are six *APOE* allele pairs: ε2/ε2, ε2/ε3, ε2/ε4, ε3/ε3, and ε4/ε4. Having the ε3 pair does not make someone more or less likely to develop AD. The ε2 pair has a lower risk compared to the ε3 pair. However, one copy of the ε4 form increases the AD risk by around three times compared to two copies of the ε3 form, and two copies of the ε4 form increases the risk by eight to twelve times (Liu *et al.*, 2013; Loy *et al.*, 2014; Michaelson, 2014).

In EOAD, only 1% of cases are due to common, fully penetrant mutations in three distinct genes *APP*, *PSEN1*, and *PSEN2* (Cruchaga *et al.*, 2012; Loy *et al.*, 2014; Bellenguez *et al.*, 2022). These genes produce the protein amyloid precursor protein (APP) (on chromosome 21) and, the

enzymes presenilin (PSEN) PSEN1 (on chromosome 14), and PSEN2 (on chromosome 1) that generate Aβ peptides (Cruchaga *et al.*, 2012). Those who have trisomy 21 (Down's syndrome) carry three copies of the APP thus almost all adults over 40 with Down´s syndrome develop AD (Doran *et al.*, 2017).

Studies have shown that there are sex-specific differences in AD susceptibility, age of onset, and symptom development (Li and Singh, 2014; Laws *et al.*, 2018; Yu *et al.*, 2020). It has been noted that prevalence is typically higher in women, however, the incidence is not higher, suggesting that both sexes are equally susceptible (Li and Singh, 2014; Dumitrescu *et al.*, 2019; Wang *et al.*, 2020b).

Conditions like diabetes mellitus, hypertension, obesity, and low HDL cholesterol, hearing loss, traumatic brain injury are linked to an elevated risk of AD (Livingston *et al.*, 2020). Low educational attainment, increased dietary fat, lack of physical activity, alcohol misuse, smoking and other aspects of lifestyle are modifiable risk factors for AD development (Scarmeas *et al.*, 2009; Xu *et al.*, 2015; Delpak and Talebi, 2020).

1.3.1.2 Hypotheses for the Progression of Alzheimer's Disease

Even though AD has been a major area of study for many years, the process that leads to AD remains unclear. The amyloid cascade hypothesis and the phosphorylation of the tau protein hypothesis are the two etiological ideas that have received the most support from the scientific community (Murphy and LeVine, 2010). The amyloid cascade hypothesis proposes that the neurodegenerative process in AD is caused by the formation and accumulation of deposits of Aβ peptides, which have negative effects on synaptic plasticity and neuronal functioning (Hardy and Higgins, 1992; Korczyn, 2008).

1.3.1.2.1 The amyloid cascade hypothesis

This hypothesis is focused on the human protein APP. This single domain transmembrane protein is present in various types of neurons and glial cells (Murphy and LeVine, 2010). The breakdown of APP produces Aβ peptides. APP is fragmented by the endoproteases, α-, β- and γ-secretases. The protein can be cleaved in an amyloidogenic and a non-amyloidogenic form (**Figure 1.7**) (Murphy and LeVine, 2010; Lu *et al.*, 2013; Van Cauwenberghe *et al.*, 2016; Michaels *et al.*, 2020).

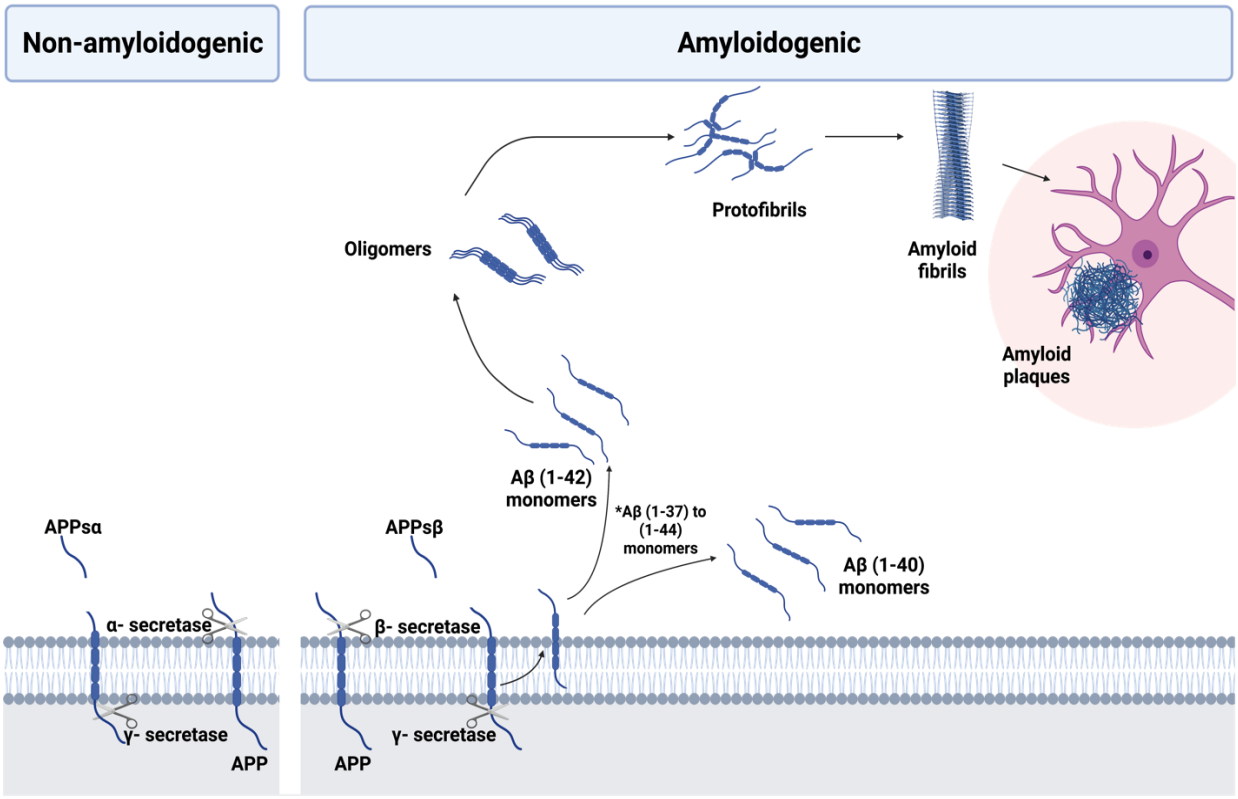

Figure 1.7. Amyloidogenic and non-amyloidogenic processing of APP. In the non-amyloidogenic pathway, APP is cleaved by α- and γ-secretases. Cleavage by β- and γ-secretases results in the amyloidogenic pathway. The amyloidogenic pathway generates Aβ peptides. Aβ(1-40) is the most abundant isoform whereas Aβ(1-42) is more hydrophobic, more neurotoxic, and more prone to aggregation which favours the amyloid self-assembly process and plaque formation in the brain. *Aβ peptide length varies between 37-44 amino acids. Created with BioRender.com.

1.3.1.2.1.1 Non-amyloidogenic pathway

Physiologically, APP is most often cleaved by α -secretase (non-amyloidogenic process in **Figure 1.7**) (Murphy and LeVine, 2010; Lu *et al.*, 2013; Van Cauwenberghe *et al.*, 2016; Michaels *et al.*, 2020). The result of this cleavage is a soluble fragment known as APPsα that stays in the extracellular space. The APPsα fragment has been shown to control neuronal excitability, enhance synaptic plasticity, learning, and memory, as well as improve neurons' resistance to oxidative and metabolic stress (Gertsik *et al.*, 2014; Nhan *et al.*, 2015; Folch *et al.*, 2018; Ribarič, 2018)

1.3.1.2.1.2 Amyloidogenic pathway

In the amyloidogenic pathway APP is cleaved by β- and γ-secretases (Murphy and LeVine, 2010; Lu *et al.*, 2013; Van Cauwenberghe *et al.*, 2016; Michaels *et al.*, 2020). First, β-secretase

cuts APP and produces a membrane-tethered, intracellular C-terminal portion of 99 amino acids (CTFβ or C99) and a short, soluble APPs β fragment. Later, C99 is non-precisely cut by γ -secretase, resulting in the production of extracellular Aβ peptides of different sizes. Aβ peptide length varies between 37-44 amino acids (**Figure 1.7**) (Murphy and LeVine, 2010; Lu *et al.*, 2013; Van Cauwenberghe *et al.*, 2016; Michaels *et al.*, 2020). Aβ(1-40) is the most abundant peptide, representing 80-90% of the total Aβ pool. The longer peptide, Aβ(1-42), is more hydrophobic and this favours the amyloid self-assembly process, shifting from a monomeric form to a β-sheet structure susceptible to aggregate and deposit in the brain (**Figure 1.7**) (Murphy and LeVine, 2010).

1.3.1.3 Treatment

Despite significant financial and research commitments, the supply of AD medications on the market is limited. Only four approved drugs—donepezil, rivastigmine, galantamine, and memantine—were offered for the symptomatic management of AD for more than 20 years (Abeysinghe *et al.,* 2020).Donepezil, rivastigmine and, galantamine are acetylcholinesterase inhibitors. Inhibiting acetylcholine catabolism in synaptic clefts enhances neurotransmission (Abeysinghe *et al.,* 2020). On the other hand, memantine, is an antagonist of the N-methyl D-aspartate receptor (NMDAR) ion channel. It controls the amount of Ca^{2+} that enters neurons and prevents glutamate from causing excitotoxicity (Abeysinghe *et al.*, 2020; Wang *et al.*, 2021b). In patients with known stages of AD, these medications are tolerated and reduce the progression of neurological symptoms, such as cognition, emotion, awareness, irritability, and delusion, but they do not have the power to reverse the disease (Wang *et al.*, 2021b).

The generation of AD drugs has been focused on targeting Aβ and tau proteins. The main methods include suppressing tau phosphorylation, inhibiting Aβ generation, inhibiting Aβ and tau aggregation, using active immunotherapy methods, such as vaccinations and, clearing the disease using monoclonal antibodies (mAbs) (Sevigny *et al.*, 2016; Tatulian, 2022). Aducanumab is a mAb against aggregated Aβ and was the first medicine with the potential to treat AD. Aducanumab was authorized by the US Food and Drug Administration (FDA) in June 2021(Dhillon, 2021). More recently, lecanebab, another mAb, that binds with to Aβ soluble protofibrils has demonstrated promise for those with AD in early stages. In a phase 3 clinical trial, lecanebab slowed cognitive decline in people with early AD by 27%. Lecanebab is under review by the FDA and is expected to become available in late 2023 (van Dyck *et al.*, 2023).

1.4 PRION AND PRION-LIKE MECHANISMS IN NDs

The idea of an infectious protein, or prion, was put forth by Stanley B. Prusiner and his team (1996). In contrast to typical infectious agents like bacteria or viruses, prions are a misfolded version of the prion protein (PrP), a normal cellular protein found in the brain. The pathogenic, isoform of this protein is known as PrP^{Sc}, while the normal cellular form is known as PrP^{C}. PrP^{C} changes into the infectious form when it interacts with PrP^{Sc}, which causes a conformational shift. The cycle is repeated by the newly created harmful proteins in a self-sustaining loop, escalating the toxicity and finally killing the cell or impairing its function (Prusiner, 1996; Prusiner, 1998).

In the brain, these misfolded prions have a predisposition to congregate and form amyloid fibrils, which ultimately cause neurodegeneration and prion diseases, also referred to as transmissible spongiform encephalopathies (TSEs) (Prusiner, 1996; Prusiner, 1998). TSEs, include well-known examples like scrapie in sheep, bovine spongiform encephalopathy (BSE) or "mad cow disease" in cattle, Creutzfeldt-Jakob disease (CJD) in people, and chronic wasting disease (CWD) in deer and elk, among others. These illnesses can develop suddenly, inheritably, or as a result of contact with contaminated tissues (Prusiner, 1996; Prusiner, 1998).

Prions constitute a unique way of transmission because all that is required for them to spread is a structural change in a normal protein induced from a misfolded protein. Because prions defy accepted notions of infectious agents and have ramifications for public health and food safety, their peculiar properties continue to interest researchers. In fact, several studies have shown that a number of NDs can be experimentally transmitted through a prion-like mechanism in a variety of cellular and animal models of various diseases (Soto, 2012; Goedert, 2015; Walker and Jucker, 2015). Studies employing Aβ (Meyer-Luehmann *et al.*, 2006; Bolmont *et al.*, 2007; Eisele *et al.*, 2010; Morales *et al.*, 2012), tau (Bolmont *et al.*, 2007; Frost *et al.*, 2009; Guo and Lee, 2011), and a-syn (Desplats *et al.*, 2009; Hansen *et al.*, 2011) have demonstrated that exposure to tissue homogenates from patients with NDs or transgenic mouse models rich in protein aggregates causes the generation of disease pathophysiology in the recipient cellular or animal models. Furthermore, pathological induction has been shown to cause a disease even in not genetically predisposed animals more analogous to infectious prions (Luk *et al.*, 2012a; Guo *et al.*, 2016). Depleting the inoculum of protein aggregates can diminish pathological induction (Meyer-Luehmann *et al.*, 2006; Desplats *et al.*, 2009; Frost *et al.*, 2009; Eisele *et al.*, 2010; Guo and Lee, 2011; Hansen *et al.*,

2011; Luk *et al.*, 2012b; Morales *et al.*, 2012). However, transmission using tissue homogenates generally has a higher efficiency than transmission using isolated proteins, indicating that other cellular cofactors may be involved in the pathogenic induction (Supattapone, 2014). These results suggest that primary proteins involved in NDs share characteristics of prions as infectious agents.

1.5 AMYLOID POLYMORPHISM: CONFORMATIONAL STRAINS AND THEIR RELEVANCE IN NDs

Although most amyloid fibrils adopt the basic PIRIBS scaffold, individual amyloids can adopt a wide range of different shapes known as polymorphs or conformational strains. In contrast to the more common 3-dimensional folds of globular and membrane proteins, amyloids flatten into 2-dimensions exposing the amides in their backbone to the maximum amount of hydrogen-bonding or "stacking" with neighbouring chains that are identical (Sawaya *et al.*, 2021). The length of the fibril is determined by the stacking of thousands of identical flat protein molecules (Sawaya *et al.*, 2021).

In prion diseases, PrP^{Sc} can self-replicate in different "conformational strains" with gives the protein aggregates a structural variability that can result in different pathologies (Collinge and Clarke, 2007; Barron, 2017; Morales, 2017; Caughey *et al.*, 2022). These prion strains are comparable to different strains of common pathogens (Morales, 2017). Studies have revealed the presence of different two-dimensional folds that make different conformational strains for Aβ, tau, and α-syn (Lu *et al.*, 2013; Tycko, 2015; Li and Liu, 2022). These findings might explain the significant heterogeneity of AD and PD, as well as the different tauopathies and synucleinopathies. In fact, at least seven different diseases are linked to the buildup of tau and Aβ aggregates, including AD, frontotemporal dementia, progressive supranuclear palsy, corticobasal degeneration, argyrophilic grain disease, and chronic traumatic encephalopathy, as well as three associated with the deposition of α-syn, such as PD, multiple system atrophy, and Lewy body dementia (Williams, 2006; Goedert *et al.*, 2017). Similar to how different prion diseases are triggered by different prion strains, different tauopathies and synucleinopathies can be identified by their clinical signs, their pathology specific to certain brain regions, their preference for accumulating in particular cell types, and/or their distinctive morphological and biophysical characteristics, toxicity, and seeding ability (Williams, 2006; Goedert *et al.*, 2017; Melki, 2018).

A study identified 18 distinct tau strains which showed to have unique biochemical and biological characteristics in cell culture (Kaufman *et al.*, 2016). These strains were administered to transgenic mice, which led to the development of strain-specific intracellular tau aggregates in various cell types and parts of the brain that propagated at various rates (Kaufman *et al.*, 2016). These findings highlight the significance of these conformational strains, suggesting that different tau strains can result in a variety of neuropathological manifestations, some of which are similar to those seen in human tauopathies. Similarly, Sanders *et al.* (2014) isolated different tau strains from 29 patients who had five different tauopathies and showed that different tauopathies are linked to specific conformational strains.

It has also been demonstrated that α-syn assembles in various structures resulting in diverse histopathological and behavioural abnormalities (Stefanis, 2012; Bousset *et al.*, 2013; Goedert *et al.*, 2017). Comparably, Aβ deposits can adopt various structural strains which could help to explain the apparent heterogeneity in the brains of AD patients (Petkova *et al.*, 2005; Paravastu *et al.*, 2008b; Lu *et al.*, 2013; Wang *et al.*, 2020a). The ability of Aβ to aggregate into various conformations has been demonstrated by studies using electron microscopy, atomic force microscopy, and solid-state nuclear magnetic resonance (Goldsbury *et al.*, 2005; Petkova *et al.*, 2005; Elkins *et al.*, 2016). High-resolution structural analyses show that different experimental setups can produce synthetic Aβ aggregates significantly diverse in structure (Goldsbury *et al.*, 2005; Petkova *et al.*, 2005; Elkins *et al.*, 2016). Following numerous iterations of self-propagation *in vitro*, different Aβ strains were able to faithfully template their structure using monomeric Aβ peptides as seeds (Goldsbury *et al.*, 2005; Petkova *et al.*, 2005; Elkins *et al.*, 2016). Similar to this, seeding experiments using Aβ aggregates extracted from brains who had a variety of clinicopathological AD symptoms produced structurally unique synthetic Aβ fibrils (Stöhr *et al.*, 2012; Scherpelz *et al.*, 2016). More recently, Ghosh *et al.* (2021) investigated whether structures of Aβ fibrils from cerebral tissue of nondemented elderly subjects differ from structures from AD patients. They found statistically significant differences findings offering more evidence of the existence of biologically significant Aβ strains.

1.6 SPECIES BARRIER IN PRION AND PRION-LIKE DISEASES

The capacity of some prions to spread between species was used to prove that prion diseases can be contagious and to enable the development of effective experimental models in lab animals like mice and hamsters. For instance, misfolded prion protein from hamsters can change normal proteins from mice into new infectious forms of prion and BSE has been proven to pass to people (Castilla *et al.*, 2008; Manson and Diack, 2016). Usually, the process is most effective when spread between members of the same or closely related species. Scrapie may be spread from sheep to goats but cannot be spread to either chimps or humans (Afanasieva *et al.*, 2011). CJD, on the other hand, can be spread both between humans and from humans to chimpanzees (Afanasieva *et al.*, 2011). Although the spread of prion diseases across some species is feasible, the "species barrier" phenomenon occurs when prion diseases that are fully contagious within the same mammalian or yeast species spread poorly or not at all between species.

The specific molecular mechanisms driving these interspecies barriers remain unknown due to a paucity of high-resolution structural data on the prion protein and prion-like proteins. In the next section we will discuss the most important factors contributing to permissibility of different amyloids to cross the species barrier.

1.6.1 Crossing the species barrier: factors contributing to permissibility

The major factors contributing to the species barrier are the sequences of the two prion proteins and the protein variant (polymorph) (Edskes *et al.*, 2009). Transgenic mice expressing the deer or elk PrP sequences have been shown to be effectively infected by deer or elk prions, whereas wild-type mice are not affected (Browning *et al.*, 2004). The prion transmission barrier is not always symmetric. In some circumstances, prions cannot be passed from one species to another, yet the barrier is absent or very weak the other way around. For instance, when Syrian hamsters were infected with prion material taken from mice, pathological symptoms began to manifest, yet when Syrian hamsters were infected with infectious material from mice, no pathological symptoms appeared (Kimberlin *et al.*, 1987; Kocisko *et al.*, 1995).

The efficiency of interspecies prion transmission declines as the fundamental structures of the proteins varies (Edskes *et al.*, 2009).. However, one prion protein may misfold into a variety of infectious conformations, and these variations in "strain conformation" can change the specificity of infection. The structural fold between different proteins can be very similar despite

limited amino acid sequence homology. For example, various *Saccharomyces* species produce the nitrogen regulatory proteins Ure2, which can form prions named [URE3]. Species barriers for [URE3]s rely on the prion strain. One [URE3] prion strain of species A may transmit with 100% effectiveness to species B, but another strain may transmit with 0% efficiency between the same two species (Edskes *et al.*, 2009).

The explanation for these events is that each sequence includes a variety of potential strains (polymorphs). While a wide overlap of polymorphs suggests a low barrier, a limited overlap of polymorphs between the donor and recipient results in a high species barrier. This model predicts that a particular strain shared by the donor and receiver could thus overcome a high species barrier (Collinge and Clarke, 2007).

1.7 AMYLOID SEEDING AND CROSS-SEEDING

With the evidence of prions crossing the species barrier, the possibility that amyloid proteins involved in different prion-like diseases doing the same thing has been studied (Ren *et al.*, 2019; Subedi *et al.*, 2022). Amyloid proteins have the ability of seeding protein aggregation, which gives them the innate capacity to disseminate the misfolding and aggregation process (amyloid self-assembly) (homologous seeding in **Figure 1.8**) in a way analogous to infectious prions (Soto *et al.*, 2006; Soto, 2012; Iadanza *et al.*, 2018). Although, misfolded aggregates may also elongate by integrating different amyloid proteins if they have a strong structural complementarity (Ren *et al.*, 2019; Subedi *et al.*, 2022). This process is called heterologous seeding or cross-seeding (**Figure 1.8**) (O'Nuallain *et al.*, 2004; Dubey *et al.*, 2014; Anand *et al.*, 2017; Anand *et al.*, 2018; Tavassoly *et al.*, 2018). Cross-seeding has been identified as a crucial biological process and occurs when different amyloid proteins operate as nucleators for others (Harper and Lansbury, 1997; Dubey *et al.*, 2014; Anand *et al.*, 2017; Anand *et al.*, 2018; Tavassoly *et al.*, 2018; Ren *et al.*, 2019).

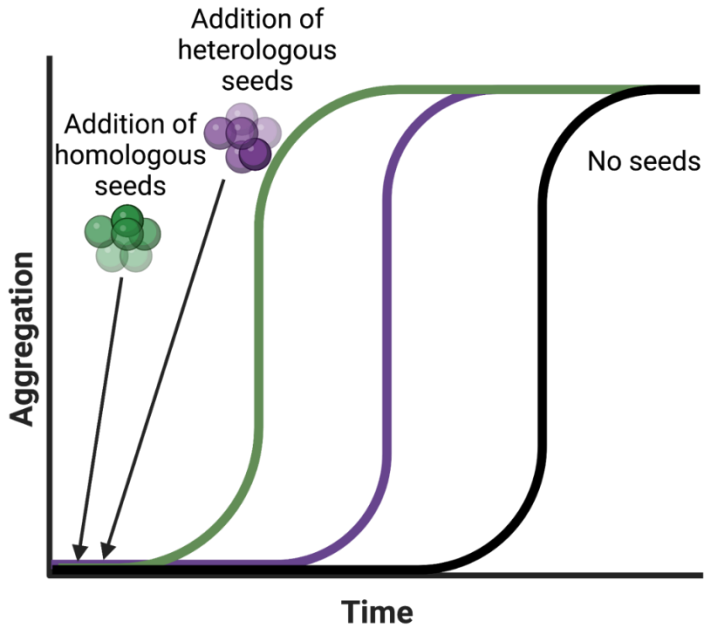

Figure 1.8. Amyloid seeding and cross-seeding. Amyloid fibrils are formed by the nucleation dependant polymerization model (black curve). Addition of preformed seeds leads to a shorter lag phase and a faster aggregation. Seeds can be identical (homologous) leading to "amyloid seeding" which is more efficient than when seeds come from a different (heterologous) protein causing, *i.e.*, "cross-seeding". Created with BioRender.com.

Cross-seeding may offer an explanation for a number of observations in various diseases, such as, the simultaneous presence of different misfolded proteins in one disease; the coexistence of multiple protein misfolding diseases in one person; the epidemiological finding that one protein misfolding disease may be a risk factor for the development of a second one; and the exacerbation of clinical features when multiple misfolded protein aggregates accumulate (Morales *et al.*, 2010; Ren *et al.*, 2019; Subedi *et al.*, 2022). For instance, several *in vitro* studies have investigated the interactions between Aβ and other human amyloid proteins linked to human illness. It has been shown that α-synuclein (Ono *et al.*, 2012; Chia *et al.*, 2017) (associated with PD), protein A (AA) (Rising *et al.*, 2021) (associated with amyloidosis), and human islet amyloid polypeptide (Hu *et al.*, 2015) (associated with type 2 diabetes) can accelerate Aβ aggregation.

Recently, the cross-seeding hypothesis has gone beyond disease-associated proteins to using functional amyloids (Chiti and Dobson, 2006; Fowler *et al.*, 2007; Javed *et al.*, 2020; Koloteva-Levine *et al.*, 2021) or non-amyloid protein fibers (Ono *et al.*, 2014). The potential for protein misfolding and aggregation leading to NDs to be initiated through cross-seeding with functional

amyloids is an emerging area of investigation. For instance, Javed *et al.* (2020) showed that FapC produced by *Pseudomonas aeruginosa*, can seed Aβ and increase its toxicity in *in vitro* and *in vivo* settings. Most of these cross-seeding studies have revealed that the inclusion of different amyloid proteins accelerates Aβ aggregation *in vitro* (Chiti and Dobson, 2006; Fowler *et al.*, 2007; Ono *et al.*, 2014; Javed *et al.*, 2020; Koloteva-Levine *et al.*, 2021). As a result, there is thought to be a possible link between other amyloid exposure and the start of AD disease.

Relevant for my work, several studies have proven the cross-seeding ability of the bacterial amyloid curli. Lundmark *et al.* (2005) revealed that curli from *E. coli* exerts amyloid-accelerating properties for protein A in murine amyloidosis. Curli was also found to promote the aggregation of PD related protein, α-syn in Aged Fischer 344 Rats and the nematode, *C. elegans* (Chen *et al.*, 2016). Curli serves as a catalytic agent for Semen Enhancers of Viral Infection (SEVI) synthesis from prostatic acid phosphatase (PAP248-286) (Hartman *et al.*, 2013). PAP248-286 facilitates HIV infection if it is in the form of amyloid aggregates known as SEVIs. Although monomeric PAP248-286 aggregates relatively slowly in isolation. Resulting SEVI fibrils that were nucleated with curli retain the capacity to promote HIV infection (Hartman *et al.*, 2013). The ability of curli to interact with proteins with different sequences suggest that its seeding specificity is relaxed, and it may seed and facilitate the aggregation of other amyloidogenic proteins.

1.7.1 Implications of cross-seeding in NDs: AD as a particular example

Currently there are no effective therapies or cures for NDs. Specifically, efforts to create medications or nonpharmacological methods to prevent, halt, or slow down AD have failed. AD is one of the disorders with the lowest percentage of medication development success. Ninety nine percent of therapeutic drug candidates are abandoned after providing no clinical effect (Sevigny *et al.*, 2016; Cummings *et al.*, 2019; Vaz and Silvestre, 2020).

Since AD is characterized by the development Aβ aggregates, traditionally they have been a focus of therapeutic action (Hardy and Higgins, 1992). However, it has been challenging to pinpoint the precise causes of protein aggregation, which is a dynamic process that involves the development of intermediate structures as well as the dissociation of mature fibrils (Arosio *et al.*, 2015; Lee and Terentjev, 2017; Almeida and Brito, 2020). The field has also evolved showing that that soluble aggregation intermediates, often known as oligomers, constitute the most toxic agents in AD and recent research on strain diversity, prion-like behaviour, and molecular interactions

between various amyloidogenic proteins has revealed both novel treatment targets and possibly unforeseen challenges (Bitan *et al.*, 2003; Kayed *et al.*, 2003a; Haass and Selkoe, 2007; Sengupta *et al.*, 2016; Sardar Sinha *et al.*, 2018).

My MSc. research is focused on the potential cross-seeding between Aβ and the bacterial amyloid curli. As many proteins develop amyloid-like misfolded aggregates as a normal biological function (Fowler *et al.*, 2006; Fowler *et al.*, 2007; Dueholm *et al.*, 2010; Evans *et al.*, 2018; Jain and Chapman, 2019; Ren *et al.*, 2019), cross-seeding with bacterial functional amyloids may play a significant but as-yet-unknown role in the development of protein misfolding diseases, like AD. It is fundamental to understand the effects that one type of protein would have on the aggregation propensity and characteristics of other proteins present in its environment.

Particularly, curli fibrils and Aβ fibrils share similar 3D structures, which involves their β-sheets engaging in hydrogen bonds that form a steric zipper along the fibril axis (Perov *et al.*, 2019; Sewell *et al.*, 2020). The fibrils of these two proteins share the PIRIBS scaffold (Paravastu *et al.*, 2008a; Sleutel *et al.*, 2023). This suggests that common structural features between curli and Aβ peptides are shared at the molecular level.

Our team has previously shown that curli is synthesized inside the body during murine *Salmonella* infection (Miller *et al.*, 2020). In this animal model, and in human infections, *S.* Typhimurium can cross the intestinal epithelium. Curli genes are shared between *Salmonella* and *E. coli* and are functionally interchangeable (Römling *et al.*, 1998). *E. coli* is a known commensal of the human gut. Curli fibrils are also highly immunogenic (Tükel *et al.*, 2010; Gallo *et al.*, 2015). Curli is recognized by eukaryotic toll like receptors 1 and 2 (TLR1-TLR2), and CD14 (Tursi and Tükel, 2018; Miller *et al.*, 2021). Activation of the innate immune system leads to an increase in PI3K expression and enhances inflammation (Tursi and Tükel, 2018; Miller *et al.*, 2021). Inflammation of the gastrointestinal (GI) tract leads to an increase in intestinal permeability, and consequently facilitate leakage of molecules, like curli, which likely promotes a systemic exposure to curli (Miller *et al.*, 2021).

In AD, the aggregation and accumulation of Aβ plaques between neurons are one of the hallmarks of the disease. The GI tract also exhibits Aβ accumulation in humans and mice and a growing body of evidence suggests that peripheral Aβ (*e.g.* gut derived Aβ) could contribute to the formation of Aβ plaques in the brain (Cintron *et al.*, 2015; Sun *et al.*, 2020; Kauwe and Tracy,

2021; Lam *et al.*, 2021; Qian *et al.*, 2022; Jin *et al.*, 2023).These observations have brought forward the possibility that curli and amyloidogenic proteins of the host, like peripheral Aβ could interact which may have implications for understanding the underlying mechanisms involved in the development and progression of AD and shed light to new therapeutic strategies.

CHAPTER 2. RATIONALE, HYPOTHESIS AND OBJECTIVES

2.1 RATIONALE AND HYPOTHESIS

Amyloid cross-seeding may contribute to the pathology of several proteinopathies. AD is characterized by the development Aβ aggregates. However, it has been challenging to pinpoint the precise causes of Aβ aggregation. For my MSc. research, we wonder if a bacterial amyloid like curli was able to promote Aβ misfolding. Curli fibrils and Aβ fibrils share similar 3D structures. Curli is synthesized in the gut during murine *Salmonella* infection and the GI tract also exhibits Aβ accumulation. These observations have brought forward the possibility that curli and amyloidogenic proteins of the host, like peripheral Aβ could interact.

I hypothesised that curli produced by *Salmonella* can physically interact with and influence the polymerization and toxicity of Aβ peptides associated with Alzheimer's disease.

2.2 OBJECTIVES

My MSc. research was organized into **three Objectives:**

1. To optimize *in vitro* Aβ aggregation assays.
2. To examine if curli and Aβ peptides interact *in vitro*.
3. To determine whether curli influences the toxicity of Aβ peptides in mammalian cell lines.

CHAPTER 3. OPTIMIZING THE METHODOLOGY TO STUDY AGGREGATION OF Aβ PEPTIDES *in vitro*

3.1 ABSTRACT

There are several disorders that are connected to the self-assembly of peptides and proteins into amyloid fibrils. Aβ peptides are associated with Alzheimer's disease and are one of the most researched examples. However, regulating Aβ aggregation and producing repeatable findings is particularly challenging. Here, we studied three different factors that are known to influence Aβ aggregation, 1) Aβ pre-treatment for preparation of monomeric Aβ, 2) the pH and composition of the aggregation buffer and, 3) temperature. We combined western blot analysis of SDS-PAGE and the gold standard technique for amyloid aggregation, the Thioflavin T assay to optimize aggregation conditions of Aβ peptides according to our research interests and offer advice for similar research.

3.2 INTRODUCTION

Due to its connection with AD, Aβ is likely the amyloidogenic peptide that has been studied the most. The amyloid cascade hypothesis was proposed as the underlying process behind the AD model saying that the aggregation process of Aβ into fibrils was the main etiological agent of the disease (Hardy and Higgins, 1992). At the same time, it was discovered that Aβ was formed during normal cellular metabolism demonstrating that Aβ is not just produced by AD patients (Haass *et al.,* 1992).

Amyloid aggregation is a heterogeneous process with several concurrently feasible routes and structures (Arosio *et al.,* 2015). Therefore, even minutely changing circumstances can result in significant modifications to the kinetics, contents, and morphologies of the produced aggregates (Hellstrand *et al.,* 2010). Hence, it is not unexpected to see structural heterogeneity in high-resolution Aβ(1-40) and Aβ(1-42) fibrils when aggregation conditions are distinct (Lührs *et al.*, 2005; Morinaga *et al.*, 2010; Lindberg *et al.*, 2015; Tycko, 2015; Xiao *et al.*, 2015; Wang *et al.*, 2020a).

When studying Aβ aggregation, the preparation of the peptide sample is critical. Starting with a fully monomeric Aβ solution is the ideal strategy to optimise reproducibility since existence of pre-aggregates, regardless of its kind, can have significant effects (Foley and Raskatov, 2020).

Thus, it is necessary to accomplish monomerization of the peptide and subsequently store these monomers under nonaggregating circumstances before starting any experiments. Conditions to achieve this include treatment and storage with organic solvent at high pH, or the use of chaotropic substances (Fezoui *et al.*, 2000).

Numerous methods to making homogeneous preparations of monomeric Aβ are described in the literature, however, their efficacy varies and frequently depends on the source of the peptide (recombinant expressed and in-house purified, chemically synthetized, etc.) (Fezoui *et al.*, 2000; Broersen *et al.*, 2011; Stine *et al.*, 2011; Ryan *et al.*, 2013). Here, we study the preparation of monomeric Aβ peptides using 1,1,1,3,3,3-hexafluoroisopropanol (HFIP) and a combination of HFIP and dimethyl sulfoxide (DMSO). We compare both pre-treatments on their efficacy to make a homogeneous monomeric Aβ. Samples were characterized by Western blot analysis of SDS-PAGE, a technique commonly used to identify SDS-stable Aβ assemblies (Lambert *et al.*, 1998; Walsh *et al.*, 2000; Dahlgren *et al.*, 2002; Pryor *et al.*, 2012) and by Thioflavin T (ThT) assay (Khurana *et al.*, 2005; Biancalana and Koide, 2010; Freire *et al.*, 2014; Xue *et al.*, 2017). In addition, we used the ThT assay to monitor Aβ(1-42) fibril formation and examine the impact of other two aspects that are known to affect aggregation kinetics, buffer/pH and temperature. This with the objective of optimizing ThT assay conditions to obtain meaningful, reliable, and reproducible kinetic data.

3.3 MATERIALS AND METHODS

3.3.1 Peptides and Antibodies

Synthetic Aβ(1–42) (cat#: 4014447) was obtained from Bachem Americas, Inc. Lyophilized peptide was stored in their original packaging at -20 °C until use.

The anti-β-amyloid antibody [clone 6E10: targets residues 1–16 of the Aβ peptide: cat# 803016] was obtained from BioLegend. The NIR-labeled secondary antibody used to probe the primary anti-β-amyloid antibody was Amersham™ CyDye™ 800 Goat-Anti-Mouse from Cytiva.

3.3.2 HFIP pre-treatment

Prior to resuspension, the Aβ(1–42) vial was centrifuged to force the lyophilized peptide to the bottom of the tube and prevent loss of any material when opening it. The peptide (1 mg) was resuspended in ice-cold 1,1,1,3,3,3-hexafluoro-2-propanol (HFIP-Sigma-Aldrich) and vortexed at

low speed. HFIP is volatile and evaporates quickly. Using ice-cold HFIP reduces the evaporation rate which facilitates aliquoting. The resulting solution (2 mg/mL) was aliquoted and stored at -80 °C until use. HFIP was allowed to evaporate in the fume hood by opening the tube's lid for at least 1 h or until no liquid is observed. The resulting clear peptide film was resuspended in aggregation buffer (1X PBS pH 7.4) to the desired concentration.

3.3.3 HFIP/DMSO pre-treatment

HFIP-treated aliquots were lyophilized for 24 h. The lyophilized aliquots were stored at -80 °C until use. The dry film was initially resuspended in DMSO (5 mM final concentration) prior to addition of aggregation buffer to the desired concentration.

3.3.4 Western Blot analysis of SDS-PAGE

HFIP- and HFIP/DMSO- treated Aβ(1-42) were resuspended to 0.2 mg/mL (40 μM) in aggregation buffer (1X PBS pH 7.4). Immediately after resuspension, samples (10 μL) were resolved by SDS-PAGE using 4 to 12% Tris-Glycine Novex™ gels and SDS running buffer.

After gel electrophoresis, proteins in the gels were transferred to nitrocellulose membranes using the iBlot2 system (Thermo Fisher). Membranes were incubated for 1 h while shaking at room temperature in TBS containing 5% (w/v) non-fat dry milk (blocking buffer). Blots were probed with the 6E10 antibody (1:4000 dilution) overnight (4°C), while shaking. Membranes were washed with TBS three times for 5 min, 15 min, and 5 min with shaking. Membranes were probed with the Amersham™ CyDye™ 800 Goat-Anti-Mouse NIR-labeled secondary antibody (Cytiva) in TBS (5% skim milk) (1:10,000) for 90 min at room temperature, shaking and protected from light. Membranes were washed prior imaging in a LI-COR Odyssey CLx.

3.3.5 ThT aggregation assay

HFIP- and HFIP/DMSO-treated Aβ(1-42) were resuspended to 0.05 mg/mL (10 μM) in aggregation buffer (1X PBS pH 7.4). Immediately after resuspension, samples were characterized by ThT assay. A 50 μM ThT working solution (in aggregation buffer) was made from a 10 mM Thioflavin T (ThT, Sigma) stock solution (in distilled water) previously filtered through a 0.2 μm filter. The samples were loaded in triplicate into three wells in a Costar® 96-well, clear-flat bottomed, black polystyrene plate (Corning). Each reaction consisted of 40 μL peptide (final concentration of 0.02 mg/mL, i.e., 4 μM), 40 μL aggregation buffer and 20 μL ThT (10 μM). The plate was subsequently sealed with a clear optical adhesive film and ThT fluorescence was

measured every 10 min using a FLUOstar Omega plate reader (BMG Labtech) at 25 °C. An excitation filter of 440 nm and an emission of 480 nm were used(Naiki *et al.*, 1989). The average fluorescence measured control wells containing only 10 μM ThT solution was subtracted from all test measurements.

3.3.6 Effects of buffer on aggregation kinetics

Published work was reviewed that included ThT fluorescence measurements of Aβ aggregation and for which aggregation conditions (especially the aggregation buffer) were given. 20 mM sodium phosphate buffer pH 7.0 (Klug *et al.*, 2003; Król *et al.*, 2021), 50 mM potassium phosphate buffer pH 7.3 (Perov *et al.*, 2019), 10 mM MES buffer pH 5.5 (Burdick *et al.*, 1992), 1X PBS buffer pH 7.4 (Thakur *et al.*, 2011; Vadukul *et al.*, 2020; Quartey *et al.*, 2021) and 20 mM Tris Buffer pH 8.0 (Vestergaard *et al.*, 2008; Coalier *et al.*, 2013; Prakash *et al.*, 2019) were selected to assess the effects of buffer and pH on Aβ aggregation kinetics.

HFIP-treated Aβ(1-42) was resuspended in the five different aggregation buffers and samples were characterized by ThT assay as previously described. Briefly, aggregation reactions were composed of 0.02 mg/mL (4 μM) HFIP-treated Aβ(1-42) and 10 μM Thioflavin T (ThT) resuspended in the different aggregation buffers. Reactions (100 μL) were prepared in 96-well optical clear-bottomed plates. The plate was sealed and incubated in a FLUOstar Omega plate reader (BMG Labtech) at 25 °C for 24-40 h. ThT fluorescence was measured every 10 min (450 nm excitation, 480 nm emission).

3.3.7 Effects of temperature on aggregation kinetics

HFIP-treated Aβ(1-42) was resuspended to 0.05 mg/mL (10 μM) in aggregation buffer (20 mM Tris Buffer pH 8.0). Immediately after resuspension, samples were characterized by ThT assay as described above. The aggregation kinetics were assessed at 25 ºC and 37 ºC.

3.4 RESULTS

3.4.1 Aβ peptide pre-treatment

Western blot analysis of SDS-PAGE revealed that HFIP pre-treatment yielded Aβ(1–42) dimers, trimers, and tetramers (**Figure 3.1 A**, lane 1). Although HFIP/DMSO-treated samples showed the same dimer, trimer, and tetramer bands, smearing above 35 kDa was also observed (**Figure 3.1 A**, lane 2). Thus, large oligomeric species were present immediately after resuspension

of HFIP/DMSO-treated samples. The initial ThT fluorescence value (t= 0 h) in reference fluorescence units (RFU) for HFIP/DMSO-treated samples was higher (~10,000 RFU) than in HFIP-treated samples (~2,000 RFU) (**Figure 3.1 B**). The ThT data was consistent with the Western blot analysis suggesting that immediately after resuspension those oligomeric species observed in the western blot for the HFIP/DMSO-treatment are the species that are causing the increase in the initial ThT fluorescence value.

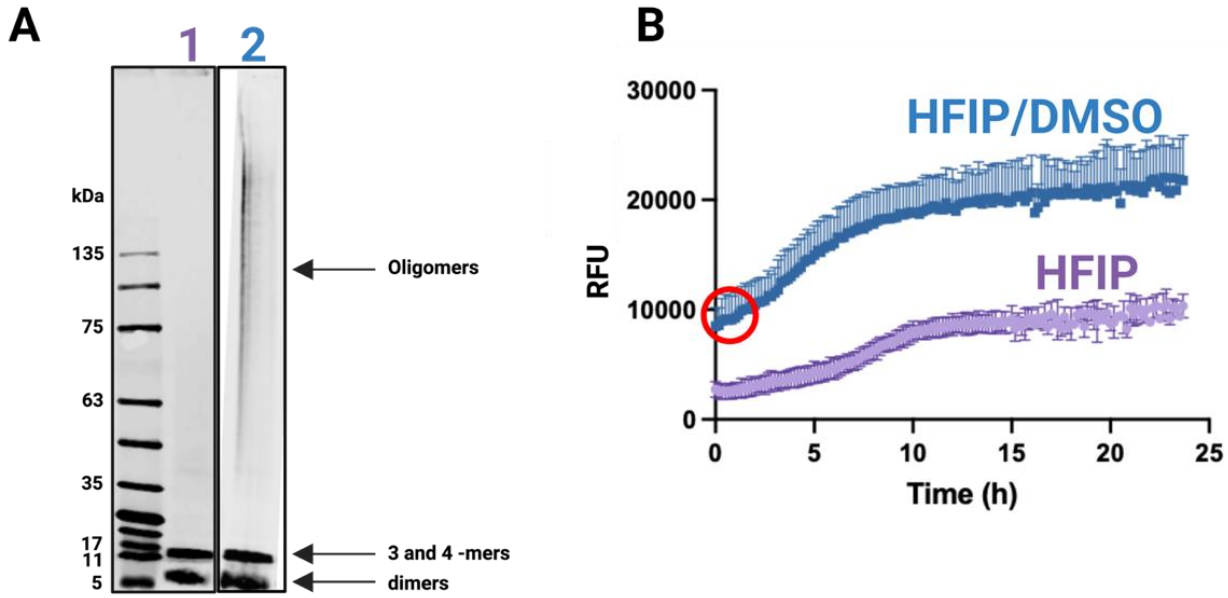

Figure 3.1. Analysis of Aβ pre-treatments for the formation of monomeric Aβ(1-42). A) Representative Western blots of HFIP- (lane 1) and HFIP/DMSO-treated (lane 2) Aβ(1-42) incubated for 0 h, separated by SDS-PAGE and probed with the anti Aβ antibody, 6E10. B) Aggregation kinetics of HFIP (purple curve)- and HFIP/DMSO-treated (blue curve) Aβ(1-42) measured by ThT fluorescence. HFIP/DMSO-treated Aβ(1-42) starts with a higher fluorescence compared to HFIP-treated Aβ(1-42).

3.4.2 Effects of buffer and pH on aggregation kinetics of Aβ

Changes in the aggregation kinetics of Aβ(1-42) due to different buffers were assessed using the ThT assay (**Figure 3.2**). The curves were normalized to the Max ThT fluorescence (RFU). All buffers produced sigmoidal curves with clear lag, elongation, and plateau stages except for 10 mM MES buffer pH 5.5. The resulting curve using MES buffer started with a high RFU value that gradually dropped within the first five hours (red curve in **Figure 3.2**). 20 mM sodium phosphate buffer pH 7.0 and 50 mM potassium phosphate buffer pH 7.3 showed similar aggregation curves

(blue and yellow curves in **Figure 3.2**), with a brief lag phase (less than one hour) and fast elongation phases with an almost vertical slope. The use of 1X PBS buffer pH 7.4 increased the lag phase to approximately three hours, along with a longer elongation phase and later plateau stage (at ~15 hours) (purple curve in **Figure 3.2**). The clearest sigmoidal curve was observed in 20 mM Tris Buffer pH 8.0 (black curve in **Figure 3.2**). This curve showed the expected sigmoidal shape with a long lag phase of approximately 12 hours and the beginning of the plateau phase was observed after 25 hours from the beginning of the experiment.

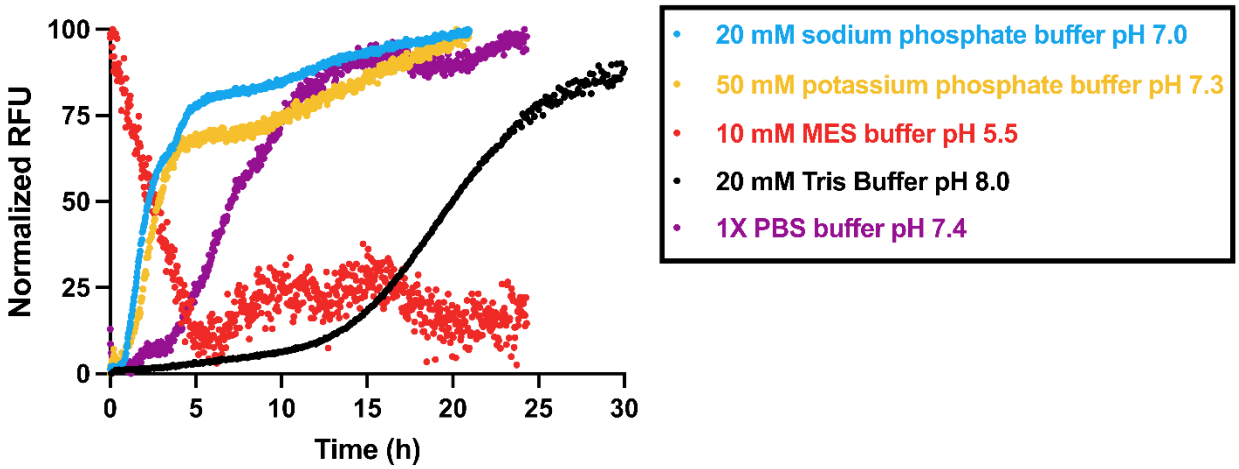

Figure 3.2. Effect of buffer on the aggregation kinetics of Aβ(1-42). Changes in the aggregation kinetics of Aβ(1-42) due to different buffers and pHs using the ThT fluorescence assay at 25 °C.

We also wanted to study how different buffers affected the aggregation of the shorter peptide, Aβ(1-40), thus an analogous approach was followed. We decided to exclude MES buffer because of the odd curve shape for Aβ(1-42), as well as Tris buffer because of the delayed aggregation time; Aβ(1-40) aggregates slower than Aβ(1-42) (Snyder *et al.*, 1994; Batzli and Love, 2015). Snyder *et al.* (1994) reported that at pHs above 7.4, aggregation of Aβ(1-40) could take days. Waiting a long period of time to collect Aβ(1-40) data would not be feasible. The curves in **Figure 3.3** for Aβ(1-40) aggregation support our previous observations with Aβ(1-42) where incubation of the peptide in buffers with higher pHs affects nucleation and results in longer lag phases.

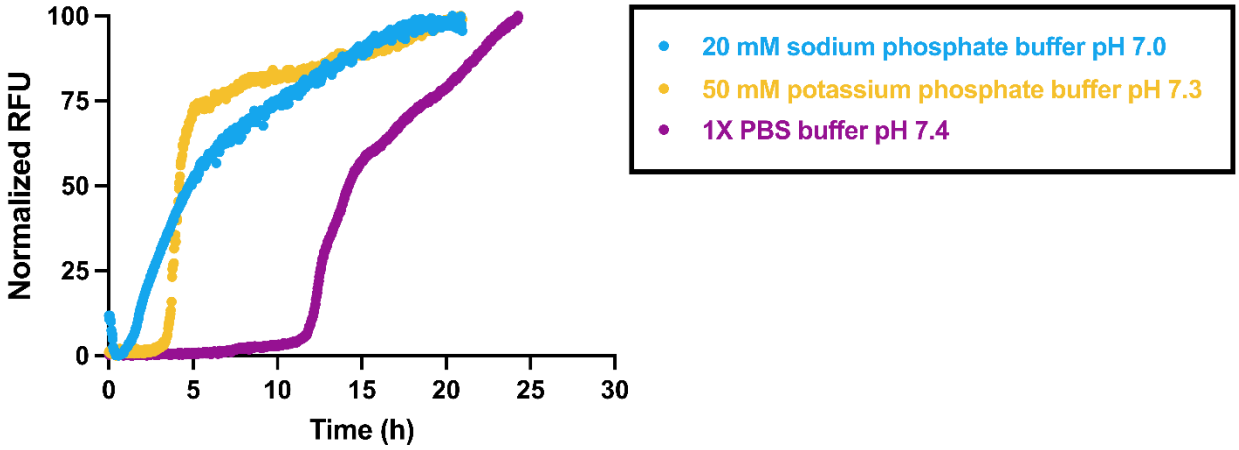

Figure 3.3. Effect of buffer on the aggregation kinetics of Aβ(1-40). Changes in the aggregation kinetics of Aβ(1-40) due to different buffers and pHs using the ThT fluorescence assay at 25 °C.

Based on the results above, we decided to use 20 mM Tris Buffer pH 8.0 for Aβ(1-42) experiments, and 1X PBS buffer pH 7.4 for Aβ(1-40). For studying Aβ and curli interactions, we thought it would be beneficial to have a long and well-defined lag phase to easily observe changes in the aggregation curves.

3.4.3 Effects of temperature on aggregation kinetics of Aβ

We explored the aggregation kinetics of the Aβ(1-42) peptide at two different temperatures, 25 and 37 °C, using the ThT assay. The curves were normalized to the Max ThT fluorescence (RFU). We observed a temperature-dependence in the aggregation kinetics of Aβ(1-42) (**Figure 3.4**), with an increase in the overall rate of fibril production and recognizable alterations in the reaction's time course at 37 °C. At 37 °C, the sigmoidal-like kinetic traces were lost, there was an almost complete absence of a lag phase, and a drastic increase in the sharpness of the transition to the plateau phase. The loss of a lag phase by increasing the temperature from 25 to 37 °C led us to select 25 ºC as the working temperature for further Aβ(1-42) aggregation experiments.

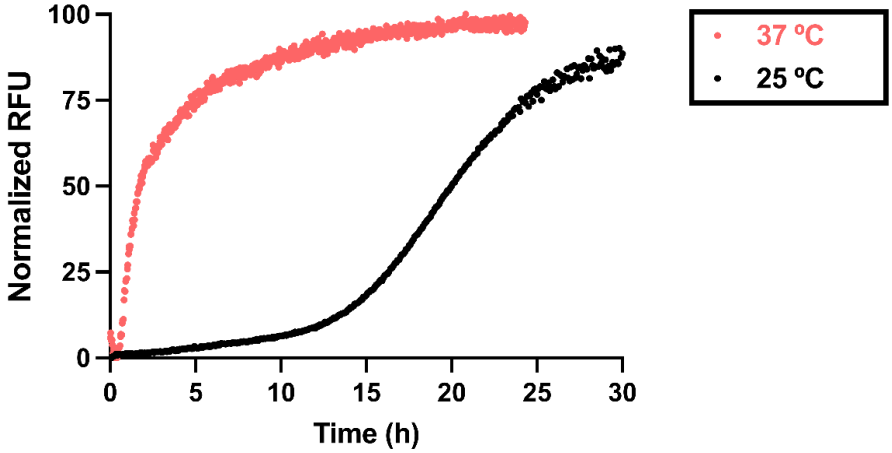

Figure 3.4. Effect of temperature on the aggregation kinetics of Aβ(1-42). ThT fluorescence assay was used to monitor Aβ(1-42) fibril formation at 37 and 25 ºC.

We proceeded to assess Aβ(1-40) aggregation at 37 ºC. Although the lag phase was not affected by either of the two temperatures, we found that at 37 ºC the resulting aggregation curves have a more consistent sigmoidal shape compared to the curves at 25 ºC (**Figure 3.5**). Therefore, 37 ºC was selected for further Aβ(1-40) experiments.

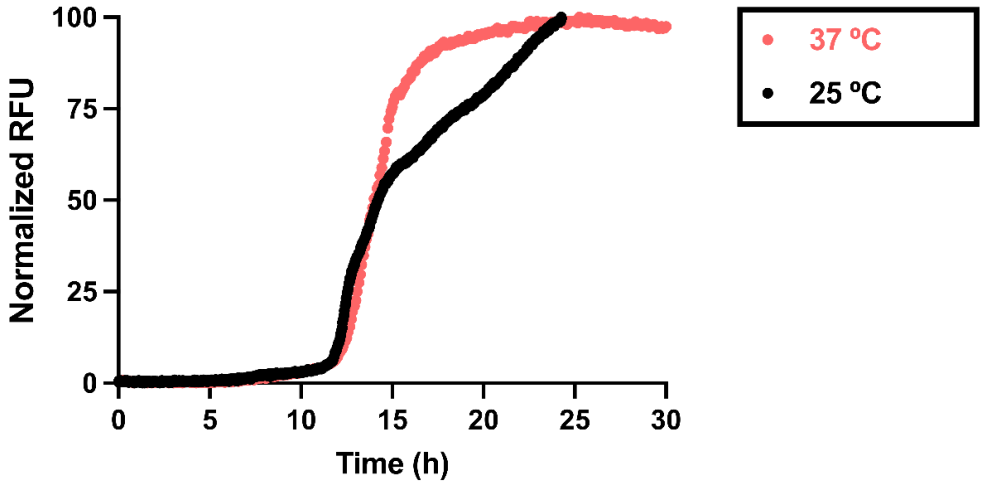

Figure 3.5. Effect of temperature on the aggregation kinetics of Aβ(1-40). ThT fluorescence assay was used to monitor Aβ(1-40) fibril formation at 37 and 25 ºC.

3.5 DISCUSSION

In our study, pre-treatment of Aβ(1-42) with HFIP resulted in more homogenous peptide solutions compared to HFIP/DMSO-treated samples. This observation provides the essential

framework for controlled aggregation experiments. Multiple researchers and commercial suppliers suggest the use of DMSO to solubilize hydrophobic peptides like Aβ since it is a highly polar, water-soluble organic solvent (Shen and Murphy, 1995; Stine *et al.*, 2003). However, detection of Aβ(1-42) smearing in western blot analysis demonstrate that HFIP/DMSO pre-treatment fails to keep the Aβ(1-42) peptides as monomers. The high ThT fluorescence for HFIP/DMSO-treated samples confirms the presence of ThT-positive molecules. When ThT binds to amyloid fibrils, it emits a strong fluorescence signal (Naiki *et al.*, 1989). It has been proposed that ThT binds to four consecutive β-strands (Biancalana *et al.*, 2009; Wu *et al.*, 2009). This supports the existence of secondary structures in HFIP/DMSO-treated Aβ(1-42).

Fluorinated alcohols, such as HFIP and trifluoroethanol, disrupt hydrophobic forces in aggregated amyloid preparations (Barrow and Zagorski, 1991; Barrow *et al.*, 1992). Numerous studies have reported that the CD spectra for HFIP-treated Aβ(1-40) and Aβ(1-42) show that the secondary structure is mostly α-helical (50-70%) and random coil (30- 50%), with very little β-sheet (1%) (Barrow and Zagorski, 1991; Barrow *et al.*, 1992; Fezoui and Teplow, 2002; Stine *et al.*, 2003). According to these CD investigations, our HFIP pre-treatment should eliminate any pre-existing β-sheet secondary structure, resulting primarily in α-helix and random coil. Regardless of the limitations of the two techniques that were used in this study, observations on HFIP pre-treatment make clear that treating the peptide with HFIP yields a more homogeneous mixture of unaggregated Aβ species than the HFIP/DMSO pre-treatment.

Changes in buffer composition and pH led to the production of different aggregation curves for both Aβ peptides. Differences in Aβ aggregation curves under different aggregation buffers are common and Aβ is not the only amyloid with pH-dependent behavior. The amyloid protein, α-synuclein has also been reported to be affected by changes in pH (Sarell *et al.*, 2009; Haldar and Chattopadhyay, 2011). Thus, buffer and pH selection are one of the most important steps in designing a ThT amyloid aggregation assay. Particularly, pH changes can either accelerate or decrease Aβ kinetics by affecting its solubility (Bhowmik *et al.*, 2014). In AD, inflammation often causes acidic microenvironments (Kinney *et al.*, 2018). Aβ fibril formation is pH-sensitive thus those changes from physiological pH to a pH that is closer to Aβ isoelectric point (pI) of 5.3, will reduce the solubility of Aβ and will increase and promote aggregation and the amyloid formation rate (Hortschansky *et al.*, 2005). MES buffer (pH 5.5) had the closet pH to the Aβ pI. Therefore,

Aβ aggregation might have been extremely favoured in this buffer. This could explain the shape of the curve that had a high RFU value at the start (detection of Aβ fibrils) and a gradual loss of fluorescence (insoluble Aβ fibrils accumulating at the bottom).

Our results showed that buffers with lower pHs affect nucleation and result in shorter lag phases. Similar conclusions have been reached by Schützmann *et al*.(2021) who tested a range of pHs, from 4.8 to 7.6 and showed that Aβ assembly is accelerated 8,000-fold when using more acidic pH *in vitro*. In the study, increasing pH always resulted in an increase in the lag phase and a reduction of the aggregation rate(2021). Along the same lines, Tian and Viles (2022) showed that primary nucleation is highly pH dependent whereas secondary nucleation and elongation rates are independent of pH. Snyder *et al.* (1994) showed that aggregation is very rapid (seconds) near the pI of the peptide (pH 5-6), outside of this range (e.g. pH 7.0–7.4), aggregation of Aβ(1-42) remains rapid (minutes), whereas aggregation of its shorter counterpart, Aβ(1-40) is slow, from hours to days. Although kinetic parameters were not calculated in this part of my research, our data agrees with these observations, with higher pH affecting primary nucleation and resulting in longer lag phases.

Ionic strength is another factor that alters Aβ aggregation by modifying electrostatic interactions between protein molecules (Zidar and Merzel, 2011; Ziaunys *et al.*, 2021; Wang *et al.*, 2022). These electrostatic interactions can be shielded by high ionic strength, which is brought on by elevated ion concentrations, especially salts. This reduces repulsive forces and encourages protein aggregation. In contrast, environments with low ionic strength cause the shielding effect to be less effective, resulting in greater electrostatic interactions between charged protein molecules and a reduction in aggregation (Zidar and Merzel, 2011; Ziaunys *et al.*, 2021; Wang *et al.*, 2022). Ionic strength of sodium and potassium, or chloride ions increase in frontal and parietal cortex regions up to 25% and 20% in AD compared to healthy individuals (Vitvitsky *et al.*, 2012). This ion imbalance might contribute to the pathophysiology of AD. Abelein *et al.* (2016). investigated how ions modulate Aβ aggregation and toxicity. They proposed that salt lowers the free-energy barrier for Aβ folding to the fibril state, favouring the development of the mature fibrils (Abelein *et al.*, 2016). Here, we used buffers with similar pH although we observed drastic differences between them (*i.e.*, 1X PBS pH 7.4, 20 mM sodium phosphate buffer 7.0 and 50mM potassium phosphate buffer pH 7.3). Considering the buffer composition differences in the

aggregation curves are likely associated to the different ionic strength of the solutions. However, it remains to be explored how the buffer constituents influence Aβ morphology.

Aβ aggregation was found to be dependent upon temperature. Our findings are consistent with what others have shown (Kusumoto *et al.*, 1998; Ghavami *et al.*, 2013; Batzli and Love, 2015). Kusumoto *et al.* (1998) studied the temperature dependence of the Aβ fibril elongation rate constant using Quasielastic light scattering (QLS) which allows for simultaneous monitoring of size and molecular weight of particles in solution. They showed the temporal evolution of the hydrodynamic radius of Aβ fibrils incubated between 24 ºC and 4 °C. When Aβ was incubated at 24 °C the elongation rate was 18.6 nm/h (Kusumoto *et al.*, 1998). Decreasing the temperature to 20 °C resulted in a decrease in the elongation rate by a factor of 20 (1.0 nm/h) (Kusumoto *et al.*, 1998). Ghavami *et al.* (2013) used molecular dynamic (MD) simulation methods and revealed that the core hydrophobic amyloid backbone of Aβ monomers is more available for interactions by increasing the temperature from 37 to 42 °C. They proceeded to complement their work with experimental methods, including the ThT aggregation assay (Ghavami *et al.*, 2013). The idea that the core part of the fibrillation process is more exposed at higher temperatures was further supported by the finding that the lag time for Aβ was decreased gradually by increasing the temperature from 37 to 42 °C (Ghavami *et al.*, 2013). Therefore, rising temperature leads to more rapid amyloid formation.

3.6 CONCLUSIONS

Taken together, our results define specific conditions for formation of unaggregated Aβ suitable for kinetic experiments *in vitro*. We conclude that modifiable factors like, aggregation buffer (pH and ionic strength) and temperature play important roles during Aβ aggregation, which is stimulated by lower pHs, ionic strength and higher temperature. On this basis, comprehension of how soluble Aβ folds to form cross-β-sheet rich aggregates and particularly how different factors, such as temperature, ionic strength, etc. can affect this process is crucial for deciphering the molecular basis of fibrillogenesis.

Our results provide unique conditions that control the intricate process of Aβ assembly. Although we selected different conditions for each peptides —1X PBS pH 7.4 at 37 ºC for Aβ(1-40) and, 20 mM Tris buffer pH 8.0 at 25 ºC for Aβ(1-42)—we based our decision on using the

conditions that would ensure getting the most controlled, consisted and reproducible data even if that meant to use 25 ºC and pH 8 for Aβ(1-42) to delay the aggregation and create an appropriate time frame for our aggregation kinetics tests. We highlight the importance of characterizing the amyloid protein that is being used and strategically optimize and define the best conditions to use in the assays according to the research questions. This implies that detailed information on the methods that were selected and the reasons why those were selected should be mentioned. As we also experienced challenge in controlling aggregation and obtaining reproducible findings, we offer some advice for dealing with the reproducibility problem in Aβ aggregation studies:

- The monomerization process comes first and is likely the most crucial step. Any pre-aggregates that will alter the aggregation rate must be monomerized using a meticulous process. Testing and comparing different solvents and combining different protocols is a good way to optimize this step.
- The settings of the aggregation experiment as well as any pre-treatments (amounts, volumes, timings, final concentrations, reagent preparation, buffer recipes, type of plate reader, protocols, scripts, etc.) should be recorded in as much detail as possible.
- A large number of replicates are necessary to clearly detect outliers. We recommend $n = 6$ as the minimum.
- Differences across ThT assays that are identical are likely to happen thus, looking for patterns in aggregation curves might occasionally be more relevant.
- Protein interactions are also increased by increased mixing or agitation; thus, it is best to avoid vigorous pipetting when preparing samples. Agitation during aggregation is often used during the assay but if using a highly aggregation-prone protein like Aβ(1-42) using quiescent conditions is advisable.

CHAPTER 4. THE BACTERIAL AMYLOID CURLI AFFECTS THE AGGREGATION OF Aβ(1-40) AND Aβ(1-42) DIFFERENTLY AND CHANGES THEIR TOXICITY IN CELL CULTURE

4.1 ABSTRACT

Salmonella and *E. coli* make the functional amyloid curli which shares structural similarities to Aβ fibrils associated with Alzheimer's disease. In this study we assessed the ability of curli to influence Aβ aggregation *in vitro*. Biophysical methods such as Western blot analysis and thioflavin T fluorescence for aggregation kinetics were used to evaluate the impact of curli on Aβ aggregation. Additionally, we used human fibroblast cells from donors from both sexes and different AD susceptibility to measure the toxicity of the aggregates of Aβ alone or in combination with curli. The results showed that curli decreases oligomeric Aβ(1-42) and might enhance its aggregation. Additionally, we found that curli promotes the aggregation of Aβ(1-40) which is known for its reduced propensity to aggregate by its own. Overall, this study shows that curli, a bacterial amyloid, can physically interact with pathological amyloids like Aβ. However, additional research is necessary to better understand the underlying mechanisms and the relevance of these interactions in disease pathology.

4.2 INTRODUCTION

Amyloid proteins have a characteristic cross-β structure and the ability to form fibrils has historically been linked to the progression and pathogenesis of many neurodegenerative diseases including Alzheimer's disease, Parkinson's disease, Amyotrophic lateral sclerosis and prion diseases (Soto, 2003; Soto and Pritzkow, 2018). In such diseases, unique amyloid proteins self-assembly into toxic conformers like amyloid deposits (Soto, 2003; Soto and Pritzkow, 2018). Moreover, there are non-neuronal diseases such T2D, cancer, and systemic amyloidosis, where amyloid aggregation also leaves its mark (Yang-Hartwich *et al.*, 2015; Haque *et al.*, 2017; Benson, 2023). Although these diseases have been a major area of study for many years, the process that leads to the misfolding of their associated proteins into the amyloid form remains unclear. Not all amyloids are associated with disease and there are increasing instances where amyloid proteins play important roles in biological processes in a range of species, from fungi and bacteria to plants, animals, and mammals (Otzen and Riek, 2019).

Given that co-aggregation and amyloid cross-seeding have been identified as crucial biological processes (Dubey *et al.*, 2014; Anand *et al.*, 2017; Anand *et al.*, 2018; Tavassoly *et al.*, 2018) it is fundamental to understand the effects that aggregation of one type of protein would have on the aggregation propensity and characteristics of other proteins and metabolites present in its environment. This has promoted a need to find other possible ways to approach research around amyloidogenic diseases including the effect of other host amyloid proteins or perhaps a microbial link including bacterial amyloids. For instance, formation of senile plaques composed of Aβ peptides, particularly the Aβ(1-42) is a key pathogenic feature of AD (Querfurth and LaFerla, 2010). Several *in vitro* studies have investigated the interactions between Aβ and other amyloid proteins linked to human illness. It has been shown that PD, α-syn (Ono *et al.*, 2012; Chia *et al.*, 2017); amyloidosis, protein A (AA) (Rising *et al.*, 2021); and T2D, human islet amyloid polypeptide (hIAPP) (Hu *et al.*, 2015) accelerate Aβ aggregation. Aβ cross-seeding research has gone beyond disease-associated proteins using functional amyloids (Chiti and Dobson, 2006; Fowler *et al.*, 2007; Javed *et al.*, 2020; Koloteva-Levine *et al.*, 2021) or non-amyloid protein fibers (Ono *et al.*, 2014). Overall, most of these studies have revealed that the inclusion of different amyloid proteins accelerates Aβ *in vitro* aggregation. As a result, there could be a link between endogenous amyloid exposure and the start of AD disease.

Recent research by our team has shown that the bacterial amyloid curli produced by *Salmonella* is synthesized inside the murine intestine during *Salmonella* infection (Miller *et al.*, 2020). Some aspects of this infection model are thought to model human gastroenteritis caused by *Salmonella*, meaning that curli exposure could also occur in humans. Curli fibers play a fundamental role in bacterial cell-cell aggregation, which aids in survival and persistence once *Salmonella* cells exit the host (Collinson *et al.*, 1993; MacKenzie *et al.*, 2017). Furthermore, the curli genes are shared between *Salmonella* and *E. coli* and are functionally interchangeable (Römling *et al.*, 1998). *E. coli* are common members of the human gut microbiota, which again could mediate curli exposure in humans. Curli fibrils are also highly immunogenic (Tükel *et al.*, 2010; Gallo *et al.*, 2015) and interestingly, share a similar 3D structure as Aβ fibrils (Perov *et al.*, 2019; Sewell *et al.*, 2020). These observations have brought forward the possibility that curli and amyloidogenic proteins of the host could interact. Thus, here we investigate the hypothesis that the bacterial amyloid curli can physically interact with, and influence, AD-related Aβ function.

4.3 MATERIALS AND METHODS

4.3.1 Peptides and Antibodies

Synthetic Aβ(1–40) (cat#: 4014442), and Aβ(1–42) (4014447) were obtained from Bachem Americas, Inc. Disruption of any pre-existing β-sheet structures was performed by reconstitution of the peptides in ice-cold HFIP (Sigma-Aldrich) to a concentration of 1 mg/mL. Aliquots of the peptide solution were stored at -80°C. HFIP was evaporated prior to peptide use in any assay.

The anti Aβ antibody [clone 6E10: targets residues 1–16 of the Aβ peptide: cat# 803016] was obtained from BioLegend. The primary anti-curli immune serum was prepared according to(Miller *et al.*, 2020). The NIR-labeled secondary antibodies used to probe the primary anti-β-amyloid antibody and the anti-curli immune serum were Amersham™ CyDye™ 800 Goat-Anti-Mouse and CyDye™ 700 Goat-Anti-Rabbit from Cytiva.

4.3.2 Curli purification

Curli purification was performed by a former lab member as described in (Sivaranjani *et al.*, 2022).

4.3.3 Curli sample preparation

Curli stock solutions were made by weighing out a desired amount of purified curli and resuspending in distilled water to achieve a final concentration of 1, 2, or 8 mg/mL. Aliquots of these solutions were used as mature curli samples, making sure to evenly mix the stock and using wide-bore pipette tips to deliver the required volume. Aliquots were frozen at -80°C for at least 1 h prior lyophilization for 24 h. For depolymerized curli samples, aliquots were removed, and formic acid was added to >90% v/v and the mixture was frozen at -80°C for at least 1 h prior lyophilization for 24 h. Lyophilized material for mature and depolymerized curli was stored at -20°C until use.

4.3.4 Curli and Aβ co-incubation

After evaporation of HFIP, Aβ peptides were resuspended to 0.2 mg/mL (40 μM) in aggregation buffer (1X PBS pH 7.4 for Aβ(1-40) and, 20 mM Tris buffer pH 8.0 for Aβ(1-42)). Curli solutions of were made in separate tubes from a stock solution of mature or depolymerized curli (1 mg/mL). Aliquots (10 μL) of Aβ peptide solutions were co-incubated with 10 μL of curli

solutions (i.e., at 1.0, 0.4, 0.2, and 0.02 mg/mL) for 24 h at 37°C or 25°C for Aβ (1-40) and Aβ (1-42), respectively. For time zero samples, aliquots of Aβ peptide solution were immediately frozen at -80°C.

4.3.4.1 Western Blot analysis of SDS-PAGE

SDS-PAGE and Western blot analysis were used to visualize the aggregation of Aβ peptide mixtures. Pre-incubated samples were resolved using 4 to 12% bis-Tris NuPAGE™ or Tris-Glycine Novex™ gels (Thermo Fisher) and, with MES or SDS running buffer, respectively. Proteins were transferred to 0.2-µm nitrocellulose membranes using the iBlot2 system (Thermo Fisher). Membranes were incubated in TBS containing 5% (w/v) non-fat dry milk (blocking buffer) for 1 h at room temperature with shaking. Blots were incubated overnight at 4°C with both primary antibodies, the mouse 6E10 antibody (1:4000 dilution) and the rabbit anti-curli immune serum (1:1000). Membranes were washed with TBS three times, shaking, for 5 min, 15 min, and 5 min. Membranes were probed with both Amersham™ CyDye™ 800 Goat-Anti-Mouse and CyDye™ 700 Goat-Anti-Rabbit NIR-labeled secondary antibodies (Cytiva) in TBS (5% skim milk) (1:10,000) for 90 minutes at room temperature, shaking and protected from light. Membranes were washed prior imaging in a LI-COR Odyssey CLx. Data analysis was performed using the Image Studio (version 5.2) software.

4.3.5 Amyloid aggregation kinetics: Thioflavin T assay

4.3.5.1 Preparation of ThT assays

A dilution series containing 0.005, 0.05, 0.1 and 0.25 mg/mL of mature or depolymerized curli was prepared. After HFIP evaporation, Aβ peptides were resuspended to 0.05 mg/mL (10 µM) in 1X PBS pH 7.4 for Aβ(1-40) or 20 mM Tris buffer pH 8.0 for Aβ(1-42). A 50 µM ThT working solution was made from a 10 mM Thioflavin T (ThT, Sigma) stock solution previously filtered through a 0.2 µm filter. The samples were loaded into a Costar® 96-well, clear-flat bottomed, black polystyrene plate (Corning), from low to high peptide concentration, with 6 wells per sample. Samples containing peptide and curli consisted of 40 µL peptide (final concentration of 0.02 mg/mL or 4 µM), 40 µL curli (0.002, 0.02, 0.04 or 0.25 mg/mL) and 20 µL ThT (10 µM). In control samples, either the curli or the peptide volume were substituted with aggregation buffer. The plate was subsequently sealed and ThT fluorescence was measured. The whole setup was repeated at least three times for each peptide and each form of curli.

4.3.5.2 ThT Assay

ThT fluorescence was measured using a FLUOstar Omega plate reader (BMG Labtech) at 37°C for Aβ(1-40) or at 25°C for Aβ(1-42). Fluorescence was measured through the bottom of the plate using an excitation filter of 440 nm and an emission of 480 nm. Measurements were taken every 10 min for a total of 20 - 40 hours. The plate was shaken for 5 s before the first cycle. The fluorescence measured from negative control wells, containing only 10 µM ThT, was subtracted from all test measurements.

4.3.5.3 Kinetic parameters

Data from the ThT assays were analyzed by non-linear regression to fit the theoretical Boltzmann sigmoid model using PRISM (Graphpad Software Inc.) according to equation 1 (Cabaleiro-Lago *et al.*, 2008; Khemtemourian *et al.*, 2021):

$$y = y_0 + \frac{y_{max} - y_0}{1 + e^{-(t - t_{1/2})^k}} \qquad (1)$$

were, y_0 and y_{max} are initial and final ThT fluorescence values, $t_{1/2}$ is the half-time which is the time at which the fluorescence is halfway between the initial and the final fluorescence value and k is the slope of the curve.

The lag time can be calculated using equation 2:

$$lag\ time = t_{1/2} - \frac{2}{k} \qquad (2)$$

4.4.7 Cell culture assays

4.4.7.1 Cell Lines and Conditions

The study was carried out on four cell lines derived from human skin fibroblasts with different *APOE* genotypes. Male fibroblasts (*APOE* ε2/3 and *APOE* ε3/4) and, female fibroblasts (*APOE* ε2/3 and *APOE* ε4/4) from in-patients with and without metabolic disease were obtained from the Montreal Children's Hospital Cell Repository. These cell lines were cultured in high-glucose Dulbecco's Modified Eagle's Medium (DMEM) supplemented with 10% fetal bovine serum at 37 ^{o}C in an atmosphere of 5% CO_2. Morphology and confluence of the cells was assessed daily because high levels of confluency can dramatically affect cell behavior and culture kinetics(Topman *et al.*, 2011). When cells reached 70% confluency, the medium with cells was collected and centrifuged at 1000×g for 5 min. Supernatants were removed, and fresh medium was added.

4.4.7.2 Treatment preparation

Curli (mature and depolymerized) and HFIP-treated Aβ(1-40) were dissolved in 1X PBS buffer pH 7.4 or 20 mM Tris Buffer pH 8.0 for Aβ(1-42) to a final stock concentration of 6 mg/mL for curli, or 0.4 mg/mL (80 µM) for the peptides. Treatments were prepared from curli and peptide stock solutions. Treatments containing Aβ(1-40) were incubated at 37 ºC for 24 h, whereas treatments containing Aβ(1-42) were incubated at room temperature for 24 h.

4.4.7.3 Cell viability

Cells were counted with a Countess™ 3 Automated Cell Counter and seeded in 96-well plates at 10,000 cells/well. Plates were incubated at 5% CO_2, 95% humidity, and 37 ºC. One day after seeding the cells, the old medium was replaced with fresh medium containing the different treatments (50 µL media + 50 µL treatment). Each group contained six replicates and the whole set-up was repeated twice. Control wells for background (no cells), untreated cells (vehicle, *e.g.*, 1:1, media:PBS) and dead cells (lysed cells) were included in each plate. Cells were returned to the incubator (5% CO_2, 95% humidity, and 37 ºC) for 24 h.

The mitochondrial metabolic activity based on the MTT conversion assay was used as an index of cell viability. A stock solution of 5 mg/mL 3-(4,5-dimethylthiazol-2-yl)-2,5-diphenyltetrazolium bromide (MTT) was prepared by dissolving MTT in PBS and filtering through a 0.22 µm filter. The MTT working solution (0.5 mg/mL) was made by mixing 1 volume of stock MTT solution with 9 volumes of high-glucose DMEM containing 1% FBS. After treatment of cells for 24 h, the experimental media was carefully removed, and the cells were incubated with 50 µL of the MTT working solution at 37 ºC. After 2 h, solubilization of MTT formazan product was done by addition of 150 µL dimethyl sulfoxide (DMSO) followed by incubation for 45 min at 36 ºC. MTT formazan was quantified by determining the absorbance at 570 nm using a SpectraMax M5 Multi-Mode Microplate Reader (Molecular Devices). After subtracting the background, the optical densities were expressed as a percentage of the average OD of the control untreated cells (vehicle, 100% cell viability) and the dead cells (0%).

4.5 RESULTS

4.5.1 Depolymerized curli cross-reacts with Aβ(1-42) by affecting its aggregation.

Investigation of the aggregation behavior of Aβ(1-42) with curli was performed by Western blots probed with the 6E10 and the anti-curli antibodies (**Figure 4.1**). Control Aβ(1-42) samples at time 0 showed two discrete bands of ~8 and ~16 kDa corresponding to Aβ(1-42) dimers and tetramers (**Figure 4.1 A** and **B**, lane 1) consistent with Western blotting analysis of freshly made Aβ(1-42) (Walsh *et al.*, 2000; Sureshbabu *et al.*, 2009). After 24 h incubation, control Aβ(1-42) peptide was detected as a smear above 35 kDa (**Figure 4.1 A** and **B**, lane 2). Samples mixed with increasing amounts of depolymerized curli exhibited weaker 6E10 immunoreactivity in the smear (analysed by densitometry **Figure 4.1 C**) and no discrete band at ~8 kDa. Moreover, SDS resistant material was observed to accumulate at the top of the wells (**Figure 4.1 A**, lanes 3–6). On the contrary, mixtures of Aβ(1-42) with mature curli did not exhibit significant differences in the smear (**Figure 4.1 B** and **C**) and the ~8 kDa was still present at all curli concentrations. Curli did not show any differences with or without the peptide using this technique (**Supplementary Figure 1**). Thus, depolymerized curli appears to stimulate the aggregation of Aβ(1-42) but mature curli does not influence Aβ(1-42).

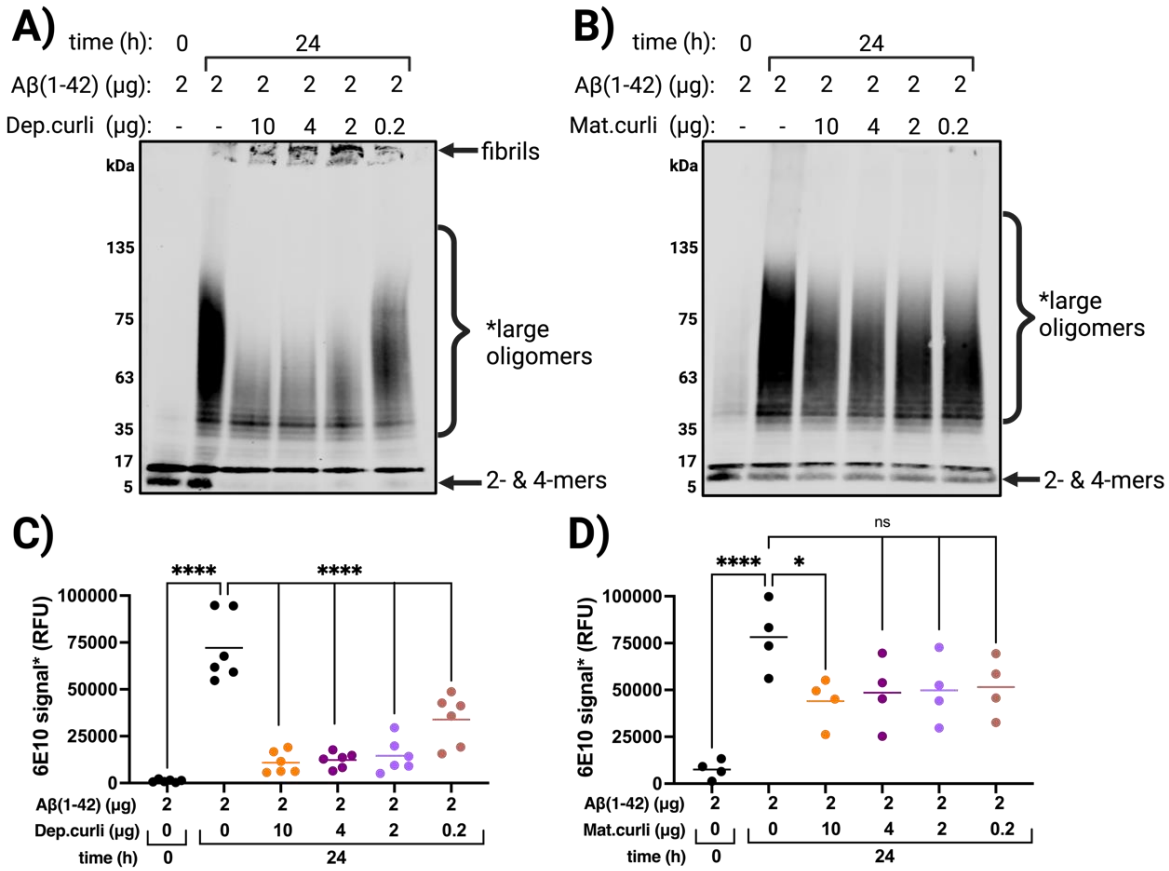

Figure 4.1. Western blot analysis of oligomerization of Aβ(1–42) peptide after co-incubation with depolymerized curli or mature curli fibrils. Aβ(1–42) peptide was incubated either alone or with 0.2-10 μg of A) depolymerized curli or B) mature curli. Aβ oligomerization was monitored with the 6E10 antibody that targets residues 1-16 of Aβ. Quantification in reference fluorescence units (RFU) of the 6E10 signal in the "large oligomers" section was performed using the Image Studio software. C) Depolymerized curli significantly reduces large Aβ oligomers, while D) mature curli does not. (n = 4-6). ns: $p > 0.05$; *: p: ≤ 0.05; **: $p \leq 0.01$; ***: $p \leq 0.001$; ****: $p \leq 0.0001$ by one-way ANOVA.

We used the thioflavin T assay(Gade Malmos *et al.*, 2017) to further investigate the interactions between curli and Aβ(1-42) (**Figure 4.2**). The aggregation curve shapes for Aβ(1-42) displayed a typical sigmoidal shape(LeVine, 1993), with a lag phase at low fluorescence, followed by a visible elongation phase where fluorescence values started to increase until a plateau was reached. In the experimental dataset for depolymerized curli, the lag phase for Aβ(1-42) alone was considerably shorter than in the mature dataset shifting from ~3h to ~13 h (**Figure 4.2 A** and **B**). Variability in Aβ experiments is common and strong qualitative findings are considered robust (Foley and Raskatov, 2020; Faller and Hureau, 2021). The RFU scales were different for the

depolymerized vs. mature datasets because I had to change the settings of the plate reader when using mature curli. Mature curli experiments using the same settings as depolymerized curli gave high RFU values that were above the maximum fluorescence intensity of the instrument. Therefore, I had to employ a different gain value (1900 for depolymerized vs. 900 for mature curli) to keep the RFU reads within the range of the instrument. Increasing concentrations of mature curli increased the starting RFU value (up to ~3000 fold), however, regardless of this increase, the shape of the curves for Aβ(1-42)/mature curli mixtures and Aβ(1-42) were similar (**Figure 4.2 B**).

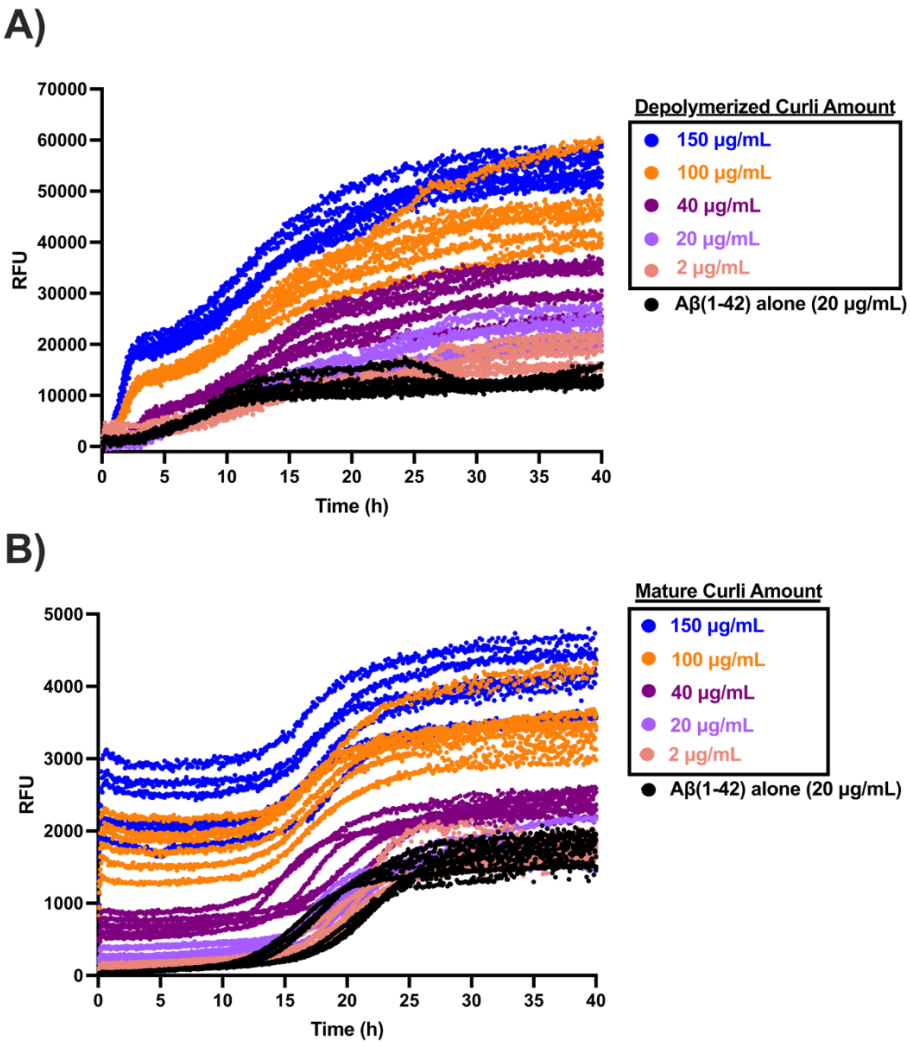

Figure 4.2. Aggregation kinetics of Aβ(1-42) with depolymerized and mature curli. Aβ(1-42) was incubated at 25 °C in the presence or absence of A) depolymerized or B) mature curli (2-150 µg/mL) and aggregation was monitored by Thioflavin T fluorescence. Reference fluorescence units (RFU) were measured every 10 min for 40 h. (n = 6). Mature and depolymerized curli alone samples were included but not plotted in these graphs.

Closer inspection of the curves in **Figure 4.2 A** showed that two distinct transitions occurred when the curli concentration was ≥40 µg/mL as monitored by ThT fluorescence. **Figure 4.3** shows the two transitions (1st and 2nd transition regions). Analysis of double sigmoidal curves is done by analyzing each transition independently (Cukalevski *et al.*, 2015b; Braun *et al.*, 2022). Due to the presence of double sigmoidal curves in our dataset, *post-hoc* analysis of the curves in **Figure 4.2 A** was first done for the second transition (corresponding to the grey region in **Figure 4.3**).

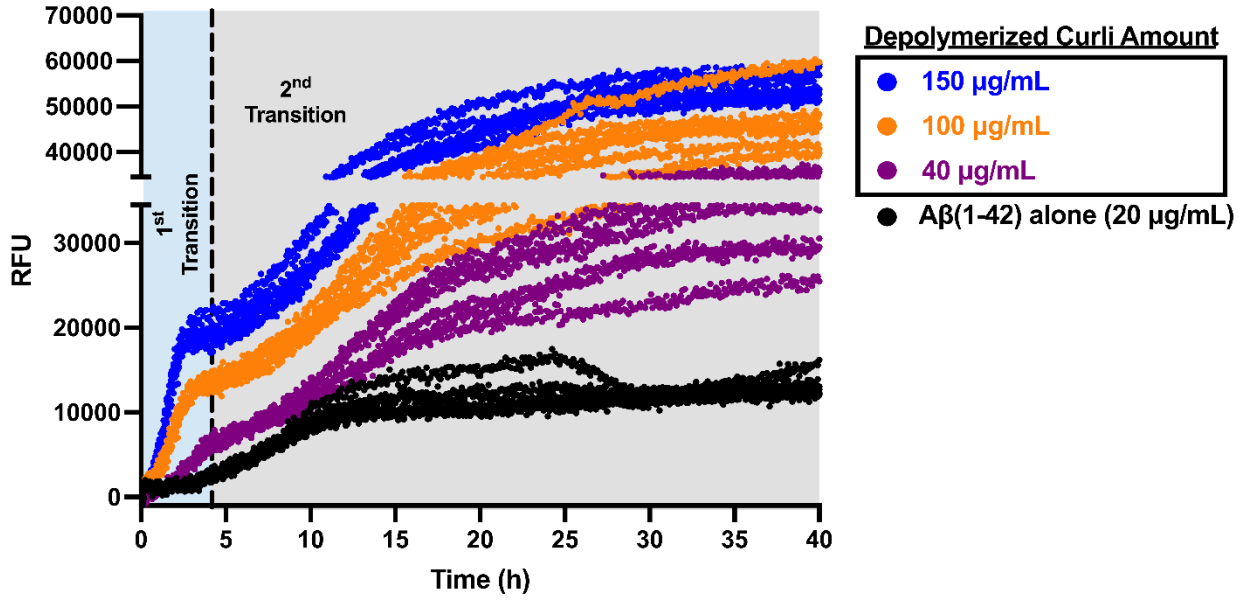

Figure 4.3. Aggregation curves of mixtures of Aβ(1-42) with depolymerized curli show a two-transition aggregation process. Two distinct transitions were observed as monitored by ThT fluorescence. The 1st transition (shown in the blue region of the graph) occurs within the first 5 hours of the experiment while the 2nd transition (shown in the grey region of the graph) occurs later.

When examining the second transition (grey region in **Figure 4.3**) we observed that depolymerized curli increased the Max ThT fluorescence in a dose-dependent manner (**Figure 4.4 B**). The shape of the second transition in the Aβ(1-42)/depolymerized curves was similar to the shape of the aggregation curve of Aβ(1-42) alone. This was supported by no changes in the slope of the curves containing curli (**Figure 4.4 C**). The half-time ($t_{1/2}$), as a measure of the elongation phase was considerably increased by the presence of depolymerized curli (**Figure 4.4 D**).

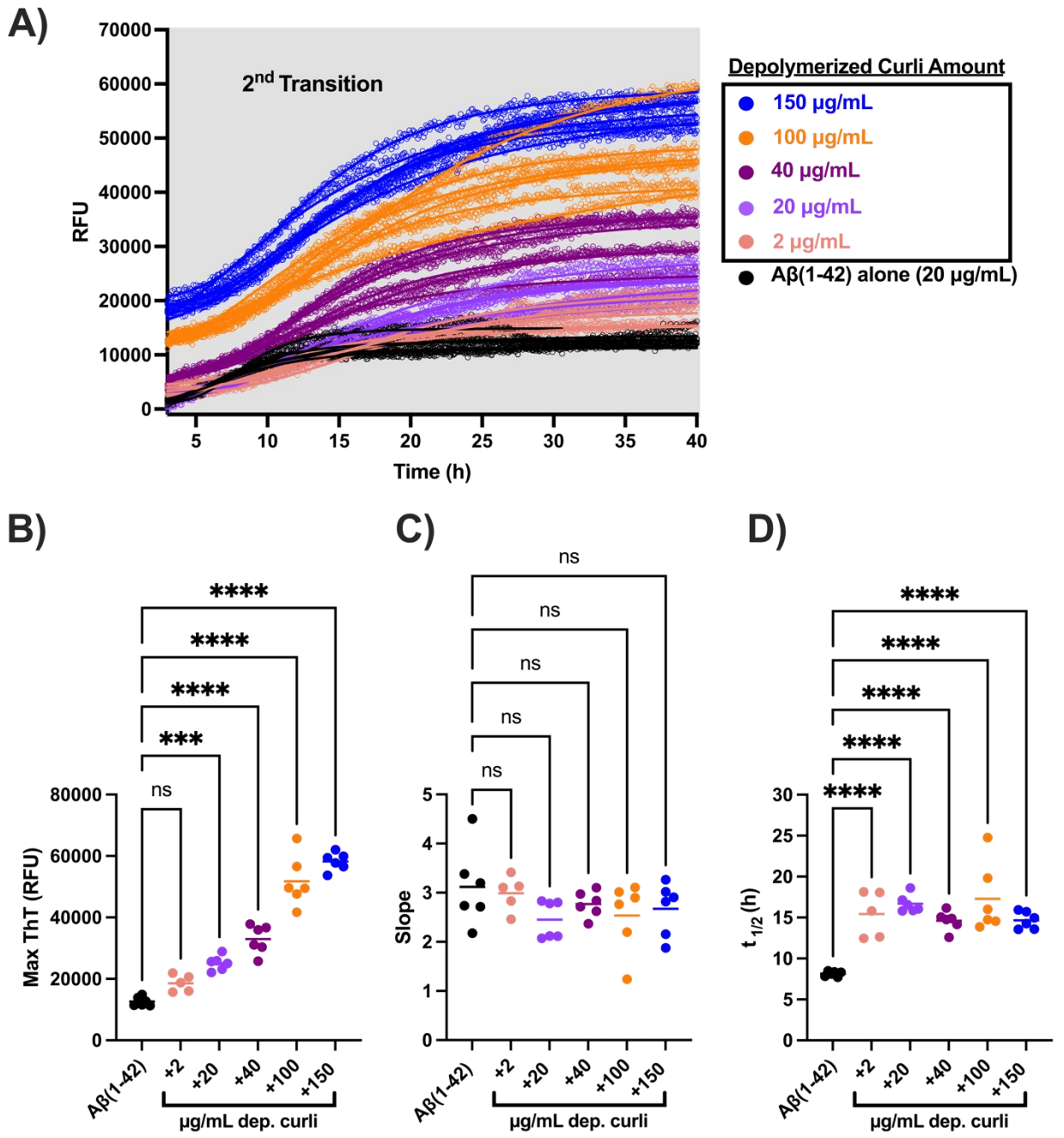

Figure 4.4. Comparing the aggregation kinetics of mixtures of Aβ(1-42) and depolymerized curli in the second transition. A) Solid lines represent the aggregation curves of each mixture fit to the Boltzmann sigmoid model, after the first transition has occurred (data repeated from Figure 4.3). The curves in (A) were used to compare the kinetic parameters of the mixtures to kinetic parameters of Aβ(1-42) alone: B) max ThT fluorescence, C) curve slope, and D) time needed to reach half of the maximum ThT fluorescence (half-time; $t_{1/2}$). Values were compared by one-way ANOVA: ns: $p > 0.05$; *: $p \leq 0.05$; **: $p \leq 0.01$; ***: $p \leq 0.001$; ****: $p \leq 0.0001$.

To better understand the interactions between Aβ(1-42) and depolymerized curli, we used the Aβ(1-42)+40 μg/mL and Aβ(1-42)+150 μg/mL depolymerized curli curves from **Figure 4.3** and plotted them in separate panels along with their pure components (**Figure 4.5 A** and **E**). Typical sigmoidal curves were observed for depolymerized curli alone samples (light pink and blue curves in **Figure 4.5A** and **E**). The 40 μg/mL depolymerized curli curves plateaued at about the baseline value after ~8h of incubation while the 150 μg/mL depolymerized curli alone curves plateaued around 10,000 RFU after ~3h of incubation (**Figure 4.5A** and **E**). Kinetic parameters of the first (blue region) and second transition (grey region) were compared to Aβ(1-42) and depolymerized curli alone. Results showed a significant increase in the max ThT fluorescence of both transitions compared to the pure components (**Figure 4.5 B** and **F**). The max ThT fluorescence in the second transition was higher than the sum of the max fluorescence of both pure components suggesting more complex interactions between these two amyloidogenic proteins than just an increase due to the higher total protein concentration (**Figure 4.5B** and **F**). The shape of the first transition in the two-component curves seemed similar to the shape of the curves from depolymerized curli alone (**Figure 4.5 A** and **E**). Although there was an increase in the slope of the first transition compared to the slope of curli alone, this value only reached statistical significance for the 40 μg/mL curves ($p=0.0011$) and not for the 150 μg/mL ($p=0.2521$) (**Figure 4.5 C** and **G**). No differences were found between the slope of the second transition in the mix and the slope of Aβ(1-42) alone curves (**Figure 4.5C** and **G**). The $t_{1/2}$ of the first transition was reduced for the 40 μg/mL curves ($p<0.0001$) whereas for the 150 μg/mL the value was not different compared to the curli alone curves ($p=0.7109$). The presence of depolymerized curli significantly increased the $t_{1/2}$ of the second transition compared to any of the pure components (**Figure 4.5 D** and **H**). These data emphasize that that the second transition observed in the mixed systems has a longer elongation time than the elongation time of Aβ(1-42) alone.

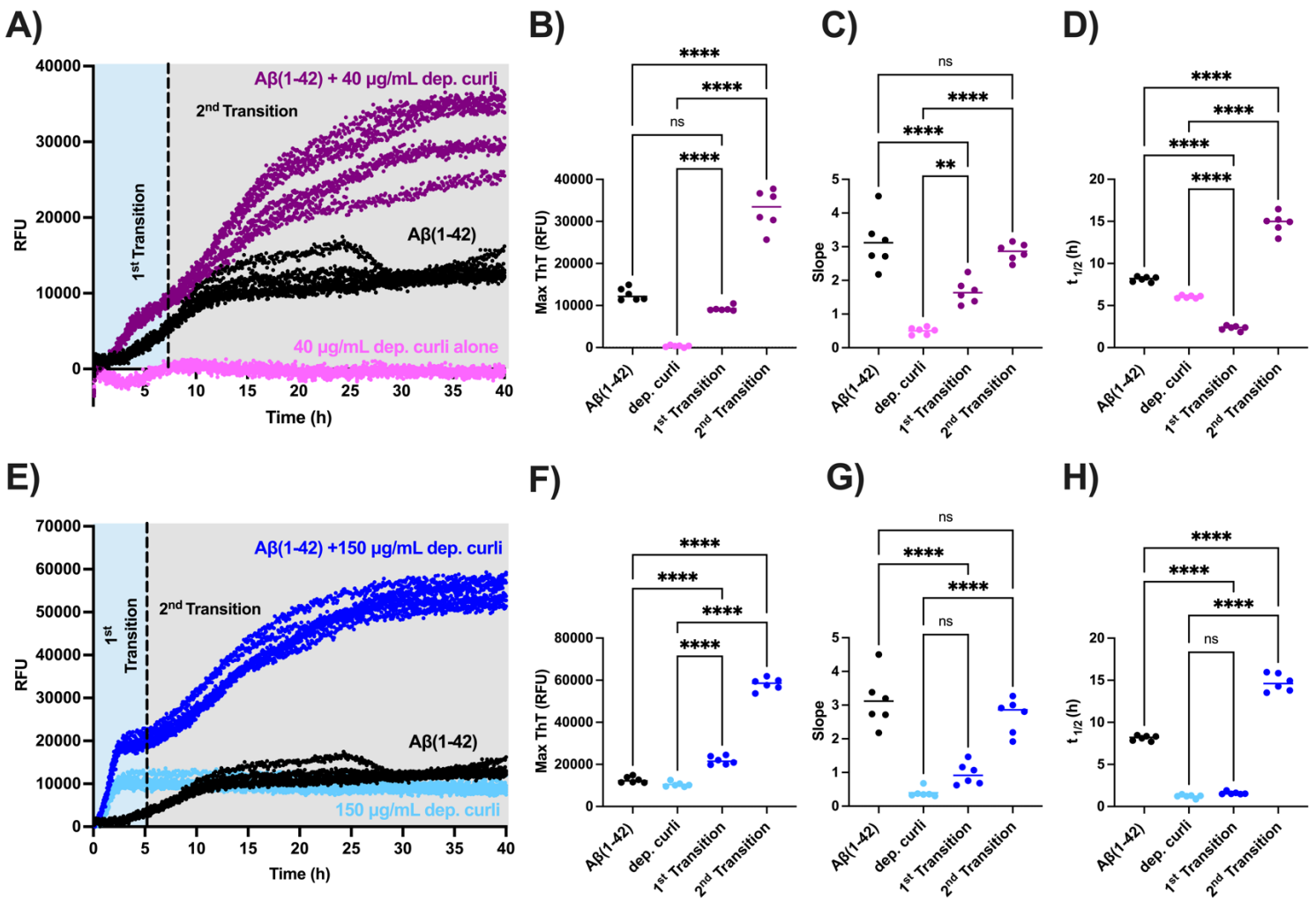

Figure 4.5. Comparing the aggregation kinetics of mixtures of Aβ(1-42) and depolymerized curli in the first and second transitions. A) Aβ(1-42)+40 and E) Aβ(1-42)+150 μg/mL depolymerized curli curves from Figure 4.3 were plotted along with their pure component curves. Curves were fitted to the Boltzmann sigmoid model and the pure component curves were used to compare the kinetic parameters of the 1st and 2nd transitions of the mixtures. Values were compared by one-way ANOVA: ns: $p > 0.05$; *: $p \leq 0.05$; **: $p \leq 0.01$; ***: $p \leq 0.001$; ****: $p \leq 0.0001$.

Curves of Aβ(1-42) with mature curli from **Figure 4.2 B** were further analyzed including mature curli alone samples. Pure curli samples showed a flat line throughout all the experimental window (**Figure 4.6**). The RFU value for this flat line increased in a dose-dependent manner. This value was subtracted from their respective concentration containing the Aβ(1-42) peptide in order to correct the high starting RFU value and compare to the pure Aβ(1-42) aggregation curves (**Figure 4.7 A**). The resulting curves were fitted to the Boltzmann sigmoid model and kinetic parameters were calculated (**Figure 4.7 B-D**). Addition of mature curli did not affect any kinetic parameters except for the max ThT fluorescence at 100 and 150 µg/mL, but at these high concentrations, the variability within replicates was higher. These results indicate that the data obtained for Aβ(1-42)/mature curli mixtures from western blot analysis tie well with observations from the thioflavin T assay. No interactions were observed when Aβ(1-42) and mature curli fibrils were incubated together.

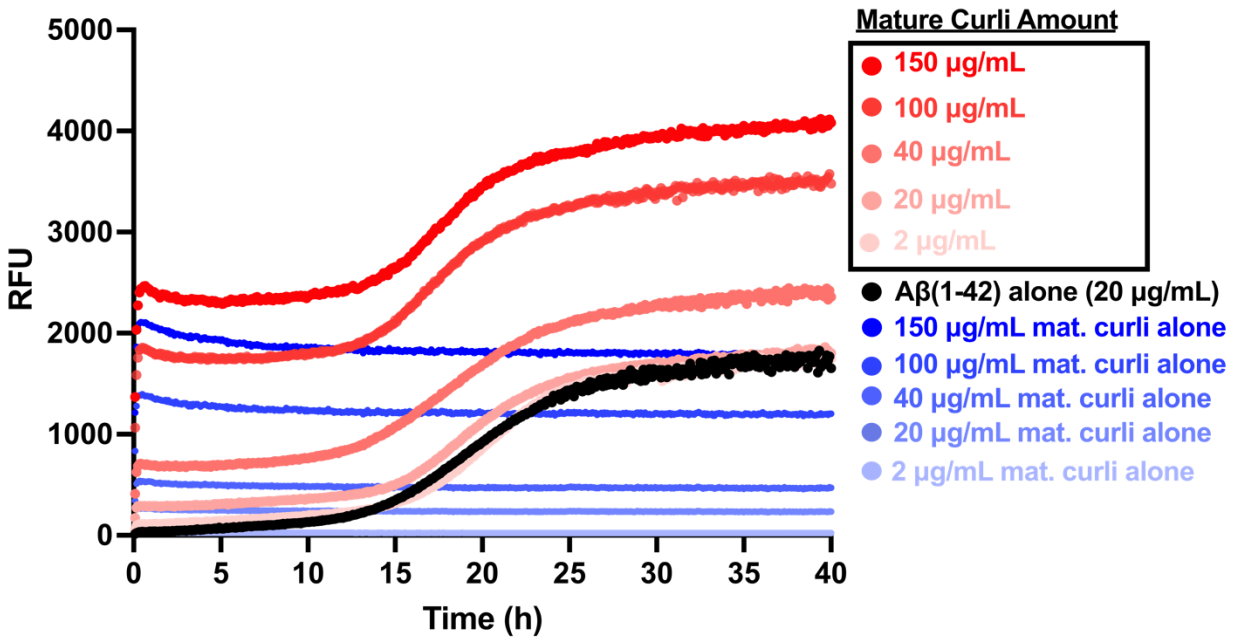

Figure 4.6. Aggregation kinetics for mixtures of Aβ(1-42) and mature curli, and pure components. Curves from Fig. 4.2 B were averaged, and the coloured scheme was changed for easier visualization. Pure mature curli samples display a flat line throughout all the experiment (in blue).

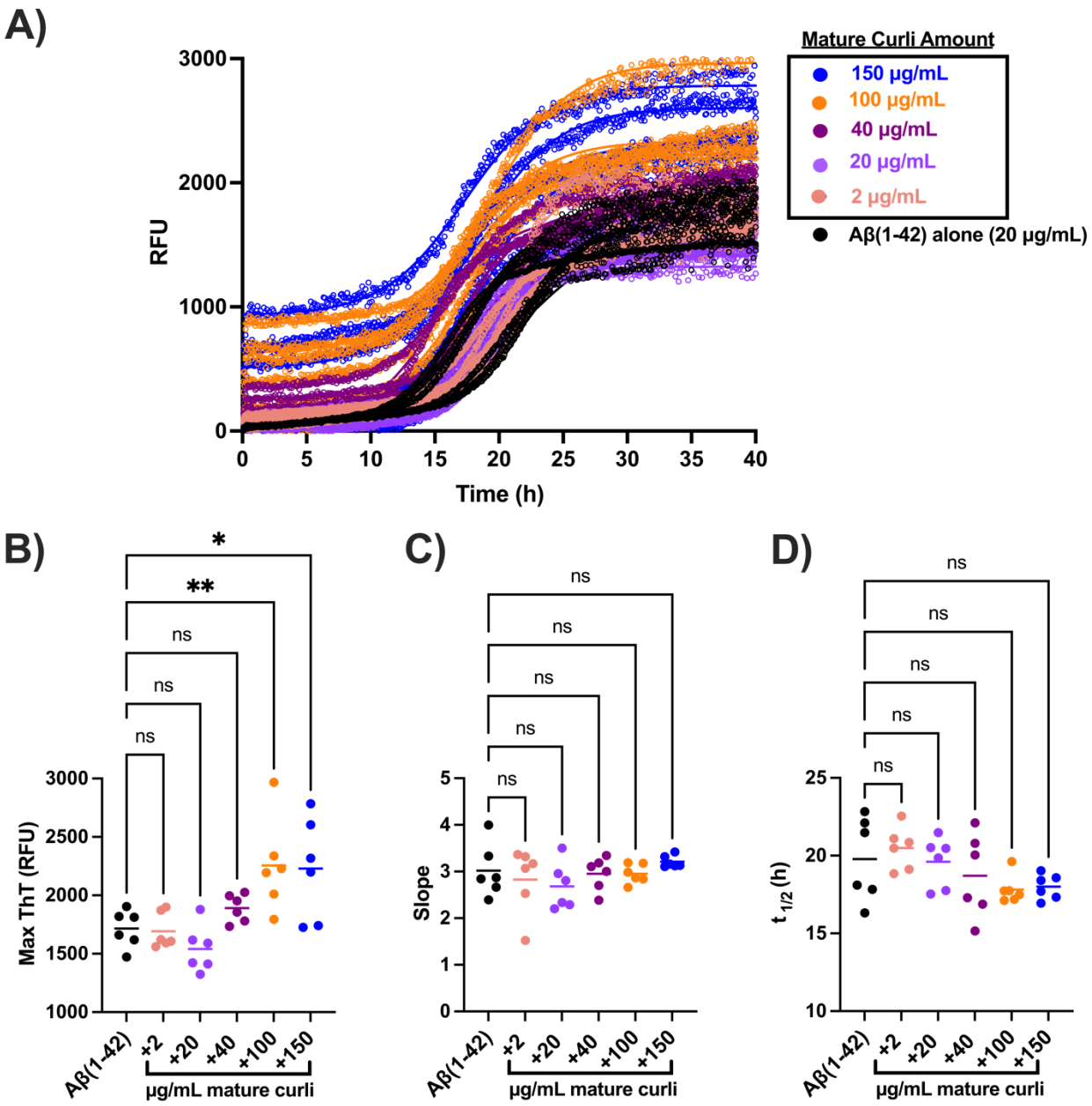

Figure 4.7. Comparing the aggregation kinetics of mixtures of Aβ(1-42) and mature curli. A) Solid lines represent the aggregation curves of each mixture fit to the Boltzmann sigmoid model (data repeated from Figure 4.2 B). The curves in (A) were used to compare the kinetic parameters of the mixtures to kinetic parameters of Aβ(1-42) alone: B) max ThT fluorescence, C) curve slope, and D) time needed to reach half of the maximum ThT fluorescence (half-time; $t_{1/2}$). Values were compared by one-way ANOVA: ns: $p > 0.05$; *: $p \leq 0.05$; **: $p \leq 0.01$; ***: $p \leq 0.001$; ****: $p \leq 0.0001$.

4.5.2 Aβ(1-40) aggregation is accelerated by depolymerized curli.

The aggregation behavior of Aβ(1-40) with curli was studied using Western blots probed with the anti-Aβ and anti-curli antibodies (**Figure 4.8** and **Figure 4.9**). Control Aβ(1-40) samples at time 0 showed two discrete bands of ~4 and ~8 kDa corresponding to Aβ(1-40) monomers and dimers (arrows each panel in **Figure 4.8** and **Figure 4.9**). Aβ(1-40) monomers and dimers were still observed even after 24 h when mixed with either mature or depolymerized curli. When using depolymerized curli, the aggregation was monitored at different timepoints (6, 8, 12, 18, 24 h) (**Figure 4.8 A-E**). Co-incubation of Aβ(1-40) with depolymerized curli for 6 h resulted in the formation of 6E10-positive insoluble material that accumulated at the top of the wells (**Figure 4.8 A**). This material was absent at 6 h when Aβ(1-40) was incubated alone (lane 2 in **Figure 4.8 A**). There was increased accumulation of insoluble Aβ(1-40) material in wells containing depolymerized curli after 8 and 12 h of co-incubation (**Figure 4.8 B and C**). In contrast, insoluble material was only present in the Aβ(1-40) alone wells after 12 h (**Figure 4.8 C**). Our data indicated that depolymerized curli accelerates Aβ(1-40) fibril formation. For the mixtures of Aβ(1-40) and mature curli, all appeared similar to Aβ(1-40) alone (**Figure 4.9**). Like with Aβ(1-42), these data suggested that mature curli fibrils only had a minor, possibly non-specific, effect on Aβ(1-40) aggregation.

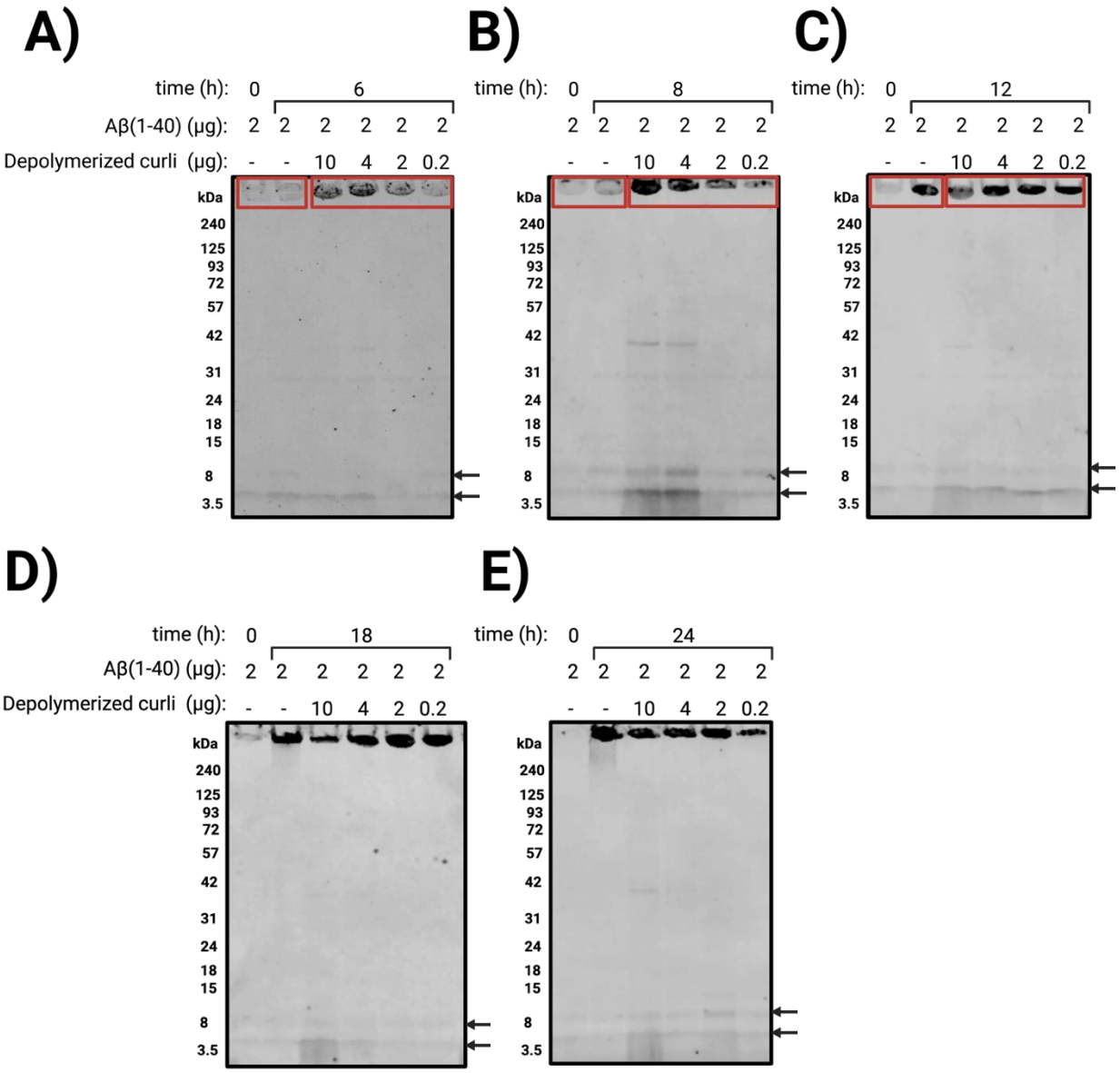

Figure 4.8. Western blot analysis of oligomerization of Aβ(1–40) peptide after co-incubation with depolymerized curli. 2 μg of Aβ(1–40) peptide were incubated either alone (lanes 1 and 2) or with 10, 4, 2 and 0.2 μg of depolymerized curli (lanes 3-6) for A) 6 h, B) 8 h, C 12 h, D) 18 h or E) 24 h. Presence of insoluble material at the top of the wells was observed in samples containing depolymerized curli as early as 6 h of co-incubation (red box). Aβ oligomerization was detected with the 6E10 mouse monoclonal antibody that targets residues 1-16 of Aβ, followed by fluorophore-conjugated 800RD Goat-Anti-Mouse IgG secondary antibody.

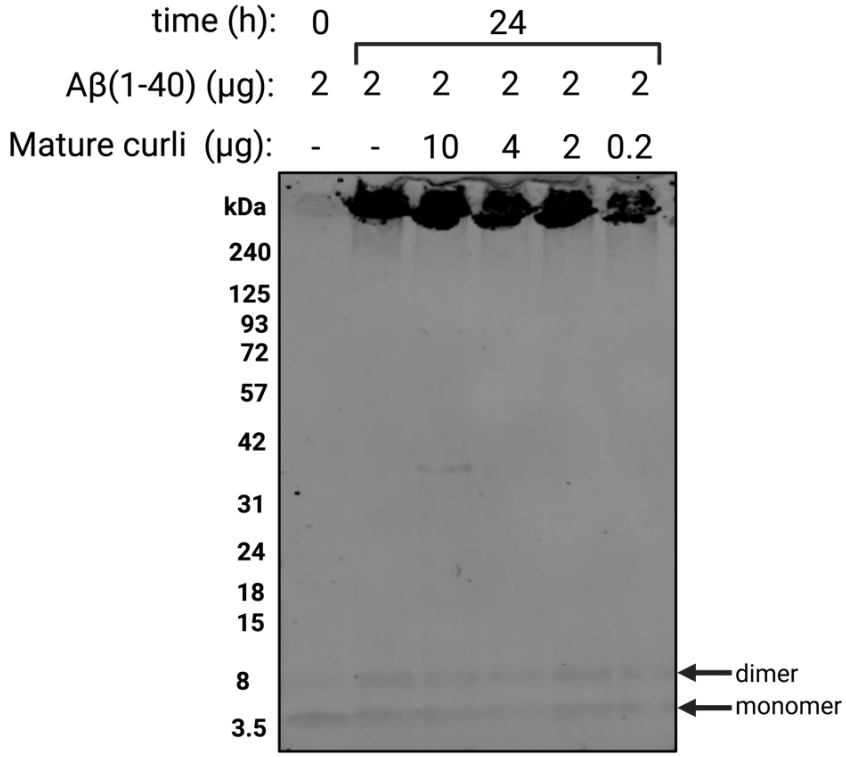

Figure 4.9. Western blot analysis of oligomerization of Aβ(1–40) peptide after co-incubation with mature curli fibrils. 2 μg of Aβ(1–40) peptide were incubated either alone (lanes 1 and 2) or with 0.2-10 μg of mature curli (lanes 3-6) for 24 h. Aβ oligomerization was monitored with the 6E10 mouse monoclonal antibody that targets residues 1-16 of Aβ, followed by fluorophore-conjugated 800RD Goat-Anti-Mouse IgG secondary antibody.

The interactions between Aβ(1-40) with curli were studied using the ThT assay (**Figure 4.10**). The aggregation curve for Aβ(1-40) alone depicted a long lag phase (12-14 h) with a relatively low fluorescence intensity, followed by a rapid growth phase until it plateaued after 16-18 h from the beginning of the experiment (black curves in **Figure 4.10**). Addition of depolymerized curli reduced the lag phase in a dose-dependent manner (**Figure 4.10 A**). As for mature curli, plate reader settings were adjusted as done for Aβ(1-42)/mature curli. This change made the RFU scales different for each dataset (**Figure 4.10**). In line with observations in our previous experiments with mature curli, the starting RFU value of Aβ(1-40)/mature curli samples increased, specially at the highest concentration of curli (150 μg/mL). Although, mature curli did not seem to affect the overall shape of the curve nor the time of the lag phase (**Figure 4.10 B**).

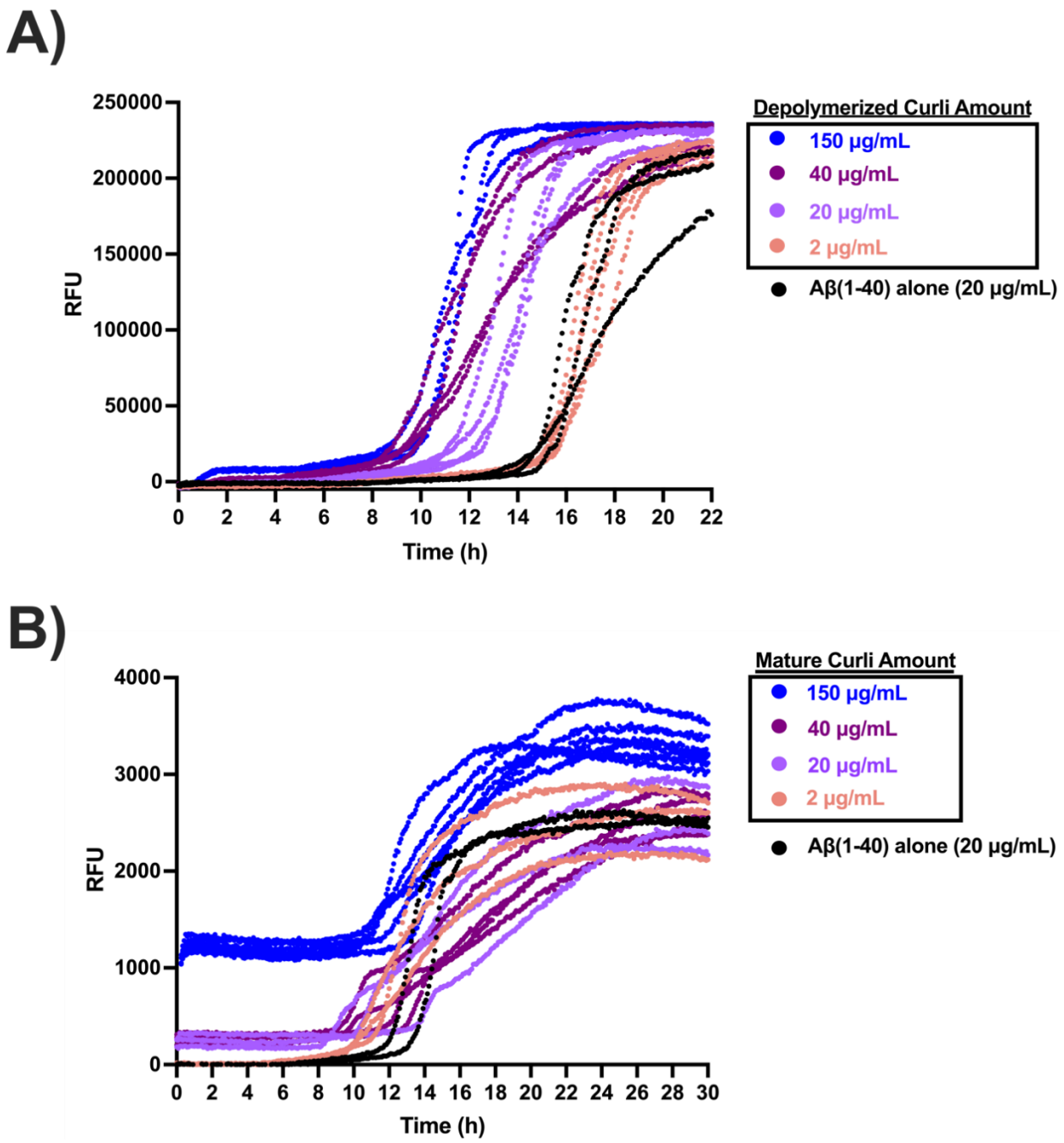

Figure 4.10. Aggregation kinetics of Aβ(1-40) with depolymerized or mature curli. Aβ(1-40) was incubated at 37 °C in the presence or absence of A) depolymerized or B) mature curli (2-150 µg/mL) and aggregation was monitored by Thioflavin T fluorescence. Reference fluorescence units (RFU) were measured every 10 min (n = 6). Mature and depolymerized curli alone samples were included but not plotted in these graphs.

A double sigmoidal transition was also observed in the mixture with the highest concentration of depolymerized curli (150 μg/mL). We separated these curves from figure **Figure 4.10 A** and plotted them in a new graph (**Figure 4.11 A**) for better visualization. Analysis of each transition in these curves was performed and kinetic parameters were compared with the kinetic parameters of the pure components. The first transition plateaued at around 10,000 RFU after ~1.5 h from the beginning of the experiment and curves of 150 μg/mL depolymerized curli alone showed a similar behaviour (light blue curves in **Figure 4.11 A**). In fact, there were no changes in any of the kinetic parameters between the first transition in the mixture and curli alone (**Figure 4.11 B-D**). These data suggest that the first transition that is observed in the mixture likely corresponds to the aggregation of curli while the second transition indicates the aggregation of Aβ(1-40). The second transition occurs earlier than the single transition in the Aβ(1-40) pure sample. This suggests that depolymerized curli accelerates Aβ(1-40) oligomerization, measured as a statistically significant shorter half-time (**Figure 4.11 A** and **D**).

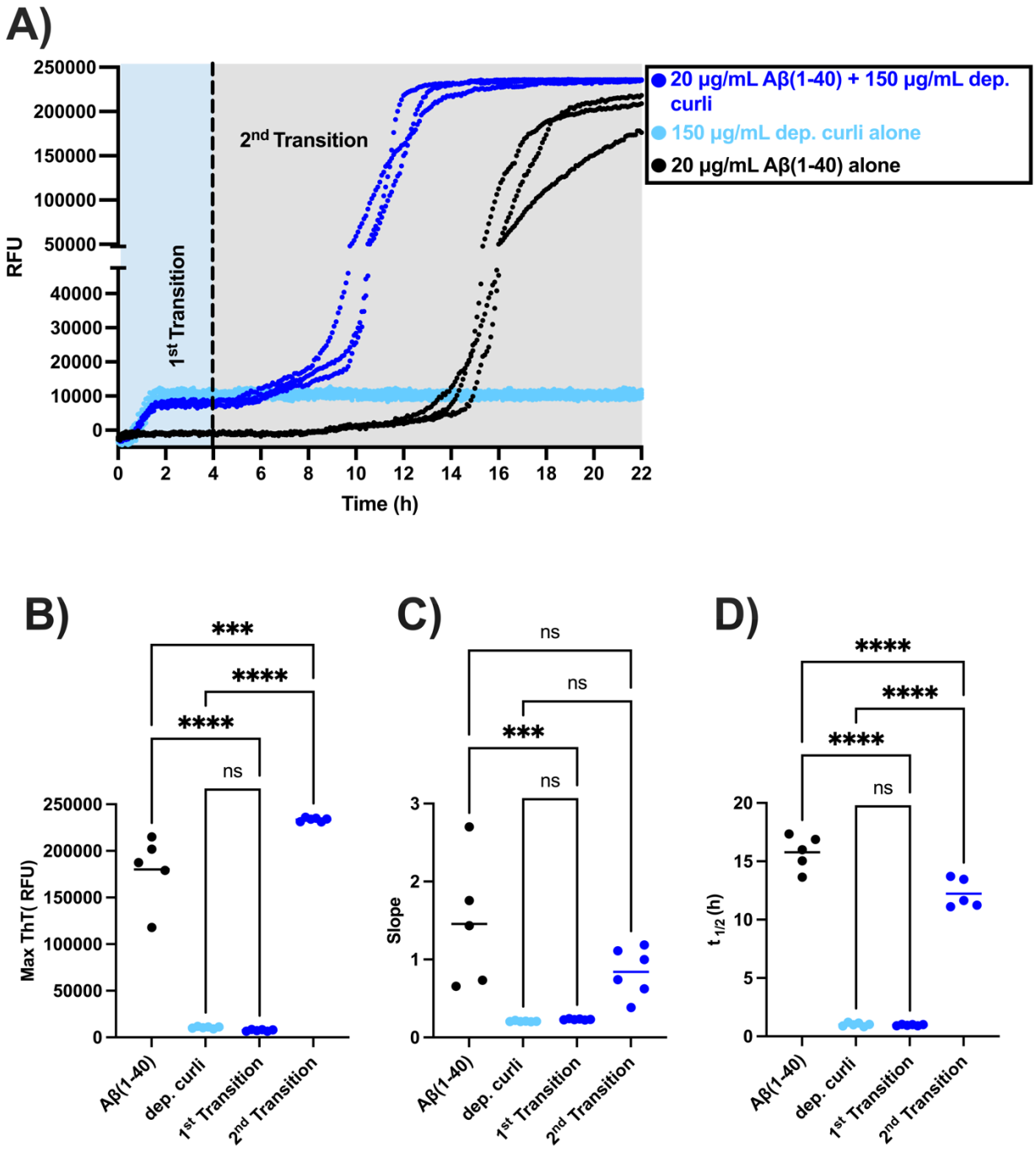

Figure 4.11. Comparing the aggregation kinetics of mixtures of Aβ(1-40) and depolymerized curli in the first and second transitions. A) Aβ(1-40)+150 µg/mL depolymerized curli curves from Figure 4.10 A were plotted along with their pure component curves. Curves were fitted to the Boltzmann sigmoid model and the pure component curves were used to compare the kinetic parameters of the 1st and 2nd transitions of the mixture. Values were compared by one-way ANOVA: ns: $p > 0.05$; *: $p \leq 0.05$; **: $p \leq 0.01$; ***: $p \leq 0.001$; ****: $p \leq 0.0001$.

The rest of the curves in **Figure 4.10 A** were fitted to the Boltzmann sigmoid model, and kinetic parameters were obtained (**Figure 4.12**). A dose-dependent reduction in the half-time was evident (**Figure 4.12 D**). The time of the lag phase was calculated using equation 2 and the results indicate that depolymerized curli can interact with Aβ(1-40) and it catalyzes primary nucleation by reducing the lag time (**Figure 4.12 E**).

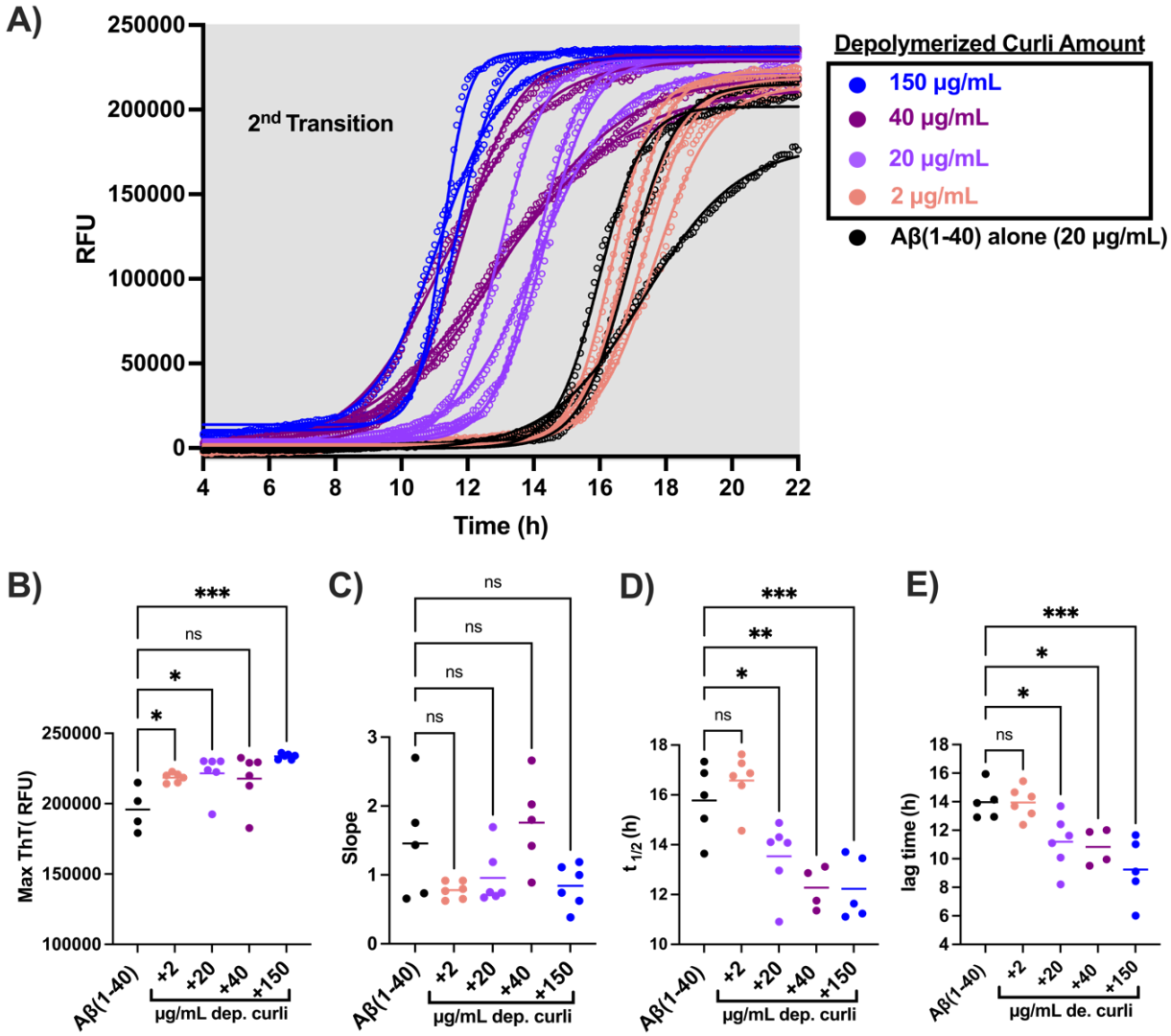

Figure 4.12. Comparing the aggregation kinetics of mixtures of Aβ(1-40) and depolymerized curli in the second transition. A) Solid lines represent the aggregation curves of each mixture fit to the Boltzmann sigmoid model, after the first transition has occurred (data repeated from Figure 4.10 A). The curves in (A) were used to compare the kinetic parameters of the mixtures to kinetic parameters of Aβ(1-40) alone: B) max ThT fluorescence, C) curve slope D) time needed to reach half of the maximum ThT fluorescence (half-time; $t_{1/2}$), and E) lag time. Values were compared by one-way ANOVA: ns: $p > 0.05$; *: $p \leq 0.05$; **: $p \leq 0.01$; ***: $p \leq 0.001$; ****: $p \leq 0.0001$.

The Aβ (1-40)/mature curli curves in **Figure 4.10 B** were fitted to the Boltzmann sigmoid model, and kinetic parameters were obtained (**Figure 4.13**). However, addition of mature curli did not affect any kinetic parameters (**Figure 4.13 B-D**). This indicates that mature curli does not influence the polymerization of Aβ(1-40).

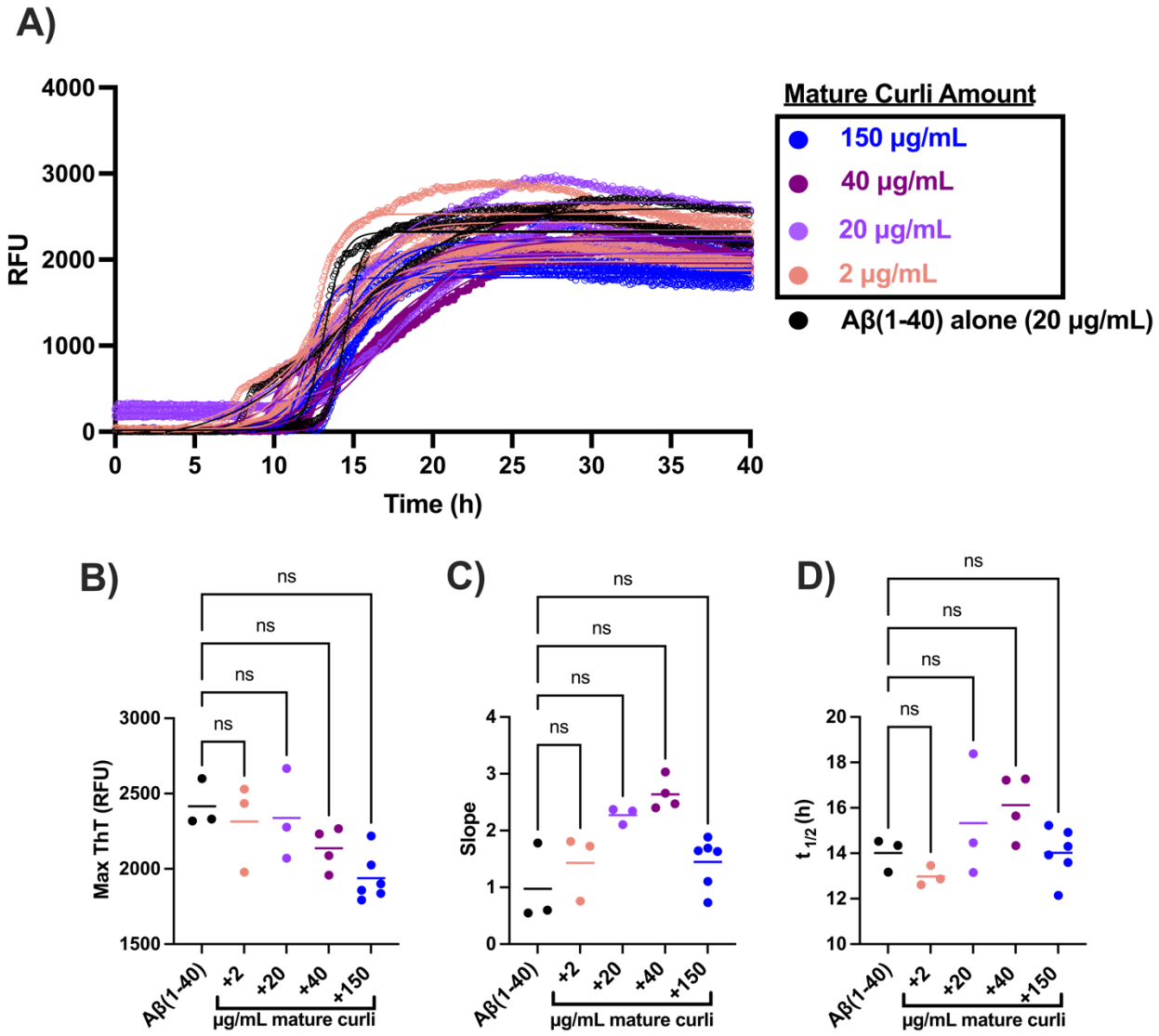

Figure 4.13. Comparing the aggregation kinetics of mixtures of Aβ(1-40) and mature curli. A) Solid lines represent the aggregation curves of each mixture fit to the Boltzmann sigmoid model (data repeated from Figure 4.10 B). The curves in (A) were used to compare the kinetic parameters of the mixtures to kinetic parameters of Aβ(1-40) alone: B) max ThT fluorescence, C) curve slope, and D) time needed to reach half of the maximum ThT fluorescence (half-time; $t_{1/2}$). Values were compared by one-way ANOVA: ns: $p > 0.05$; *: $p \leq 0.05$; **: $p \leq 0.01$; ***: $p \leq 0.001$; ****: $p \leq 0.0001$.

4.5.3 Depolymerized curli seems to rescue cell viability loss due to Aβ(1-42) in *APOE* ε4-positive human fibroblasts.

Previous research has shown that Aβ peptides, particularly Aβ(1–42), can be toxic to mammalian cell lines(Pike *et al.*, 1993; Vadukul *et al.*, 2017). We examined the effect of Aβ peptides, with or without incubation with curli, on the viability of four human fibroblast cell lines from female and male donors that differed in their *APOE* ε4 status, a risk allele for late-onset AD(Nyarko *et al.*, 2018). Cell viability was monitored by measuring changes in mitochondrial respiration, using an MTT conversion assay. Treatment with Aβ(1-42) alone for 24 h significantly decreased cell viability in all four cell lines (black bars in **Figure 4.14**). Depolymerized curli also reduced viability in male and female *APOE* ε4-negative and in female *APOE* ε4-positive fibroblasts (**Figure 4.14**, pink bars). Male *APOE* ε4-positive fibroblasts were not significantly affected by depolymerized curli (**Figure 4.14 A**, pink bars). The combination of depolymerized curli and Aβ(1-42) improved cell viability in male and female *APOE* ε4-positive cell lines, as compared to Aβ(1–42) alone (**Figure 4.14 A** and **B**). However, this effect was less pronounced in female fibroblasts ($p=0.0282$ and $p=0.0331$) compared to male fibroblasts ($p<0.0001$). In contrast, the combination did not have a significant effect on the *APOE* ε4-negative cell lines, as compared to Aβ(1-42) alone (**Figure 4.14 C** and **D**).

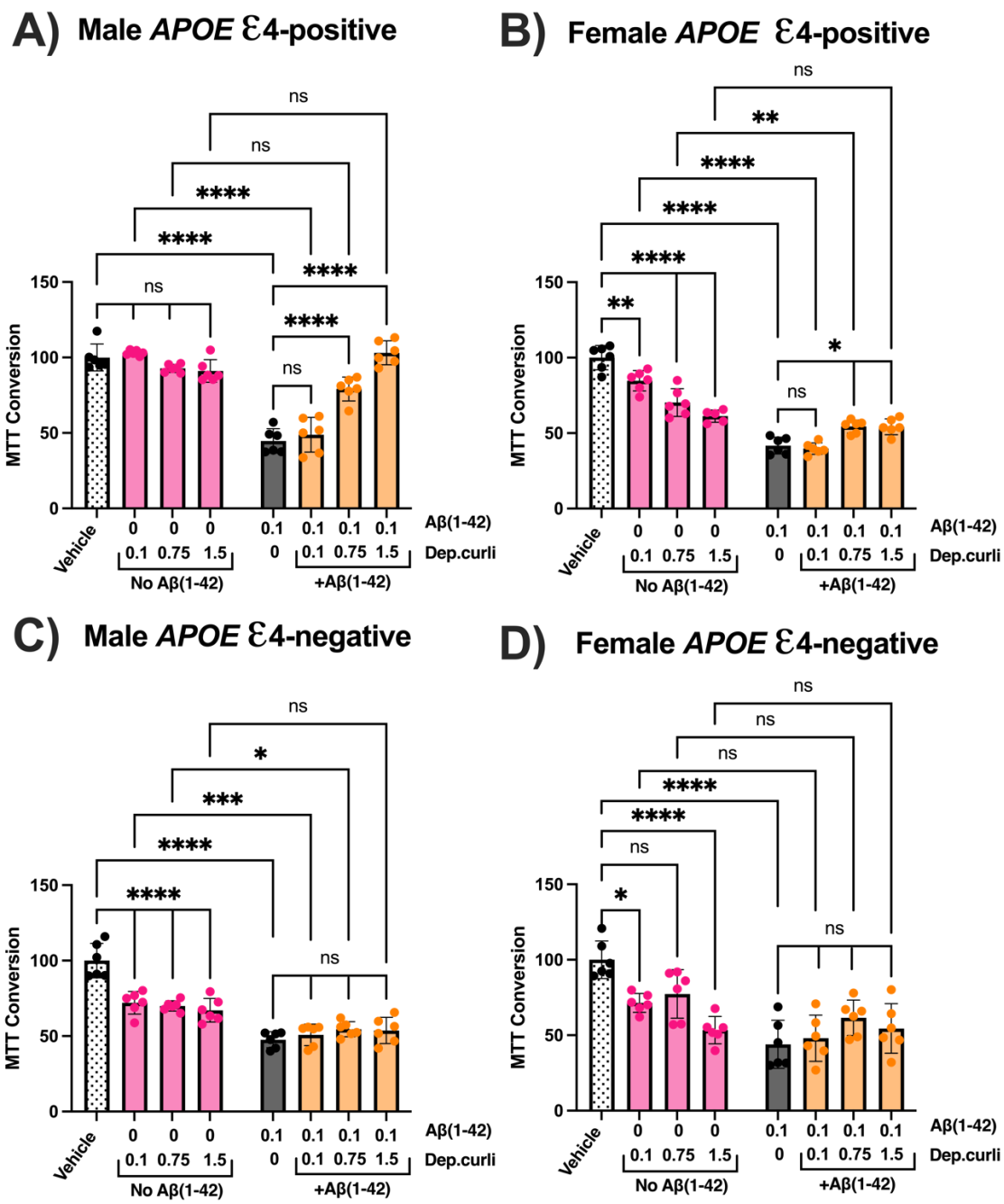

Figure 4.14. Cell viability after Aβ(1-42) and depolymerized curli treatment. MTT conversion used as a reflection of cell viability of A) Male *APOE* ε4-positive, B) female *APOE* ε4-positive, C) male *APOE* ε4-negative and D) female *APOE* ε4-negative fibroblast cultures that were treated (24 h) with concentrations of dep. curli alone, Aβ(1–42) alone or dep. curli + Aβ(1–42) as indicated along the X-axis (labels are in mg/mL). Significance was determined by two-way ANOVA with Tukey's multiple comparisons test (n = 6). *: $p < 0.05$; **: $p < 0.01$; ***: $p < 0.001$; ****: $p < 0.0001$.

We also examined the effects of Aβ(1–42)/mature curli mixtures. Mature curli on its own decreases cell viability in all cell lines (blue bars in **Figure 4.15**). The effect of the co-treatments was not different than the Aβ(1-42) or their corresponding mature curli alone effects (purple bars in **Figure 4.15**).

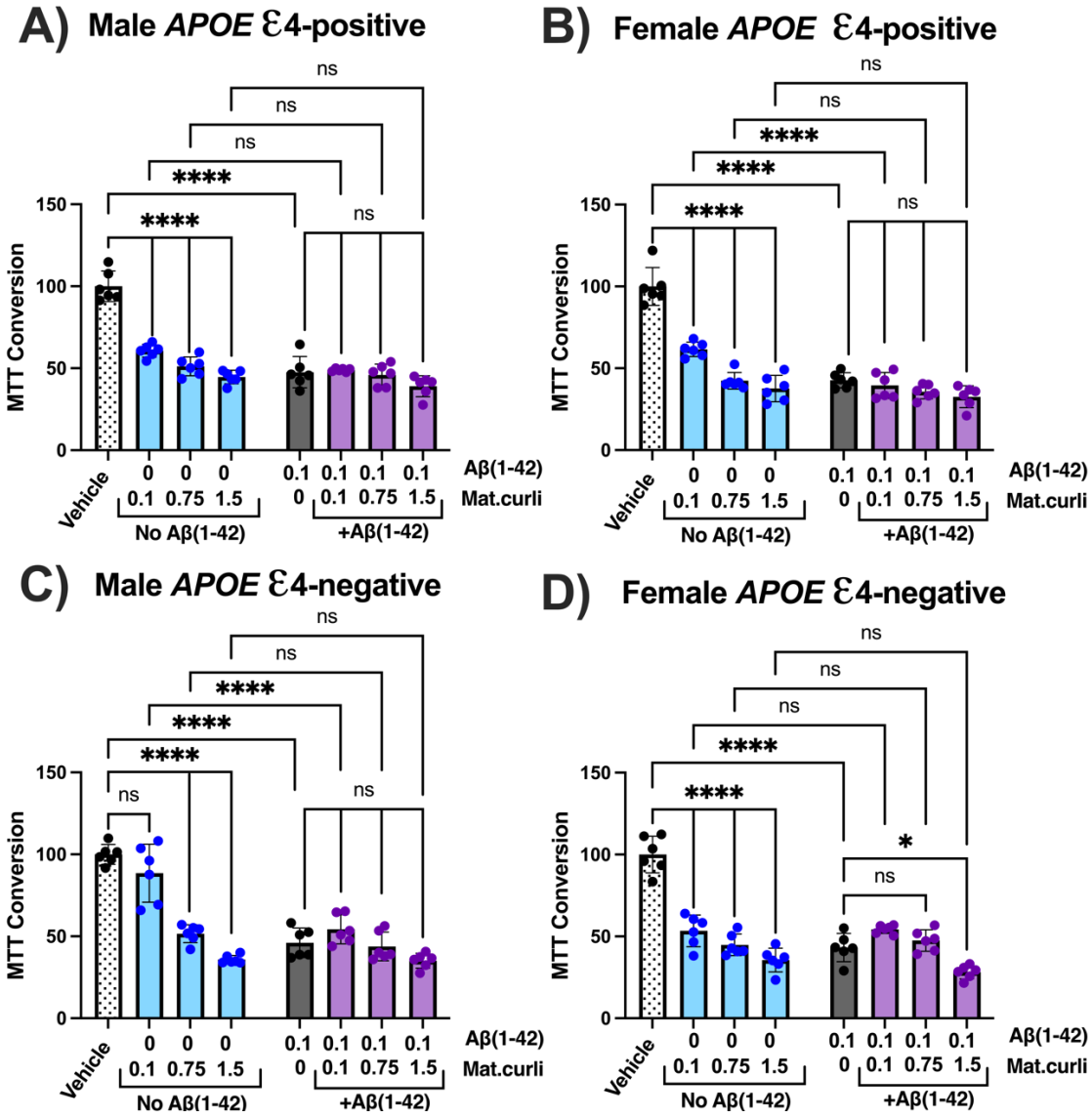

Figure 4.15. Cell viability after Aβ(1-42) and mature curli treatment. MTT conversion used as a reflection of cell viability of A) Male *APOE* ε4-positive, B) female *APOE* ε4-positive, C) male *APOE* ε4-negative and D) female *APOE* ε4-negative fibroblast cultures that were treated (24 h) with concentrations of mat. curli alone, Aβ(1–42) alone or mat. curli + Aβ(1–42) as indicated along the X-axis (labels are in mg/mL). Significance was determined by two-way ANOVA with Tukey's multiple comparisons test ($n = 6$). *: $p < 0.05$; **: $p < 0.01$; ***: $p < 0.001$; ****: $p < 0.0001$.

4.5.4 Cell viability loss due to Aβ(1-40) in human fibroblasts is not affected by depolymerized or mature curli.

Changes in cell viability were also examined for the Aβ(1–40) peptide and depolymerized curli (**Figure 4.16**). Aβ(1-40) affected all cell lines by significantly decreasing viability. Depolymerized curli exerted a significant effect in the *APOE ε4*-negative fibroblasts only (**Figure 4.16 C** and **D**). The effects seen in the co-treatments did not differ from the effect of Aβ(1-40) (orange bars in **Figure 4.16**).

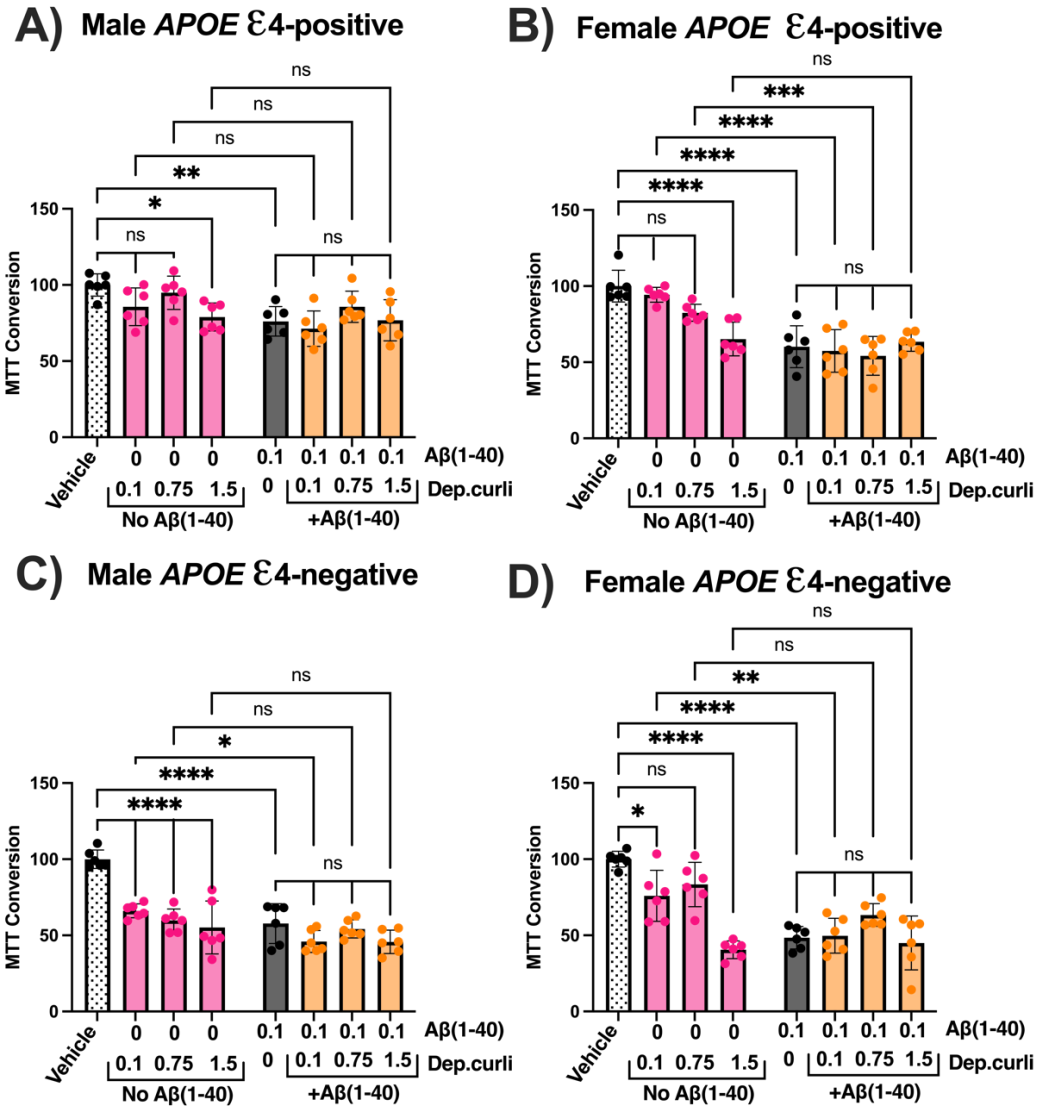

Figure 4.16. Cell viability after Aβ(1-40) and depolymerized curli treatment. MTT conversion used as a reflection of cell viability of A) Male *APOE* ε4-positive, B) female *APOE* ε4-positive,

C) male *APOE* ε4-negative and D) female *APOE* ε4-negative fibroblast cultures that were treated (24 h) with concentrations of dep. curli alone, Aβ(1–40) alone or dep. curli + Aβ(1–40) as indicated along the X-axis (labels are in mg/mL). Significance was determined by two-way ANOVA with Tukey's multiple comparisons test (n = 6). *: $p < 0.05$; **: $p < 0.01$; ***: $p < 0.001$; ****: $p < 0.0001$.

As previously observed, mature curli negatively impacted all cell lines (blue bars in **Figure 4.17**). However, the mixtures with Aβ(1–40) exerted effects that were not significantly different that effects of the pure components (purple bars in **Figure 4.17**).

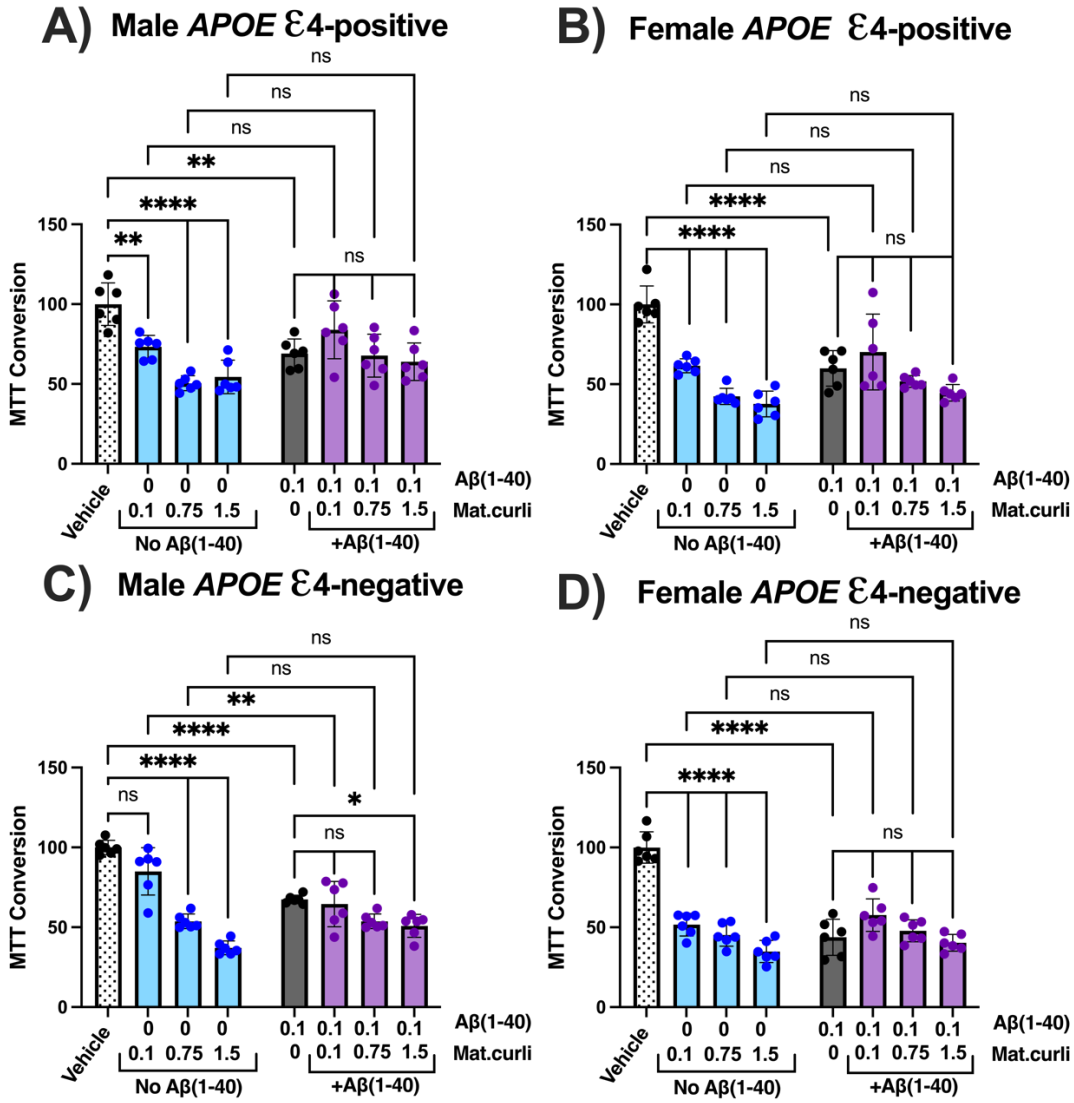

Figure 4.17. Cell viability after Aβ(1-40) and mature curli treatment. MTT conversion used as a reflection of cell viability of A) Male *APOE* ε4-positive, B) female *APOE* ε4-positive, C)

male *APOE* ε4-negative and D) female *APOE* ε4-negative fibroblast cultures that were treated (24 h) with concentrations of mat. curli alone, Aβ(1–40) alone or mat. curli + Aβ(1–40) as indicated along the X-axis (labels are in mg/mL). Significance was determined by two-way ANOVA with Tukey's multiple comparisons test (n=6). *: $p < 0.05$; **: $p < 0.01$; ***: $p < 0.001$; ****: $p < 0.0001$.

4.6 DISCUSSION

To our knowledge my thesis is the first research studying the physical interactions between the bacterial amyloid curli and Aβ peptides associated with AD. Previous research has shown that the aggregation of the PD-associated amyloid protein, α-syn increases in brain neurons of aged rats and muscle cells in nematodes after exposure to curli-producing bacteria (Chen *et al.*, 2016). Another study found that curli fibrils can cause neuroinflammation and contribute to neurodegenerative processes using genome-wide screening in a *C. elegans* model (Wang *et al.*, 2021a). However, these studies have only found correlations between the addition of the bacterial amyloid and neuroinflammation, neuronal cell death or disease pathology, but the exact mechanism of why this occurs, or how curli could modulate host-amyloid aggregation remains to be elucidated. Here, I showed that curli can physically interact with Aβ peptides at the protein-protein interaction level.

Our biophysical analysis revealed that depolymerized curli reduces oligomeric Aβ(1-42). This observation first led us to hypothesize that curli was exerting an inhibitory effect on the peptide´s aggregation. However, we noticed the presence of SDS-resistant material at the top of the wells in the mixed samples which was absent in the Aβ(1-42) control. Such material has been previously characterized as fibrillar content (Cerf *et al.*, 2009). Aβ fibrils are insoluble and resistant to degradation. Quantification of the fibrillar content in the Western blots is difficult to perform and therefore was not done because the fibrils that remain at the top of the well are probably underestimated by this technique. Nevertheless, neither small nor large oligomers were the major species in the mixed samples.

ThT exhibits affinity towards various amyloid fibrils, regardless of their unique amino acid sequences (Biancalana and Koide, 2010). Thus, ThT binds to a shared structural characteristic among fibrils, and can be correlated with the fibril content. Studies have shown a connection

between dye binding and the existence of the cross-β structure found in amyloid fibrils (LeVine, 1995; Khemtemourian *et al.*, 2021). Our data showed that depolymerized curli increases the max ThT fluorescence of the Aβ(1-42) aggregation curves. Although it might seem clear that the increase in the ThT fluorescence would be associated to the increase in the total amyloid protein, the cumulative ThT fluorescence of the two pure proteins was lower than the fluorescence in the mixed systems. It is known that different fibril structures can differentially bind ThT (Lindberg *et al.*, 2015); therefore the change in ThT may correlate with the number of fibrils or reflect a change in the morphology of the fibrils caused by depolymerized curli.

We showed that the effects of depolymerized curli are different on Aβ(1-40). When combined with the shorter alloform, depolymerized curli accelerates the aggregation of Aβ(1-40). Sarroukh *et al.* characterized the aggregation of Aβ(1-40) by bis–Tris SDS-PAGE and 6E10 monoclonal antibody recognition at different timepoints (Sarroukh *et al.*, 2011). In their study, Aβ(1-40) was mostly present as monomers at the beginning of the aggregation process. A diverse collection of oligomers resulted from further aggregation, with dimers and trimers being the predominant species (Sarroukh *et al.*, 2011). Continued aggregation of Aβ(1-40) caused the creation of species with an extraordinarily high molecular weight, which stayed in the stacking gel and were equivalent to fibrils (Sarroukh *et al.*, 2011). This is because the oligomeric content concurrently and gradually decreases during incubation, most likely turning into fibrils (Sarroukh *et al.*, 2011). The stages of Aβ(1-40) aggregation reported by Sarroukh *et al.* (2010) agreed with our observations, but most importantly these stages happen earlier in co-incubated samples. This effect was further confirmed when we looked at the ThT data. Addition of depolymerized curli leads to acceleration of Aβ(1-40) fibril formation seen as a shorter lag phase. This indicates that there is an interaction at the primary nucleation level which favours the aggregation of Aβ(1-40). Thus, the catalytic effect of depolymerized curli on Aβ(1-40) is evident. Previous studies have suggested that in multispecies aggregation the formation of a co-nuclei usually favours and affects the protein with the lowest primary nucleation rate (Cukalevski *et al.*, 2015a; Meisl *et al.*, 2022). Meisl *et al.* (2022) found that the aggregation mechanism of all disease-associated amyloid proteins including Aβ(1-40) and Aβ(1-42) is dominated by secondary processes (secondary nucleation and fibril

fragmentation) rather than primary nucleation which is the pathway that dominates curli aggregation. This could explain why curli catalyzes the formation of a co-nuclei that go on to form Aβ(1-40) fibrils.

In this work, it remains unclear the type of interactions between Aβ and curli. Interactions and cross-reactivity between amyloidogenic proteins are mainly classified in cross-catalysis and co-aggregation processes (Bondarev *et al.*, 2018; Braun *et al.*, 2022; Murakami and Ono, 2022; Subedi *et al.*, 2022). The cross-catalysis process leads to the formation of mainly pure fibrils. In co-aggregation, the formed fibrils are heterogeneous. Both Aβ/depolymerized curli systems produced two-step aggregation curves. This type of curves have been previously reported for Aβ(1-40)/Aβ(1-42) mixtures (Cukalevski *et al.*, 2015a). Cukalevski *et al.* (2015a). used isotope labels in mass spectrometry and NMR spectroscopy to confirm that Aβ(1-40)/Aβ(1-42) monomer mixtures produce homomolecular fibrils and that each sigmoid curve indicates the presence of separate aggregation eventsOther work suggested that Aβ(1-40)/Aβ(1-42) systems may experience some Aβ(1-40)/Aβ(1-42) monomer exchange (Jan *et al.*, 2008). Thus, fibrils formed under binary systems may have some degree of heterogenicity. After examining the aggregation curves of pure proteins, we speculate that at the beginning of the reaction the process is dominated by curli aggregation which corresponds to the first transition, followed by Aβ aggregation (*i.e.*, second transition). However, further research is required to fully comprehend the action mechanism of depolymerized curli and its effects on the structure and toxicity of the final aggregates.

Aβ, especially Aβ(1-42) has been shown to exert cytotoxicity contributing to synaptic dysfunction, neuronal loss, and cognitive impairment (Kayed *et al.*, 2003b; Selkoe, 2008; Vadukul *et al.*, 2017; Shahnawaz *et al.*, 2021). Aβ(1-42) cytotoxic action is thought to be related to its capacity to self-assemble into oligomers and amyloid fibrils (Kayed *et al.*, 2003b; Shahnawaz *et al.*, 2021). Our cell culture assays confirmed that 24-h-incubated Aβ(1-42) promoted a significant loss of cell viability in all the human fibroblast cell lines used in this work, independent of their *APOE* genotype. Interestingly, in *APOE ε4*-positive fibroblast cultures, addition of depolymerized curli recues Aβ(1-42)-mediated mitochondrial dysfunction but has no obvious effect on *APOE ε4*-

negative fibroblasts. The ε4 allele of the lipid transport protein in the plasma, apolipoprotein E (ApoE), is a known genetic risk factor for AD (Corder *et al.*, 1994; Raber *et al.*, 1998; Liu *et al.*, 2013; Michaelson, 2014; Nyarko *et al.*, 2018; Quartey *et al.*, 2021). Humans have three primary apoE isoforms that vary at two residues: apoE2 (Cys112, Cys158), apoE3 (Cys112, Arg158), and apoE4 (Arg112, Arg158). A dose-dependent risk for AD and an earlier beginning of the illness are linked to inheriting one or two copies of the 4 allele (Corder *et al.*, 1994; Raber *et al.*, 1998; Liu *et al.*, 2013; Michaelson, 2014; Nyarko *et al.*, 2018; Quartey *et al.*, 2021). ApoE isoforms affect the production, clearance, and cytoxicity of given oligomers and fibrils in various ways (Drouet *et al.*, 2001; Lauderback *et al.*, 2002; Butterfield and Boyd-Kimball, 2004; Yao *et al.*, 2004). Cell-death pathways have been found to be differently modulated by apoE/Aβ complexes (Drouet *et al.*, 2001; Lauderback *et al.*, 2002; Butterfield and Boyd-Kimball, 2004; Yao *et al.*, 2004). Our findings suggest that cells with an altered genotype, such as *APOE ε4*-positive fibroblasts, are more vulnerable to the effects caused by amyloid exposure.

At this stage of understanding, it could be possible that the loss of MTT conversion in the Aβ(1-42) treatment group is associated to the large oligomeric species which are absent in Aβ(1-42)/ depolymerized curli treatments. It is well acknowledged that increased synthesis of Aβ(1-42) results in Aβ oligomers and fibrils, which eventually contribute to cell death (Kayed *et al.*, 2003b; Shahnawaz *et al.*, 2021). Although fibrillar forms of Aβ have been demonstrated to be hazardous, new research suggests that soluble, oligomeric, and non-fibrillar forms of Aβ are more dangerous than mature fibrils (Walsh *et al.*, 2000; Haass and Selkoe, 2007; Walsh and Selkoe, 2007; Selkoe, 2008; Jin *et al.*, 2011). Therefore, our data suggest that depolymerized curli might be mitigating MTT conversion loss by reducing oligomeric Aβ(1-42). However, the actual mechanism underlying these cytotoxic effects needs to be defined and morphological differences need to be confirmed.

Our cell culture assays using the shorter peptide Aβ(1-40) revealed that this peptide also triggers mitochondrial dysfunction and the *APOE ε4* status also seems to play an important role especially in male cultures. Our observations agree with other reports of Aβ(1-40)-mediated toxicity (Abe and Saito, 1999; Tang and Zhang, 2001; Ramsden *et al.*, 2002; Rönicke *et al.*, 2008) as well as genotype and sex differences (Drouet *et al.*, 2001; Lauderback *et al.*, 2002; Butterfield

and Boyd-Kimball, 2004; Yao *et al.*, 2004; Lennol *et al.*, 2021). Ramsden *et al.* (2002) studied the effects of aggregated and unaggregated forms Aβ(1-40) on cultured rat cortical neurons. They found that aggregated Aβ(1-40) induced apoptotic cell death, as confirmed by MTT and TUNEL assays, while the unaggregated form had no neurotoxic effect(Ramsden *et al.*, 2002). These effects were associated to a disruption in the Ca^{2+} homeostasis by aggregated Aβ(1-40) (Ramsden *et al.*, 2002). Although our biophysical data suggests that depolymerized curli is promoting Aβ(1-40) aggregation, we did not see any differences between Aβ(1-40) alone vs. the co-incubated treatments in our functional data. However, an apparent limitation of the methodology we used is that the differences in the biophysical profiles were incubation-time-dependant. Therefore, a differently approach with a shorter pre-incubation of the treatments or even a set of different pre-incubation times could be considered for future reference.

Various studies have demonstrated that fibril surfaces can catalyze secondary nucleation by increasing the number of templating fibril ends to which soluble precursors (*i.e.*, monomers) are introduced (Ruschak and Miranker, 2007; Cohen *et al.*, 2013; Buell *et al.*, 2014; Cohen *et al.*, 2015) and that processes, such as fibril fragmentation, can also enhance aggregation (Xue *et al.*, 2008). However, addition of mature curli fibrils to any of the Aβ peptides did not show any significant changes in any of our tests. A possible explanation of why we did not observe any effects using mature curli fibrils is that fibril-catalyzed processes are highly specific events (Cukalevski *et al.*, 2015a). Therefore, mature curli fibrils are incapable of catalyzing Aβ polymerization. These observations were reflected in our MTT assays were co-treatment with mature curli did not cause differences in the effects seen with Aβ(1-42) or Aβ(1-40).

My thesis shows that curli can physically interact with Aβ peptides *in vitro* and that this bacterial amyloid can affect the aggregation kinetics of the peptides. However, the interactions between Aβ peptides and curli are likely far more complicated than suggested herein. Thus, whether what we observed here with our functional assays plays a role in AD progression and pathology is something we cannot correlate, and years of further research are needed to explore this aspect.

4.7 CONCLUSIONS

In this study, we showed that the bacterial amyloid curli can physically interact with AD-related Aβ peptides and induce an effect on their aggregation kinetics. Using Western blotting with the anti-Aβ antibody (6E10) and anti-curli immune serum, we screened for Aβ and curli oligomerization after co-incubation. We also used the widely employed ThT assay for measuring fibril formation and found that although differently the aggregation of both Aβ(1-40) and Aβ(1-42) is highly sensitive to the presence of depolymerized but not mature curli fibrils.

Depolymerized curli exerts a significant kinetic modulation on the shorter alloform Aβ(1-40). Depolymerized curli accelerate the aggregation of Aβ(1-40) by reducing the lag time. Our functional assays using human fibroblasts did not show any toxicity differences between Aβ(1-40) and Aβ(1-40)+depolymerized curli treatments however, this could be due to non-optimal experimental conditions and, perhaps, a different experimental design should be used to further study these interactions.

Additionally, we showed that depolymerized curli reduces oligomeric Aβ(1-42) in a dose-dependent manner and likely promotes aggregation which may be associated with the reduced toxicity observed in *APOE ε4*-positive fibroblast cultures treated with co-incubated samples vs. Aβ(1-42) alone. However, the exact conformational species mediating these effects were not characterized and imaging techniques to assess fibril morphology are needed.

Using the ThT assay we identified biphasic aggregation curves in both depolymerized curli+Aβ(1-40) and depolymerized curli+Aβ(1-42) systems. These biphasic curves suggest that separate aggregation processes are occurring at different time-points and more in-depth analysis is required to determine whether curli co-aggregates with the peptides and gets integrated into the final fibril or if aggregation occurs independently and separate homomolecular fibrils are formed.

We found that mature curli fibrils do not affect Aβ aggregation and we did not observe any functional differences. Thus, depolymerized curli, likely the curli´s major subunit CsgA, is a significant factor in curli-Aβ interactions. Finally, our study highlights significant implications for the influence of the APOE risk genotype and sex which warrants further studies to unveil the mechanisms underlying sex and risk factor differences *in vivo*.

Overall, the interactions of curli and Aβ peptides *in vitro* were examined in this thesis. The work in this thesis supports previous findings that bacterial amyloids may influence pathological amyloids. Therefore, further research using a combination of *in vitro* and *in vivo* models is crucial to expanding the knowledge regarding how bacterial amyloids like curli can affect the conformational states of pathological amyloids like Aβ and provide additional functional links between fibril morphology, genotype, and sex mediating pathology.

CHAPTER 5: THESIS SUMMARY, LIMITATIONS AND FUTURE DIRECTIONS

5.1 Thesis Summary

The goal of my M.Sc. research was to assess whether the bacterial amyloid curli and Aβ peptides could physically interact *in vitro*. In the past few years, an increasing amount of attention has been paid to the study of bacterial amyloids and how they could relate to neurodegenerative diseases, including AD (Friedland and Chapman, 2017; Jain and Chapman, 2019; Sampson *et al.*, 2020). Curli fibres, which are formed by S*almonella* and *E. coli* are bacterial amyloids that resemble the 3D structure Aβ fibrils associated with Alzheimer's disease (Perov *et al.*, 2019; Sleutel *et al.*, 2023). A recent study found that curli fibrils can cause neuroinflammation and contribute to neurodegenerative processes using genome-wide screening in a *C. elegans* model (Wang *et al.*, 2021a). These findings have given rise to intriguing hypothesis regarding the part that bacteria and their components play in host neurodegeneration.

While research exploring the potential interactions between bacterial amyloids and pathological amyloids has provided valuable insights (Lundmark *et al.*, 2005; Hartman *et al.*, 2013; Chen *et al.*, 2016; Javed *et al.*, 2020; Miller *et al.*, 2021; Wang *et al.*, 2021a), there is still a lack of comprehensive understanding regarding the precise mechanisms governing the interactions between bacterial and pathological amyloids. Thus, here I used an *in vitro* approach to determine if curli could physically influence the aggregation kinetics of Aβ peptides.

Reproducibility in research using Aβ peptides is a significant issue (Foley and Raskatov, 2020; Faller and Hureau, 2021). Sample variability, assay variability, methodological differences and lack of standardization contribute to the difficulty of reproducing results. These challenges hinder the comparison and replication of findings across different studies. To address these issues and efficiently work with the Aβ peptides, I developed an optimized protocol and found the most appropriate conditions to work with the Aβ peptides (Objective 1 for this thesis, presented in Chapter 3).

Then, I focused my work in proving whether curli could interact and influence Aβ aggregation. I compared polymerization Western blots and ThT aggregation curves of Aβ peptides to other samples containing the same amount of peptide but different amounts of curli (Objective 2 for this thesis, presented in Chapter 4). I showed that the bacterial amyloid curli can interact with

and affect Aβ aggregation. **Figure 5.1** shows a summary of the biophysical interactions between curli and Aβ peptides using the ThT assay.

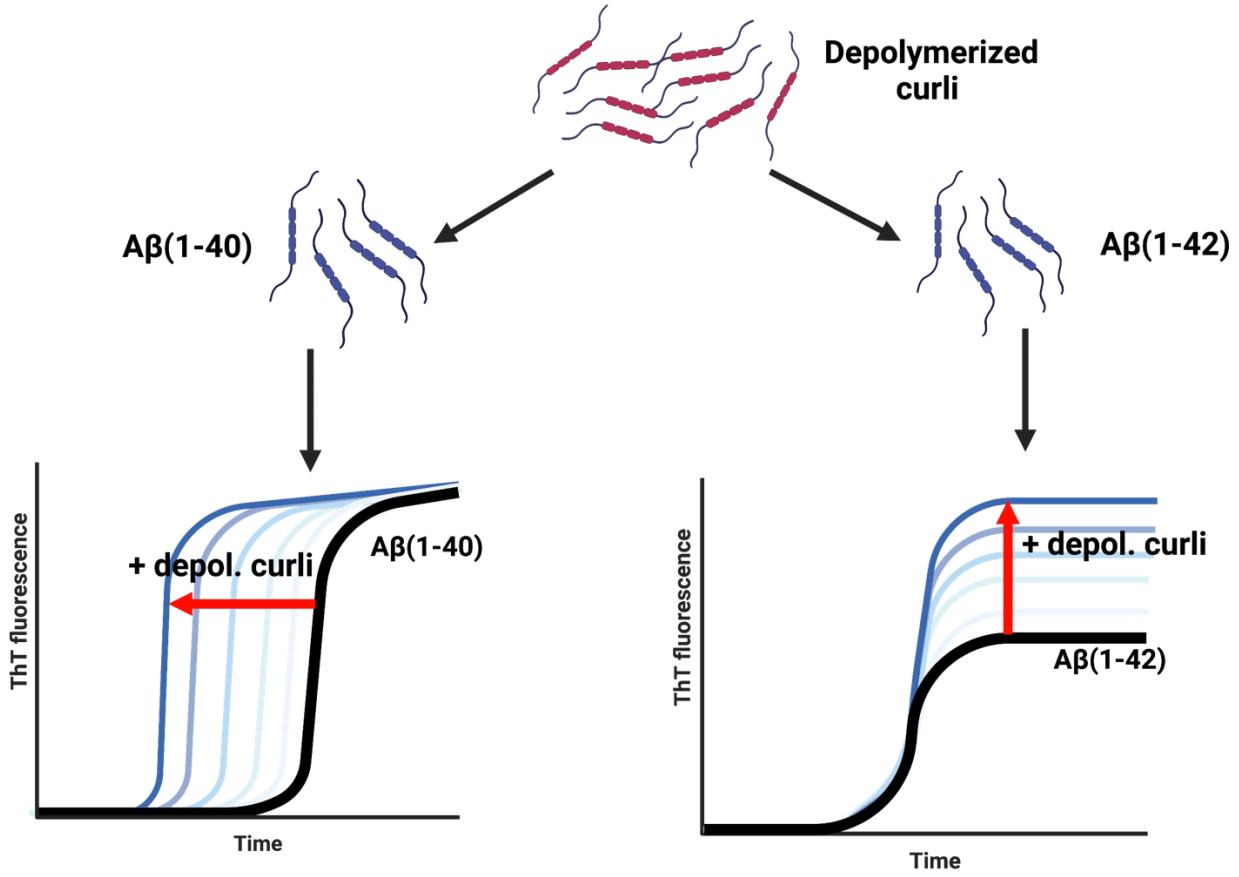

Figure 5.1. Summary of the biophysical interactions between depolymerized curli and Aβ peptides using the ThT aggregation assay. Representative kinetic aggregation curves showing the effects of depolymerized curli on the aggregation curves on Aβ peptides (in black) as observed with the ThT aggregation assay. The black curves show the expected behaviour if the two peptides were to aggregate alone, the blue curves show the behaviour if Aβ is co-incubated with depolymerized curli. For Aβ(1-40), depolymerized curli shifts the aggregation curves to the left reducing the lag time. For Aβ(1-42), depolymerized curli increases the amplitudes of the curve reaching a higher max ThT fluorescence. Mature curli fibrils were excluded from this schematic since they did not affect Aβ aggregation.

The interactions between curli and amyloid beta peptides raised intriguing questions about their role in neurodegenerative diseases and the potential contribution of curli to AD pathology. Therefore, I decided to study the functional implications of these interactions using human

fibroblasts cultures and the MTT assay to assess for cell viability after treatment with 24 h-pre-incubated samples (Objective 3 for this thesis, presented in Chapter 4).

The work in my thesis adds credence to previous studies showing that pathological amyloids may be influenced by bacterial amyloids. However, further investigation is needed to fully understand the mechanisms underlying the interactions between curli and Aβ peptides. Expanding our understanding of how pathological amyloids like Aβ can be affected by bacterial amyloids like curli and how this affects Aβ oligomerization and fibrillization pathways is crucial for developing therapeutic strategies that mitigate the neurotoxic effects of Aβ aggregates in Alzheimer's disease.

5.1 Limitations of this work

While we have published an established protocol for purification of curli fibrils (Sivaranjani *et al.*, 2022), one important limitation in my thesis is that I employed curli fibrils to obtain depolymerized curli in order to mimic CsgA. Although, purification of CsgA is possible (Zhou *et al.*, 2013), we opted against this method due to its inherent complexities. The CsgA purification process requires several days, yields low amounts of purified CsgA, and the protein has a limited shelf life of only one day. Although our chosen approach sought to imitate CsgA, we cannot say how closely the resultant depolymerized material resembles the native CsgA structure. Moreover, we decided to use mature fibrils as a control because we did not observe any interaction with them but the addition of other protein (s) as a control should be considered to assess the specificity of the interactions shown in my thesis.

Another major limitation of my work is that all the experiments were conducted *in vitro*. While *in vitro* studies allow for controlled experimental conditions, they may not accurately reflect the complex interactions that occur in the human body. The absence of biological systems and physiological factors in this study may limit the generalizability of the findings to *in vivo* situations. To comprehend the significance of the interactions between curli and Aβ in disease development and potential treatment implications, further investigation of these interactions in an *in vivo* model is required. Our lab has recently acquired experience with the nematode *C. elegans*. Therefore, using *C. elegans* as an *in vivo* model may be a useful way to learn more about the biological effects and potential implications of the interaction between these two proteins. Genetic manipulation

techniques can be employed to generate *C. elegans* strains expressing curli or Aβ peptides. With the use of this model system, it is possible to investigate the behavioural, pathogenic, and molecular aspects of curli-Aβ interactions as well as any potential implications for AD and other neurodegenerative disorders.

The techniques employed in my thesis project (Thioflavin T assay and Western blots) provide valuable information about the aggregation and detection of amyloid structures but have their own limitations. The thioflavin T assay primarily detects the presence of amyloid fibrils but does not capture the conformational changes (amyloid polymorphisms), subtle interactions between Aβ peptides and curli fibrils or which of the two proteins is aggregating. Similarly, Western blot analysis is limited in its ability to provide detailed insights into the molecular interactions between these two entities. To support conclusions and gain more information, orthogonal methods such as CD spectroscopy, DLS, TEM, and Fourier transform infrared spectroscopy (FTIR) could be applied. However, the nature of the proteins we used in this study gave us a limited number of feasible techniques.

Finally, this study focused primarily on the physical interactions between Aβ peptides and curli fibrils. Although we explored the functional consequences of these interactions using the MTT assay to assess cell viability based on mitochondrial dysfunction of human fibroblasts, understanding how these interactions affect other cellular processes, such, inflammation, calcium homeostasis, cell membrane integrity, ROS production, etc., would provide a more comprehensive understanding of their implications in disease progression and mechanisms of action.

5.2 Future directions

While my thesis provides insights into the interactions between curli and Aβ peptides it also raises several important questions for future research. One of the most intriguing questions is to elucidate the type of interactions and cross-reactivity between these two amyloidogenic proteins. At this point, we cannot say whether the interactions lead to the formation of homomolecular fibrils, composed of a single protein type, or mixed fibrils, which combine both proteins. This is an avenue that should be explored. Using techniques like High-Performance Liquid Chromatography-Mass Spectrometry (HPLC-MS), selectively labelling each protein with two fluorophores, or NMR

solution with curli or the Aβ isotope labelled we could distinguish between the two proteins and clarify if there is some level of co-aggregation or if the aggregation processes occur separately.

Amyloid proteins exhibit remarkable polymorphisms, resulting in diverse fibril structures and conformations (Heise *et al.*, 2005; Paravastu *et al.*, 2008b; Fitzpatrick *et al.*, 2017; Sawaya *et al.*, 2021; Caughey *et al.*, 2022; Li and Liu, 2022). To advance our comprehension of curli-Aβ interactions, it is imperative to further characterize these fibrils. Using advanced imaging techniques such as Cryo-EM or AFM can offer high-resolution structural information, allowing us to elucidate the polymorphic states, structural variations, and dynamics of these amyloid aggregates.

In my work, I examined the cytotoxic effects of the produced fibrils using the MTT assay as a measure of cell viability. However, examining alternative cell culture assays can offer deeper insights into the molecular processes behind the interactions between Aβ and curli. For example, we could complement our findings with cell proliferation assays to measure changes in proliferation rates or cell cycle progression, cell imaging to evaluate changes in cell morphology and differentiation, and immunofluorescence staining to investigate the localization and distribution of the fibrils within the cells.

Considering that amyloid fibrils are associated with oxidative stress and inflammation (Kinney *et al.*, 2018), quantifying reactive oxygen species (ROS) production and measuring pro-inflammatory cytokines (*e.g.*, IL-1, IL-6, TNF-alpha) in cell culture supernatants can provide valuable data.

Additionally, given that my study focused on *Salmonella* curli, future research within the White lab should investigate whether the interactions observed extend to *E. coli* curli. As *E. coli* is a member of the human gut microbiota, exploring the potential interactions with *E. coli* curli can broaden the scope of understanding as well going beyond the imposed restriction of having a *Salmonella* infection to be potentially exposed to curli.

APPENDIX

Curli aggregation assessed by Western blot

Blotted membranes were simultaneously probed with the 6E10 anti-Aβ antibody and anti-curli immune serum as primary antibody and two fluorescent labelled secondary antibodies with different spectrum wavelength with allowed us to assess curli and Aβ aggregation on the same membrane. **Supplementary Figure 1** shows representative blots of curli aggregation in the four experimental settings.

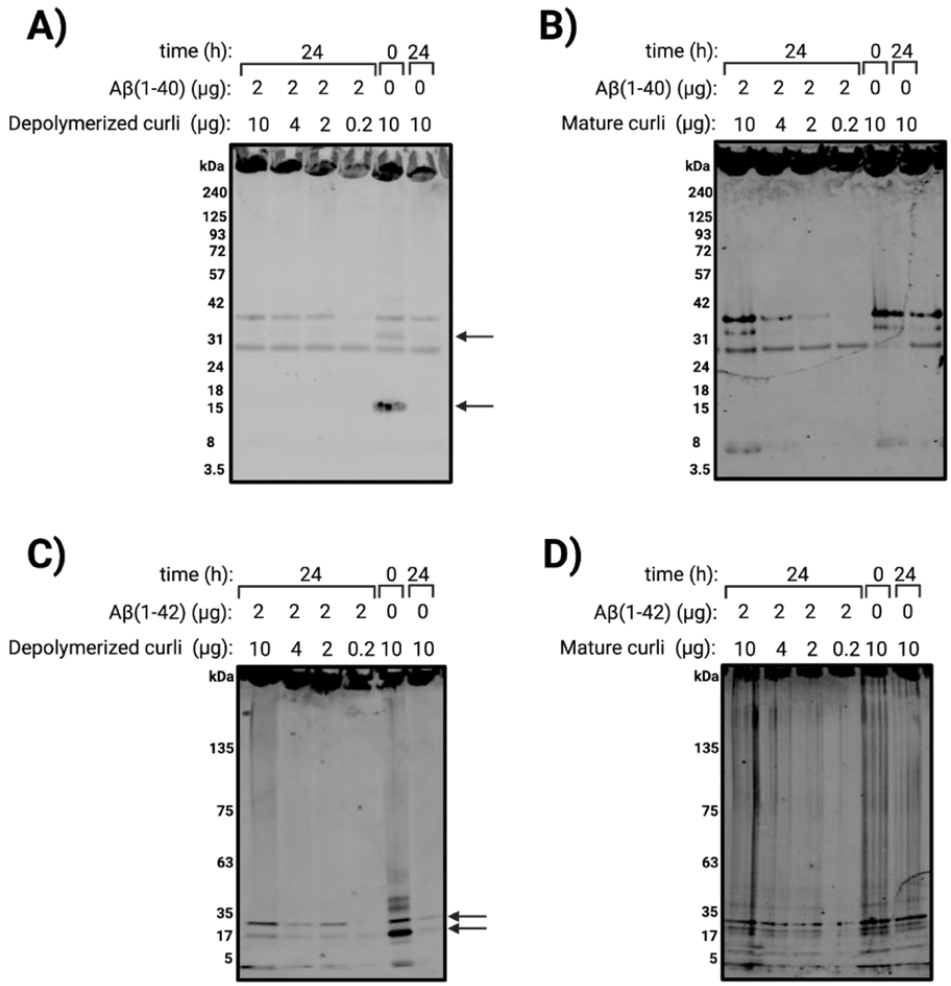

Supplementary Figure 1. Representative Western blot analysis of depolymerized and mature curli fibrils after co-incubation with Aβ(1–40) or Aβ(1–42). 2 μg of Aβ peptides were incubated with 0.2-10 μg of depolymerized curli (A and C) or mature curli (B and D). Curli was monitored with in-house anti-curli immune serum, followed by fluorophore-conjugated 700RD Goat-Anti-Rabbit IgG secondary antibody. (Li-Cor Biosciences).

REFERENCES

Abe, K., and Saito, H. (1999). Both oxidative stress-dependent and independent effects of amyloid β protein are detected by 3-(4,5-dimethylthiazol-2-yl)-2,5-diphenyltetrazolium bromide (MTT) reduction assay. *Brain Res. J.* 830**,** 146-154.

Abelein, A., Jarvet, J., Barth, A., Graslund, A., and Danielsson, J. (2016). Ionic strength modulation of the free energy landscape of Aβ40 peptide fibril formation. *J. Am. Chem. Soc.* 138**,** 6893-6902.

Abeysinghe, A.a.D.T., Deshapriya, R.D.U.S., and Udawatte, C. (2020). Alzheimer's disease; a review of the pathophysiological basis and therapeutic interventions. *Life Sci.* 256**,** 117996.

Afanasieva, E.G., Kushnirov, V.V., and Ter-Avanesyan, M.D. (2011). Interspecies transmission of prions. *Biochem. (Mosc.)* 76**,** 1375-1384.

Almeida, Z.L., and Brito, R.M.M. (2020). Structure and Aggregation Mechanisms in Amyloids. *Molecules* 25.

Anand, B.G., Dubey, K., Shekhawat, D.S., and Kar, K. (2017). Intrinsic property of phenylalanine to trigger protein aggregation and hemolysis has a direct relevance to phenylketonuria. *Sci. Rep.* 7**,** 11146.

Anand, B.G., Prajapati, K.P., and Kar, K. (2018). Aβ1-40 mediated aggregation of proteins and metabolites unveils the relevance of amyloid cross-seeding in amyloidogenesis. *BBRC* 501**,** 158-164.

Ananias, M., and Yano, T. (2008). Serogroups and virulence genotypes of Escherichia coli isolated from patients with sepsis. *Braz. J. Med. Biol.* 41**,** 877-883.

Arosio, P., Knowles, T.P., and Linse, S. (2015). On the lag phase in amyloid fibril formation. *Phys. Chem. Chem. Phys.* 17**,** 7606-7618.

Auer, S. (2014). Amyloid fibril nucleation: effect of amino acid hydrophobicity. *J Phys Chem B* 118**,** 5289-5299.

Balbach, J.J., Ishii, Y., Antzutkin, O.N., Leapman, R.D., Rizzo, N.W., Dyda, F., Reed, J., and Tycko, R. (2000). Amyloid Fibril Formation by Aβ16-22, a Seven-Residue Fragment of the Alzheimer's β-Amyloid Peptide, and Structural Characterization by Solid State NMR. *Biochemistry* 39**,** 13748-13759.

Balbach, J.J., Petkova, A.T., Oyler, N.A., Antzutkin, O.N., Gordon, D.J., Meredith, S.C., and Tycko, R. (2002). Supramolecular Structure in Full-Length Alzheimer's β-Amyloid Fibrils: Evidence for a Parallel β-Sheet Organization from Solid-State Nuclear Magnetic Resonance. *Biophys. J.* 83**,** 1205-1216.

Baldwin, A.J., Knowles, T.P., Tartaglia, G.G., Fitzpatrick, A.W., Devlin, G.L., Shammas, S.L., Waudby, C.A., Mossuto, M.F., Meehan, S., Gras, S.L., Christodoulou, J., Anthony-Cahill, S.J., Barker, P.D., Vendruscolo, M., and Dobson, C.M. (2011). Metastability of native proteins and the phenomenon of amyloid formation. *J. Am. Chem. Soc.* 133**,** 14160-14163.

Barron, R.M. (2017). Infectious prions and proteinopathies. *Prion* 11**,** 40-47.

Barrow, C.J., Yasuda, A., Kenny, P.T., and Zagorski, M.G. (1992). Solution conformations and aggregational properties of synthetic amyloid beta-peptides of Alzheimer's disease. Analysis of circular dichroism spectra. *J Mol Biol* 225**,** 1075-1093.

Barrow, C.J., and Zagorski, M.G. (1991). Solution structures of beta peptide and its constituent fragments: relation to amyloid deposition. *Science* 253**,** 179-182.

Batzli, K.M., and Love, B.J. (2015). Agitation of amyloid proteins to speed aggregation measured by ThT fluorescence: A call for standardization. *Mater. Sci. Eng. C* 48**,** 359-364.

Bellenguez, C., Küçükali, F., Jansen, I.E., et al. (2022). New insights into the genetic etiology of Alzheimer's disease and related dementias. *Nat. Genet* 54**,** 412-436.

Ben Nasr, A., Olsén, A., Sjöbring, U., Müller-Esterl, W., and Björck, L. (1996). Assembly of human contact phase proteins and release of bradykinin at the surface of curli-expressing Escherichia coli. *Mol. Microbiol.* 20**,** 927-935.

Benson, M.D. (2023). "Amyloidosis and other protein deposition diseases," in *Emery and Rimoin's Principles and Practice of Medical Genetics and Genomics*. Elsevier), 213-235.

Benzinger, T.L.S., Gregory, D.M., Burkoth, T.S., Miller-Auer, H., Lynn, D.G., Botto, R.E., and Meredith, S.C. (1998). Propagating structure of Alzheimer's β-amyloid(10–35) is parallel β-sheet with residues in exact register. *Proc. Natl. Acad. Sci. U.S.A.* 95**,** 13407-13412.

Bhoite, S., Van Gerven, N., Chapman, M.R., and Remaut, H. (2019). Curli Biogenesis: Bacterial Amyloid Assembly by the Type VIII Secretion Pathway. *EcoSal Plus* 8.

Bhowmik, D., Maclaughlin, C.M., Chandrakesan, M., Ramesh, P., Venkatramani, R., Walker, G.C., and Maiti, S. (2014). pH changes the aggregation propensity of amyloid-β without altering the monomer conformation. *Phys. Chem. Chem. Phys.* 16**,** 885-889.

Bian, Z., Brauner, A., Li, Y., and Normark, S. (2000). Expression of and cytokine activation by Escherichia coli curli fibers in human sepsis. *J. Infect. Dis.* 181**,** 602-612.

Biancalana, M., and Koide, S. (2010). Molecular mechanism of Thioflavin-T binding to amyloid fibrils. *Biochim Biophys Acta Proteins Proteom* 1804**,** 1405-1412.

Biancalana, M., Makabe, K., Koide, A., and Koide, S. (2009). Molecular Mechanism of Thioflavin-T Binding to the Surface of β-Rich Peptide Self-Assemblies. *J. Mol. Biol.* 385**,** 1052-1063.

Bitan, G., Kirkitadze, M.D., Lomakin, A., Vollers, S.S., Benedek, G.B., and Teplow, D.B. (2003). Amyloid beta -protein (Abeta) assembly: Abeta 40 and Abeta 42 oligomerize through distinct pathways. *Proc. Natl. Acad. Sci. U.S.A.* 100**,** 330-335.

Blanco, L.P., Evans, M.L., Smith, D.R., Badtke, M.P., and Chapman, M.R. (2012). Diversity, biogenesis and function of microbial amyloids. *Trends Microbiol.* 20**,** 66-73.

Bolder, S.G., Sagis, L.M., Venema, P., and Van Der Linden, E. (2007). Thioflavin T and birefringence assays to determine the conversion of proteins into fibrils. *Langmuir* 23**,** 4144-4147.

Bolmont, T., Clavaguera, F., Meyer-Luehmann, M., Herzig, M.C., Radde, R., Staufenbiel, M., Lewis, J., Hutton, M., Tolnay, M., and Jucker, M. (2007). Induction of Tau Pathology by Intracerebral Infusion of Amyloid-β-Containing Brain Extract and by Amyloid-β Deposition in APP × Tau Transgenic Mice. *Am. J. Pathol.* 171**,** 2012-2020.

Bondarev, S.A., Antonets, K.S., Kajava, A.V., Nizhnikov, A.A., and Zhouravleva, G.A. (2018). Protein Co-Aggregation Related to Amyloids: Methods of Investigation, Diversity, and Classification. *Int. J. Mol. Sci.* 19**,** 2292.

Bordeau, V., and Felden, B. (2014). Curli synthesis and biofilm formation in enteric bacteria are controlled by a dynamic small RNA module made up of a pseudoknot assisted by an RNA chaperone. *Nucleic Acids Res.* 42**,** 4682-4696.

Bousset, L., Pieri, L., Ruiz-Arlandis, G., Gath, J., Jensen, P.H., Habenstein, B., Madiona, K., Olieric, V., Böckmann, A., Meier, B.H., and Melki, R. (2013). Structural and functional characterization of two alpha-synuclein strains. *Nat. Commun.* 4**,** 2575.

Braun, G.A., Dear, A.J., Sanagavarapu, K., Zetterberg, H., and Linse, S. (2022). Amyloid-β peptide 37, 38 and 40 individually and cooperatively inhibit amyloid-β 42 aggregation. *Chem. Sci. J.* 13**,** 2423-2439.

Broersen, K., Jonckheere, W., Rozenski, J., Vandersteen, A., Pauwels, K., Pastore, A., Rousseau, F., and Schymkowitz, J. (2011). A standardized and biocompatible preparation of aggregate-free amyloid beta peptide for biophysical and biological studies of Alzheimer's disease. *Protein Eng. Des. Sel.* 24**,** 743-750.

Browning, S.R., Mason, G.L., Seward, T., Green, M., Eliason, G.A., Mathiason, C., Miller, M.W., Williams, E.S., Hoover, E., and Telling, G.C. (2004). Transmission of prions from mule deer and elk with chronic wasting disease to transgenic mice expressing cervid PrP. *Virol. J.* 78**,** 13345-13350.

Buell, A.K., Galvagnion, C., Gaspar, R., Sparr, E., Vendruscolo, M., Knowles, T.P.J., Linse, S., and Dobson, C.M. (2014). Solution conditions determine the relative importance of nucleation and growth processes in α-synuclein aggregation. *Proc. Natl. Acad. Sci. U.S.A.* 111**,** 7671-7676.

Burdick, D., Soreghan, B., Kwon, M., Kosmoski, J., Knauer, M., Henschen, A., Yates, J., Cotman, C., and Glabe, C. (1992). Assembly and aggregation properties of synthetic Alzheimer's A4/beta amyloid peptide analogs. *J. Biol. Chem.* 267**,** 546-554.

Butterfield, D.A., and Boyd-Kimball, D. (2004). Amyloid β-Peptide(1-42) Contributes to the Oxidative Stress and Neurodegeneration Found in Alzheimer Disease Brain. *Brain Pathol.* 14**,** 426-432.

Cabaleiro-Lago, C., Quinlan-Pluck, F., Lynch, I., Lindman, S., Minogue, A.M., Thulin, E., Walsh, D.M., Dawson, K.A., and Linse, S. (2008). Inhibition of Amyloid β Protein Fibrillation by Polymeric Nanoparticles. *J. Am. Chem. Soc.* 130**,** 15437-15443.

Castellino, F.J., and Ploplis, V.A. (2005). Structure and function of the plasminogen/plasmin system. *JTH* 93**,** 647-654.

Castilla, J., Gonzalez-Romero, D., Saá, P., Morales, R., De Castro, J., and Soto, C. (2008). Crossing the species barrier by PrP(Sc) replication in vitro generates unique infectious prions. *Cell* 134**,** 757-768.

Caughey, B., Standke, H.G., Artikis, E., Hoyt, F., and Kraus, A. (2022). Pathogenic prion structures at high resolution. *PLoS Pathog* 18**,** e1010594.

Cerf, E., Sarroukh, R., Tamamizu-Kato, S., Breydo, L., Derclaye, S., Dufrêne, Y.F., Narayanaswami, V., Goormaghtigh, E., Ruysschaert, J.M., and Raussens, V. (2009). Antiparallel beta-sheet: a signature structure of the oligomeric amyloid beta-peptide. *Biochem. J.* 421**,** 415-423.

Chan, C.X., El-Kirat-Chatel, S., Joseph, I.G., Jackson, D.N., Ramsook, C.B., Dufrêne, Y.F., and Lipke, P.N. (2016). Force Sensitivity in Saccharomyces cerevisiae Flocculins. *mSphere* 1.

Chan, C.X., and Lipke, P.N. (2014). Role of force-sensitive amyloid-like interactions in fungal catch bonding and biofilms. *EC* 13**,** 1136-1142.

Chapman, M.R., Robinson, L.S., Pinkner, J.S., Roth, R., Heuser, J., Hammar, M., Normark, S., and Hultgren, S.J. (2002). Role of Escherichia coli curli operons in directing amyloid fiber formation. *Science* 295**,** 851-855.

Chen, S.G., Stribinskis, V., Rane, M.J., Demuth, D.R., Gozal, E., Roberts, A.M., Jagadapillai, R., Liu, R., Choe, K., Shivakumar, B., Son, F., Jin, S., Kerber, R., Adame, A., Masliah, E., and Friedland, R.P. (2016). Exposure to the Functional Bacterial Amyloid Protein Curli Enhances Alpha-Synuclein Aggregation in Aged Fischer 344 Rats and Caenorhabditis elegans. *Sci. Rep.* 6**,** 34477.

Cherny, I., Rockah, L., Levy-Nissenbaum, O., Gophna, U., Ron, E.Z., and Gazit, E. (2005). The formation of Escherichia coli curli amyloid fibrils is mediated by prion-like peptide repeats. *J. Mol. Biol.* 352**,** 245-252.

Chia, S., Flagmeier, P., Habchi, J., Lattanzi, V., Linse, S., Dobson, C.M., Knowles, T.P.J., and Vendruscolo, M. (2017). Monomeric and fibrillar α-synuclein exert opposite effects on the catalytic cycle that promotes the proliferation of Aβ42 aggregates. *Proc Natl Acad Sci U S A* 114**,** 8005-8010.

Chiti, F., and Dobson, C.M. (2006). Protein Misfolding, Functional Amyloid, and Human Disease. *Annu. Rev. Biochem.* 75**,** 333-366.

Cintron, A.F., Dalal, N.V., Dooyema, J., Betarbet, R., and Walker, L.C. (2015). Transport of cargo from periphery to brain by circulating monocytes. *Brain Res. J.* 1622**,** 328-338.

Coalier, K.A., Paranjape, G.S., Karki, S., and Nichols, M.R. (2013). Stability of early-stage amyloid-β(1-42) aggregation species. *BBA* 1834**,** 65-70.

Cohen, A., Shirahama, T., and Skinner, M. (1982). Electron microscopy of amyloid. *Electron microscopy of proteins* 3**,** 165-205.

Cohen, S.I.A., Arosio, P., Presto, J., Kurudenkandy, F.R., Biverstål, H., Dolfe, L., Dunning, C., Yang, X., Frohm, B., Vendruscolo, M., Johansson, J., Dobson, C.M., Fisahn, A., Knowles, T.P.J., and Linse, S. (2015). A molecular chaperone breaks the catalytic cycle that generates toxic Aβ oligomers. *Nat. Struct. Mol. Biol.* 22**,** 207-213.

Cohen, S.I.A., Linse, S., Luheshi, L.M., Hellstrand, E., White, D.A., Rajah, L., Otzen, D.E., Vendruscolo, M., Dobson, C.M., and Knowles, T.P.J. (2013). Proliferation of amyloid-β42 aggregates occurs through a secondary nucleation mechanism. *Proc. Natl. Acad. Sci. U.S.A.* 110**,** 9758-9763.

Collinge, J., and Clarke, A.R. (2007). A General Model of Prion Strains and Their Pathogenicity. *Science* 318**,** 930-936.

Collinson, S.K., Clouthier, S.C., Doran, J.L., Banser, P.A., and Kay, W.W. (1996). Salmonella enteritidis agfBAC operon encoding thin, aggregative fimbriae. *J. Bacteriol* 178**,** 662-667.

Collinson, S.K., Doig, P.C., Doran, J.L., Clouthier, S., Trust, T.J., and Kay, W.W. (1993). Thin, aggregative fimbriae mediate binding of Salmonella enteritidis to fibronectin. *J. Bacteriol* 175**,** 12-18.

Collinson, S.K., Emödy, L., Müller, K.H., Trust, T.J., and Kay, W.W. (1991). Purification and characterization of thin, aggregative fimbriae from Salmonella enteritidis. *J. Bacteriol* 173**,** 4773-4781.

Collinson, S.K., Parker, J.M., Hodges, R.S., and Kay, W.W. (1999). Structural predictions of AgfA, the insoluble fimbrial subunit of Salmonella thin aggregative fimbriae. *J. Mol. Biol* 290**,** 741-756.

Corder, E., Saunders, A.M., Risch, N., Strittmatter, W., Schmechel, D., Gaskell Jr, P., Rimmler, J., Locke, P., Conneally, P., and Schmader, K. (1994). Protective effect of apolipoprotein E type 2 allele for late onset Alzheimer disease. *Nat. Genet* 7**,** 180-184.

Cruchaga, C., Chakraverty, S., Mayo, K., Vallania, F.L.M., Mitra, R.D., Faber, K., Williamson, J., Bird, T., Diaz-Arrastia, R., Foroud, T.M., Boeve, B.F., Graff-Radford, N.R., St. Jean, P., Lawson, M., Ehm, M.G., Mayeux, R., Goate, A.M., and For The, N.I.a.L.N.F.S.C. (2012). Rare Variants in APP, PSEN1 and PSEN2 Increase Risk for AD in Late-Onset Alzheimer's Disease Families. *PLoS One* 7**,** e31039.

Cukalevski, R., Yang, X., Meisl, G., Weininger, U., Bernfur, K., Frohm, B., Knowles, T.P.J., and Linse, S. (2015a). The Aβ40 and Aβ42 peptides self-assemble into separate homomolecular fibrils in binary mixtures but cross-react during primary nucleation. *Chem Sci* 6**,** 4215-4233.

Cukalevski, R., Yang, X., Meisl, G., Weininger, U., Bernfur, K., Frohm, B., Knowles, T.P.J., and Linse, S. (2015b). The Aβ40 and Aβ42 peptides self-assemble into separate homomolecular fibrils in binary mixtures but cross-react during primary nucleation. *Chem. Sci.* 6**,** 4215-4233.

Cummings, J., Feldman, H.H., and Scheltens, P. (2019). The "rights" of precision drug development for Alzheimer's disease. *Alzheimer's Res. Ther.* 11**,** 76.

Dahlgren, K.N., Manelli, A.M., Blaine Stine Jr, W., Baker, L.K., Krafft, G.A., and Ladu, M.J. (2002). Oligomeric and fibrillar species of amyloid-β peptides differentially affect neuronal viability. *J Biol Chem* 277**,** 32046-32053.

De Oliveira, D.C.V., Fernandes Junior, A., Kaneno, R., Silva, M.G., Araujo Junior, J.P., Silva, N.C.C., and Rall, V.L.M. (2014). Ability of Salmonella spp. to produce biofilm is dependent on temperature and surface material. *Foodborne Pathog. Dis.* 11**,** 478-483.

Delpak, A., and Talebi, M. (2020). On the impact of age, gender and educational level on cognitive function in Alzheimer's disease: A quantitative approach. *Arch. Gerontol. Geriatr.* 89**,** 104090.

Desai, S.K., Padmanabhan, A., Harshe, S., Zaidel-Bar, R., and Kenney, L.J. (2019). Salmonella biofilms program innate immunity for persistence in Caenorhabditis elegans. *Proc. Natl. Acad. Sci. U.S.A.* 116**,** 12462-12467.

Desplats, P., Lee, H.J., Bae, E.J., Patrick, C., Rockenstein, E., Crews, L., Spencer, B., Masliah, E., and Lee, S.J. (2009). Inclusion formation and neuronal cell death through neuron-to-neuron transmission of alpha-synuclein. *Proc. Natl. Acad. Sci. U.S.A.* 106**,** 13010-13015.

Dhillon, S. (2021). Aducanumab: First Approval. *Drugs* 81**,** 1437-1443.

Di Berardo, C., Capstick, D.S., Bibb, M.J., Findlay, K.C., Buttner, M.J., and Elliot, M.A. (2008). Function and redundancy of the chaplin cell surface proteins in aerial hypha formation, rodlet assembly, and viability in Streptomyces coelicolor. *J. Bacteriol.* 190**,** 5879-5889.

Doran, E., Keator, D., Head, E., Phelan, M.J., Kim, R., Totoiu, M., Barrio, J.R., Small, G.W., Potkin, S.G., and Lott, I.T. (2017). Down Syndrome, Partial Trisomy 21, and Absence of Alzheimer's Disease: The Role of APP. *J Alzheimers Dis* 56**,** 459-470.

Drouet, B., Fifre, A., Pinçon-Raymond, M., Vandekerckhove, J., Rosseneu, M., Guéant, J.L., Chambaz, J., and Pillot, T. (2001). ApoE protects cortical neurones against neurotoxicity induced by the non-fibrillar C-terminal domain of the amyloid-β peptide. *J. Neurochem.* 76**,** 117-127.

Dubey, K., Anand, B.G., Temgire, M.K., and Kar, K. (2014). Evidence of Rapid Coaggregation of Globular Proteins during Amyloid Formation. *Biochemistry* 53**,** 8001-8004.

Dueholm, M.S., Albertsen, M., Otzen, D., and Nielsen, P.H. (2012). Curli functional amyloid systems are phylogenetically widespread and display large diversity in operon and protein structure. *PLoS One* 7**,** e51274.

Dueholm, M.S., Petersen, S.V., Sønderkær, M., Larsen, P., Christiansen, G., Hein, K.L., Enghild, J.J., Nielsen, J.L., Nielsen, K.L., Nielsen, P.H., and Otzen, D.E. (2010). Functional amyloid in Pseudomonas. *Mol. Microbiol.* 77**,** 1009-1020.

Dueholm, M.S., Sondergaard, M.T., Nilsson, M., Christiansen, G., Stensballe, A., Overgaard, M.T., Givskov, M., Tolker-Nielsen, T., Otzen, D.E., and Nielsen, P.H. (2013). Expression of Fap amyloids in Pseudomonas aeruginosa, P. fluorescens, and P. putida results in aggregation and increased biofilm formation. *Microbiologyopen* 2**,** 365-382.

Dumitrescu, L., Barnes, L.L., Thambisetty, M., et al. (2019). Sex differences in the genetic predictors of Alzheimer's pathology. *Brain* 142**,** 2581-2589.

Edskes, H.K., Mccann, L.M., Hebert, A.M., and Wickner, R.B. (2009). Prion Variants and Species Barriers Among Saccharomyces Ure2 Proteins. *Genetics* 181**,** 1159-1167.

Eisele, Y.S., Obermüller, U., Heilbronner, G., Baumann, F., Kaeser, S.A., Wolburg, H., Walker, L.C., Staufenbiel, M., Heikenwalder, M., and Jucker, M. (2010). Peripherally applied Abeta-containing inoculates induce cerebral beta-amyloidosis. *Science* 330**,** 980-982.

El Hag, M., Feng, Z., Su, Y., Wang, X., Yassin, A., Chen, S., Peng, D., and Liu, X. (2017). Contribution of the csgA and bcsA genes to Salmonella enterica serovar Pullorum biofilm formation and virulence. *Avian Pathol.* 46**,** 541-547.

Elkins, M.R., Wang, T., Nick, M., Jo, H., Lemmin, T., Prusiner, S.B., Degrado, W.F., Stöhr, J., and Hong, M. (2016). Structural Polymorphism of Alzheimer's β-Amyloid Fibrils as Controlled by an E22 Switch: A Solid-State NMR Study. *J. Am. Chem. Soc.* 138**,** 9840-9852.

Evans, M.L., Chorell, E., Taylor, J.D., Aden, J., Gotheson, A., Li, F., Koch, M., Sefer, L., Matthews, S.J., Wittung-Stafshede, P., Almqvist, F., and Chapman, M.R. (2015). The bacterial curli system possesses a potent and selective inhibitor of amyloid formation. *Mol. Cell* 57**,** 445-455.

Evans, M.L., Gichana, E., Zhou, Y., and Chapman, M.R. (2018). "Bacterial Amyloids," in *Amyloid Proteins: Methods and Protocols,* eds. E.M. Sigurdsson, M. Calero & M. Gasset. (New York, NY: Springer New York), 267-288.

Faller, P., and Hureau, C. (2021). Reproducibility Problems of Amyloid-β Self-Assembly and How to Deal With Them. *Front. Chem.* 8.

Fazeli-Nasab, B., Sayyed, R.Z., Mojahed, L.S., Rahmani, A.F., Ghafari, M., Antonius, S., and Sukamto (2022). Biofilm production: A strategic mechanism for survival of microbes under stress conditions. *Biocatal. Agric. Biotechnol.* 42**,** 102337.

Fezoui, Y., Hartley, D.M., Harper, J.D., Khurana, R., Walsh, D.M., Condron, M.M., Fink, A.L., and Teplow, D.B. (2000). An improved method of preparing the amyloid β-protein for fibrillogenesis and neurotoxicity experiments. *Neurobiol. Aging* 21**,** 77.

Fezoui, Y., and Teplow, D.B. (2002). Kinetic Studies of Amyloid β-Protein Fibril Assembly: differential effects of α-helix stabilization*. *Journal of Biological Chemistry* 277**,** 36948-36954.

Fitzpatrick, A.W.P., Falcon, B., He, S., Murzin, A.G., Murshudov, G., Garringer, H.J., Crowther, R.A., Ghetti, B., Goedert, M., and Scheres, S.H.W. (2017). Cryo-EM structures of tau filaments from Alzheimer's disease. *Nature* 547**,** 185-190.

Flemming, H.-C., and Wingender, J. (2010). The biofilm matrix. *Nat. Rev. Microbiol* 8**,** 623-633.

Folch, J., Ettcheto, M., Petrov, D., Abad, S., Pedrós, I., Marin, M., Olloquequi, J., and Camins, A. (2018). Review of the advances in treatment for Alzheimer disease: Strategies for combating β-amyloid protein. *Neurologia (Engl Ed)* 33**,** 47-58.

Foley, A.R., and Raskatov, J.A. (2020). Assessing Reproducibility in Amyloid β Research: Impact of Aβ Sources on Experimental Outcomes. *Chembiochem* 21**,** 2425-2430.

Fowler, D.M., Koulov, A.V., Alory-Jost, C., Marks, M.S., Balch, W.E., and Kelly, J.W. (2006). Functional amyloid formation within mammalian tissue. *PLoS Biol.* 4**,** e6.

Fowler, D.M., Koulov, A.V., Balch, W.E., and Kelly, J.W. (2007). Functional amyloid – from bacteria to humans. *Trends Biochem. Sci.* 32**,** 217-224.

Freire, S., De Araujo, M.H., Al-Soufi, W., and Novo, M. (2014). Photophysical study of Thioflavin T as fluorescence marker of amyloid fibrils. *Dyes Pigm.* 110**,** 97-105.

Friedland, R.P., and Chapman, M.R. (2017). The role of microbial amyloid in neurodegeneration. *PLoS Pathog.* 13**,** e1006654.

Frost, B., Jacks, R.L., and Diamond, M.I. (2009). Propagation of tau misfolding from the outside to the inside of a cell. *J. Biol. Chem.* 284**,** 12845-12852.

Gade Malmos, K., Blancas-Mejia, L.M., Weber, B., Buchner, J., Ramirez-Alvarado, M., Naiki, H., and Otzen, D. (2017). ThT 101: a primer on the use of thioflavin T to investigate amyloid formation. *Amyloid* 24**,** 1-16.

Gallo, P.M., Rapsinski, G.J., Wilson, R.P., Oppong, G.O., Sriram, U., Goulian, M., Buttaro, B., Caricchio, R., Gallucci, S., and Tükel, Ç. (2015). Amyloid-DNA Composites of Bacterial Biofilms Stimulate Autoimmunity. *Immunity* 42**,** 1171-1184.

Gerstel, U., and Römling, U. (2003). The csgD promoter, a control unit for biofilm formation in Salmonella typhimurium. *Res. J. Microbiol.* 154**,** 659-667.

Gertsik, N., Chiu, D., and Li, Y.M. (2014). Complex regulation of γ-secretase: from obligatory to modulatory subunits. *Front. Aging Neurosci.* 6**,** 342.

Ghavami, M., Rezaei, M., Ejtehadi, R., Lotfi, M., Shokrgozar, M.A., Abd Emamy, B., Raush, J., and Mahmoudi, M. (2013). Physiological temperature has a crucial role in amyloid β in the absence and presence of hydrophobic and hydrophilic nanoparticles. *ACS Chem. Neurosci.* 4**,** 375-378.

Ghosh, U., Yau, W.M., Collinge, J., and Tycko, R. (2021). Structural differences in amyloid-β fibrils from brains of nondemented elderly individuals and Alzheimer's disease patients. *Proc. Natl. Acad. Sci. U.S.A.* 118.

Goedert, M. (2015). NEURODEGENERATION. Alzheimer's and Parkinson's diseases: The prion concept in relation to assembled Aβ, tau, and α-synuclein. *Science* 349**,** 1255555.

Goedert, M., Jakes, R., and Spillantini, M.G. (2017). The Synucleinopathies: Twenty Years On. *J Parkinsons Dis* 7**,** S51-s69.

Goldsbury, C., Frey, P., Olivieri, V., Aebi, U., and Müller, S.A. (2005). Multiple assembly pathways underlie amyloid-beta fibril polymorphisms. *J. Mol. Biol.* 352**,** 282-298.

González, J.F., Tucker, L., Fitch, J., Wetzel, A., White, P., and Gunn, J.S. (2019). Human bile-mediated regulation of Salmonella curli fimbriae. *J. Bacteriol* 201**,** e00055-00019.

Greenblat, C. (2021). *Dementia* [Online]. World Health Organization: World Health Organization. Available: https://www.who.int/news-room/fact-sheets/detail/dementia [Accessed April 9, 2022 2022].

Greenwald, J., Kwiatkowski, W., and Riek, R. (2018). Peptide Amyloids in the Origin of Life. *J. Mol. Biol.* 430**,** 3735-3750.

Groveman, B.R., Dolan, M.A., Taubner, L.M., Kraus, A., Wickner, R.B., and Caughey, B. (2014). Parallel in-register intermolecular β-sheet architectures for prion-seeded prion protein (PrP) amyloids. *J Biol Chem* 289**,** 24129-24142.

Guo, J.L., and Lee, V.M. (2011). Seeding of normal Tau by pathological Tau conformers drives pathogenesis of Alzheimer-like tangles. *J Biol Chem* 286**,** 15317-15331.

Guo, J.L., Narasimhan, S., Changolkar, L., He, Z., Stieber, A., Zhang, B., Gathagan, R.J., Iba, M., Mcbride, J.D., Trojanowski, J.Q., and Lee, V.M. (2016). Unique pathological tau conformers from Alzheimer's brains transmit tau pathology in nontransgenic mice. *J. Exp. Med.* 213**,** 2635-2654.

Gustavsson, Å., Engström, U., and Westermark, P. (1991). Normal transthyretin and synthetic transthyretin fragments from amyloid-like fibrils in vitro. *BBRC* 175**,** 1159-1164.

Haass, C., Schlossmacher, M.G., Hung, A.Y., Vigo-Pelfrey, C., Mellon, A., Ostaszewski, B.L., Lieberburg, I., Koo, E.H., Schenk, D., Teplow, D.B., and Et Al. (1992). Amyloid beta-peptide is produced by cultured cells during normal metabolism. *Nature* 359**,** 322-325.

Haass, C., and Selkoe, D.J. (2007). Soluble protein oligomers in neurodegeneration: lessons from the Alzheimer's amyloid beta-peptide. *Nat. Rev. Mol. Cell Biol.* 8**,** 101-112.

Haldar, S., and Chattopadhyay, K. (2011). Effects of Arginine and Other Solution Additives on the Self-Association of Different Surfactants: An Investigation at Single-Molecule Resolution. *Langmuir* 27**,** 5842-5849.

Hall-Stoodley, L., Costerton, J.W., and Stoodley, P. (2004). Bacterial biofilms: from the Natural environment to infectious diseases. *Nat. Rev. Microbiol* 2**,** 95-108.

Hammar, M.R., Arnqvist, A., Bian, Z., Olsén, A., and Normark, S. (1995). Expression of two csg operons is required for production of fibronectin-and congo red-binding curli polymers in Escherichia coli K-12. *Mol. Microbiol.* 18**,** 661-670.

Hansen, C., Angot, E., Bergström, A.L., Steiner, J.A., Pieri, L., Paul, G., Outeiro, T.F., Melki, R., Kallunki, P., Fog, K., Li, J.Y., and Brundin, P. (2011). α-Synuclein propagates from mouse brain to grafted dopaminergic neurons and seeds aggregation in cultured human cells. *J. Clin. Investig.* 121**,** 715-725.

Haque, E., Kamil, M., Irfan, S., Hasan, A., Sheikh, S., and Ssm, M. (2017). Protein aggregation: A new challenge in type-II diabetes. *J. adv. biol. biotechnol.*

Harada, R., Okamura, N., Furumoto, S., and Yanai, K. (2018). Imaging Protein Misfolding in the Brain Using β-Sheet Ligands. *Front. Neurosci.* 12.

Hardy, J.A., and Higgins, G.A. (1992). Alzheimer's Disease: The Amyloid Cascade Hypothesis. *Science* 256**,** 184-185.

Harman, D. (2006). Alzheimer's disease pathogenesis: role of aging. *Ann. N. Y. Acad. Sci.* 1067**,** 454-460.

Harper, J.D., and Lansbury, P.T., Jr. (1997). Models of amyloid seeding in Alzheimer's disease and scrapie: mechanistic truths and physiological consequences of the time-dependent solubility of amyloid proteins. *Annu. Rev. Biochem.* 66**,** 385-407.

Hartman, K., Brender, J.R., Monde, K., Ono, A., Evans, M.L., Popovych, N., Chapman, M.R., and Ramamoorthy, A. (2013). Bacterial curli protein promotes the conversion of PAP248-286 into the amyloid SEVI: cross-seeding of dissimilar amyloid sequences. *PeerJ* 1**,** e5.

Hawe, A., Sutter, M., and Jiskoot, W. (2008). Extrinsic fluorescent dyes as tools for protein characterization. *Pharm. Res.* 25**,** 1487-1499.

Hebert, L.E., Bienias, J.L., Aggarwal, N.T., Wilson, R.S., Bennett, D.A., Shah, R.C., and Evans, D.A. (2010). Change in risk of Alzheimer disease over time. *Neurology* 75**,** 786-791.

Heise, H., Hoyer, W., Becker, S., Andronesi, O.C., Riedel, D., and Baldus, M. (2005). Molecular-level secondary structure, polymorphism, and dynamics of full-length α-synuclein fibrils studied by solid-state NMR. *Proc. Natl. Acad. Sci. U.S.A.* 102**,** 15871-15876.

Hellstrand, E., Boland, B., Walsh, D.M., and Linse, S. (2010). Amyloid β-Protein Aggregation Produces Highly Reproducible Kinetic Data and Occurs by a Two-Phase Process. *ACS Chem. Neurosci.* 1**,** 13-18.

Herwald, H., Mörgelin, M., Olsén, A., Rhen, M., Dahlbäck, B., Müller-Esterl, W., and Björck, L. (1998). Activation of the contact-phase system on bacterial surfaces—a clue to serious complications in infectious diseases. *Nat. Med.* 4**,** 298-302.

Hortschansky, P., Schroeckh, V., Christopeit, T., Zandomeneghi, G., and Fändrich, M. (2005). The aggregation kinetics of Alzheimer's beta-amyloid peptide is controlled by stochastic nucleation. *Protein Sci.* 14**,** 1753-1759.

Hu, R., Zhang, M., Chen, H., Jiang, B., and Zheng, J. (2015). Cross-Seeding Interaction between β-Amyloid and Human Islet Amyloid Polypeptide. *ACS Chem. Neurosci.* 6**,** 1759-1768.

Iadanza, M.G., Jackson, M.P., Hewitt, E.W., Ranson, N.A., and Radford, S.E. (2018). A new era for understanding amyloid structures and disease. *Nat. Rev. Mol. Cell Biol.* 19**,** 755-773.

Jain, N., and Chapman, M.R. (2019). Bacterial functional amyloids: Order from disorder. *Biochim Biophys Acta Proteins Proteom.* 1867**,** 954-960.

Jan, A., Gokce, O., Luthi-Carter, R., and Lashuel, H.A. (2008). The Ratio of Monomeric to Aggregated Forms of Aβ40 and Aβ42 Is an Important Determinant of Amyloid-β Aggregation, Fibrillogenesis, and Toxicity*. *J Biol Chem* 283**,** 28176-28189.

Jaroniec, C.P., Macphee, C.E., Astrof, N.S., Dobson, C.M., and Griffin, R.G. (2002). Molecular conformation of a peptide fragment of transthyretin in an amyloid fibril. *Proc. Natl. Acad. Sci. U.S.A.* 99**,** 16748-16753.

Jarrett, J.T., and Lansbury, P.T. (1993). Seeding "one-dimensional crystallization" of amyloid: A pathogenic mechanism in Alzheimer's disease and scrapie? *Cell* 73**,** 1055-1058.

Javed, I., Zhang, Z., Adamcik, J., Andrikopoulos, N., Li, Y., Otzen, D.E., Lin, S., Mezzenga, R., Davis, T.P., Ding, F., and Ke, P.C. (2020). Accelerated Amyloid Beta Pathogenesis by Bacterial Amyloid FapC. *Adv. Sci. (Weinh.)* 7**,** 2001299.

Jeremic, D., Jiménez-Díaz, L., and Navarro-López, J.D. (2021). Past, present and future of therapeutic strategies against amyloid-β peptides in Alzheimer's disease: a systematic review. *Ageing Res. Rev.* 72**,** 101496.

Jin, J., Xu, Z., Zhang, L., Zhang, C., Zhao, X., Mao, Y., Zhang, H., Liang, X., Wu, J., Yang, Y., and Zhang, J. (2023). Gut-derived β-amyloid: Likely a centerpiece of the gut–brain axis contributing to Alzheimer's pathogenesis. *Gut Microbes* 15**,** 2167172.

Jin, M., Shepardson, N., Yang, T., Chen, G., Walsh, D., and Selkoe, D.J. (2011). Soluble amyloid beta-protein dimers isolated from Alzheimer cortex directly induce Tau hyperphosphorylation and neuritic degeneration. *Proc. Natl. Acad. Sci. U.S.A.* 108**,** 5819-5824.

Kaufman, S.K., Sanders, D.W., Thomas, T.L., Ruchinskas, A.J., Vaquer-Alicea, J., Sharma, A.M., Miller, T.M., and Diamond, M.I. (2016). Tau Prion Strains Dictate Patterns of Cell Pathology, Progression Rate, and Regional Vulnerability In Vivo. *Neuron* 92**,** 796-812.

Kauwe, G., and Tracy, T.E. (2021). Amyloid beta emerges from below the neck to disable the brain. *PLoS Biol.* 19**,** e3001388.

Kayed, R., Head, E., Thompson, J.L., Mcintire, T.M., Milton, S.C., Cotman, C.W., and Glabe, C.G. (2003a). Common structure of soluble amyloid oligomers implies common mechanism of pathogenesis. *Science* 300**,** 486-489.

Kayed, R., Head, E., Thompson, J.L., Mcintire, T.M., Milton, S.C., Cotman, C.W., and Glabe, C.G. (2003b). Common structure of soluble amyloid oligomers implies common mechanism of pathogenesis. *Science* 300**,** 486-489.

Khemtemourian, L., Antoniciello, F., Sahoo, B.R., Decossas, M., Lecomte, S., and Ramamoorthy, A. (2021). Investigation of the effects of two major secretory granules components, insulin and zinc, on human-IAPP amyloid aggregation and membrane damage. *Chem. Phys. Lipids* 237**,** 105083.

Khurana, R., Coleman, C., Ionescu-Zanetti, C., Carter, S.A., Krishna, V., Grover, R.K., Roy, R., and Singh, S. (2005). Mechanism of thioflavin T binding to amyloid fibrils. *J. Struct. Biol.* 151**,** 229-238.

Kimberlin, R.H., Cole, S., and Walker, C.A. (1987). Temporary and permanent modifications to a single strain of mouse scrapie on transmission to rats and hamsters. *J. Gen. Virol.* 68 (Pt 7)**,** 1875-1881.

Kinney, J.W., Bemiller, S.M., Murtishaw, A.S., Leisgang, A.M., Salazar, A.M., and Lamb, B.T. (2018). Inflammation as a central mechanism in Alzheimer's disease. *TRCI* 4**,** 575-590.

Klein, R.D., Shu, Q., Cusumano, Z.T., Nagamatsu, K., Gualberto, N.C., Lynch, A.J.L., Wu, C., Wang, W., Jain, N., Pinkner, J.S., Amarasinghe, G.K., Hultgren, S.J., Frieden, C., and Chapman, M.R. (2018). Structure-Function Analysis of the Curli Accessory Protein CsgE Defines Surfaces Essential for Coordinating Amyloid Fiber Formation. *MBio* 9.

Klug, G.M., Losic, D., Subasinghe, S.S., Aguilar, M.I., Martin, L.L., and Small, D.H. (2003). Beta-amyloid protein oligomers induced by metal ions and acid pH are distinct from those

generated by slow spontaneous ageing at neutral pH. *European j. mol. biol. biochem.* 270**,** 4282-4293.
Klunk, W.E., Jacob, R.F., and Mason, R.P. (1999). Quantifying amyloid by congo red spectral shift assay. *Meth. Enzymol.* 309**,** 285-305.
Knopman, D.S., Amieva, H., Petersen, R.C., Chételat, G., Holtzman, D.M., Hyman, B.T., Nixon, R.A., and Jones, D.T. (2021). Alzheimer disease. *Nat. Rev. Dis. Primers* 7**,** 33.
Kocisko, D.A., Priola, S.A., Raymond, G.J., Chesebro, B., Lansbury Jr, P.T., and Caughey, B. (1995). Species specificity in the cell-free conversion of prion protein to protease-resistant forms: a model for the scrapie species barrier. *Proc. Natl. Acad. Sci. U.S.A.* 92**,** 3923-3927.
Koloteva-Levine, N., Aubrey, L.D., Marchante, R., Purton, T.J., Hiscock, J.R., Tuite, M.F., and Xue, W.-F. (2021). Amyloid particles facilitate surface-catalyzed cross-seeding by acting as promiscuous nanoparticles. *Proc. Natl. Acad. Sci. U.S.A.* 118**,** e2104148118.
Korczyn, A.D. (2008). The amyloid cascade hypothesis. *Alzheimers. Dement.* 4**,** 176-178.
Krebs, M.R., Bromley, E.H., and Donald, A.M. (2005). The binding of thioflavin-T to amyloid fibrils: localisation and implications. *J. Struct. Biol.* 149**,** 30-37.
Król, S., Österlund, N., Vosough, F., Jarvet, J., Wärmländer, S., Barth, A., Ilag, L.L., Magzoub, M., Gräslund, A., and Mörman, C. (2021). The amyloid-inhibiting NCAM-PrP peptide targets Aβ peptide aggregation in membrane-mimetic environments. *iScience* 24**,** 102852.
Kusumoto, Y., Lomakin, A., Teplow, D.B., and Benedek, G.B. (1998). Temperature dependence of amyloid β-protein fibrillization. *Proc. Natl. Acad. Sci. U.S.A.* 95**,** 12277-12282.
Lam, V., Takechi, R., Hackett, M.J., et al. (2021). Synthesis of human amyloid restricted to liver results in an Alzheimer disease–like neurodegenerative phenotype. *PLoS Biol.* 19**,** e3001358.
Lambert, M.P., Barlow, A.K., Chromy, B.A., Edwards, C., Freed, R., Liosatos, M., Morgan, T.E., Rozovsky, I., Trommer, B., Viola, K.L., Wals, P., Zhang, C., Finch, C.E., Krafft, G.A., and Klein, W.L. (1998). Diffusible, nonfibrillar ligands derived from Abeta1-42 are potent central nervous system neurotoxins. *Proc. Natl. Acad. Sci. U.S.A.* 95**,** 6448-6453.
Lauderback, C.M., Kanski, J., Hackett, J.M., Maeda, N., Kindy, M.S., and Butterfield, D.A. (2002). Apolipoprotein E modulates Alzheimer's Abeta(1-42)-induced oxidative damage to synaptosomes in an allele-specific manner. *Brain Res. J.* 924**,** 90-97.
Laws, K.R., Irvine, K., and Gale, T.M. (2018). Sex differences in Alzheimer's disease. *Curr Opin Psychiatry* 31.
Lee, C.T., and Terentjev, E.M. (2017). Mechanisms and rates of nucleation of amyloid fibrils. *J. Chem. Phys.* 147**,** 105103.
Levine, H. (1995). Thioflavine T interaction with amyloid β-sheet structures. *Amyloid* 2**,** 1-6.
Levine, H., 3rd (1993). Thioflavine T interaction with synthetic Alzheimer's disease beta-amyloid peptides: detection of amyloid aggregation in solution. *Protein Sci.* 2**,** 404-410.
Levine, H., 3rd (1999). Quantification of beta-sheet amyloid fibril structures with thioflavin T. *Meth. Enzymol.* 309**,** 274-284.
Li, D., and Liu, C. (2022). Conformational strains of pathogenic amyloid proteins in neurodegenerative diseases. *Nat. Rev. Neurosci.* 23**,** 523-534.
Li, R., and Singh, M. (2014). Sex differences in cognitive impairment and Alzheimer's disease. *Front. Neuroendocrinol.* 35**,** 385-403.

Lindberg, D.J., Wranne, M.S., Gilbert Gatty, M., Westerlund, F., and Esbjörner, E.K. (2015). Steady-state and time-resolved Thioflavin-T fluorescence can report on morphological differences in amyloid fibrils formed by Aβ(1-40) and Aβ(1-42). *BBRC* 458**,** 418-423.

Liu, C.C., Liu, C.C., Kanekiyo, T., Xu, H., and Bu, G. (2013). Apolipoprotein E and Alzheimer disease: risk, mechanisms and therapy. *Nat. Rev. Neurol.* 9**,** 106-118.

Livingston, G., Huntley, J., Sommerlad, A., et al. (2020). Dementia prevention, intervention, and care: 2020 report of the Lancet Commission. *Lancet* 396**,** 413-446.

Loy, C.T., Schofield, P.R., Turner, A.M., and Kwok, J.B. (2014). Genetics of dementia. *Lancet* 383**,** 828-840.

Lu, J.-X., Qiang, W., Yau, W.-M., Schwieters, Charles d., Meredith, Stephen c., and Tycko, R. (2013). Molecular Structure of β-Amyloid Fibrils in Alzheimer's Disease Brain Tissue. *Cell* 154**,** 1257-1268.

Lührs, T., Ritter, C., Adrian, M., Riek-Loher, D., Bohrmann, B., Döbeli, H., Schubert, D., and Riek, R. (2005). 3D structure of Alzheimer's amyloid-beta(1-42) fibrils. *Proc. Natl. Acad. Sci. U.S.A.* 102**,** 17342-17347.

Luk, K.C., Kehm, V., Carroll, J., Zhang, B., O'brien, P., Trojanowski, J.Q., and Lee, V.M. (2012a). Pathological α-synuclein transmission initiates Parkinson-like neurodegeneration in nontransgenic mice. *Science* 338**,** 949-953.

Luk, K.C., Kehm, V.M., Zhang, B., O'brien, P., Trojanowski, J.Q., and Lee, V.M. (2012b). Intracerebral inoculation of pathological α-synuclein initiates a rapidly progressive neurodegenerative α-synucleinopathy in mice. *J. Exp. Med.* 209**,** 975-986.

Lundmark, K., Westermark, G.T., Olsén, A., and Westermark, P. (2005). Protein fibrils in nature can enhance amyloid protein A amyloidosis in mice: Cross-seeding as a disease mechanism. *Proc. Natl. Acad. Sci. U.S.A.* 102**,** 6098-6102.

Mackenzie, K.D., Palmer, M.B., Köster, W.L., and White, A.P. (2017). Examining the Link between Biofilm Formation and the Ability of Pathogenic Salmonella Strains to Colonize Multiple Host Species. *Front. Vet. Sci.* 4**,** 138.

Mackenzie, K.D., Wang, Y., Musicha, P., Hansen, E.G., Palmer, M.B., Herman, D.J., Feasey, N.A., and White, A.P. (2019). Parallel evolution leading to impaired biofilm formation in invasive Salmonella strains. *PLoS Genet.* 15**,** e1008233.

Maji, S.K., Perrin, M.H., Sawaya, M.R., Jessberger, S., Vadodaria, K., Rissman, R.A., Singru, P.S., Nilsson, K.P., Simon, R., Schubert, D., Eisenberg, D., Rivier, J., Sawchenko, P., Vale, W., and Riek, R. (2009). Functional amyloids as natural storage of peptide hormones in pituitary secretory granules. *Science* 325**,** 328-332.

Manson, J.C., and Diack, A.B. (2016). Evaluating the Species Barrier. *J Food Saf* 4**,** 135-141.

Mccrate, O.A., Zhou, X., Reichhardt, C., and Cegelski, L. (2013). Sum of the Parts: Composition and Architecture of the Bacterial Extracellular Matrix. *J. Mol. Biol.* 425**,** 4286-4294.

Meisl, G., Xu, C.K., Taylor, J.D., Michaels, T.C.T., Levin, A., Otzen, D., Klenerman, D., Matthews, S., Linse, S., Andreasen, M., and Knowles, T.P.J. (2022). Uncovering the universality of self-replication in protein aggregation and its link to disease. *Sci. Adv.* 8**,** eabn6831.

Melki, R. (2018). How the shapes of seeds can influence pathology. *Neurobiol. Dis.* 109**,** 201-208.

Mendez, M.F. (2017). Early-Onset Alzheimer Disease. *Neurol. Clin.* 35**,** 263-281.

Meyer-Luehmann, M., Coomaraswamy, J., Bolmont, T., Kaeser, S., Schaefer, C., Kilger, E., Neuenschwander, A., Abramowski, D., Frey, P., Jaton, A.L., Vigouret, J.M., Paganetti, P., Walsh, D.M., Mathews, P.M., Ghiso, J., Staufenbiel, M., Walker, L.C., and Jucker, M. (2006). Exogenous induction of cerebral beta-amyloidogenesis is governed by agent and host. *Science* 313**,** 1781-1784.

Michaels, T.C.T., Šarić, A., Curk, S., Bernfur, K., Arosio, P., Meisl, G., Dear, A.J., Cohen, S.I.A., Dobson, C.M., Vendruscolo, M., Linse, S., and Knowles, T.P.J. (2020). Dynamics of oligomer populations formed during the aggregation of Alzheimer's Aβ42 peptide. *Nat. Chem* 12**,** 445-451.

Michaelson, D.M. (2014). APOE ε4: the most prevalent yet understudied risk factor for Alzheimer's disease. *Alzheimers. Dement.* 10**,** 861-868.

Michelitsch, M.D., and Weissman, J.S. (2000). A census of glutamine/asparagine-rich regions: implications for their conserved function and the prediction of novel prions. *Proc. Natl. Acad. Sci. U.S.A.* 97**,** 11910-11915.

Miller, A.L., Bessho, S., Grando, K., and Tükel, Ç. (2021). Microbiome or Infections: Amyloid-Containing Biofilms as a Trigger for Complex Human Diseases. *Front. Immunol.* 12.

Miller, A.L., Pasternak, J.A., Medeiros, N.J., Nicastro, L.K., Tursi, S.A., Hansen, E.G., Krochak, R., Sokaribo, A.S., Mackenzie, K.D., Palmer, M.B., Herman, D.J., Watson, N.L., Zhang, Y., Wilson, H.L., Wilson, R.P., White, A.P., and Tükel, Ç. (2020). In vivo synthesis of bacterial amyloid curli contributes to joint inflammation during S. Typhimurium infection. *PLoS Pathog.* 16.

Morales, R. (2017). Prion strains in mammals: Different conformations leading to disease. *PLoS Pathog.* 13**,** e1006323.

Morales, R., Duran-Aniotz, C., Castilla, J., Estrada, L.D., and Soto, C. (2012). De novo induction of amyloid-β deposition in vivo. *Mol. Psychiatry* 17**,** 1347-1353.

Morales, R., Estrada, L.D., Diaz-Espinoza, R., Morales-Scheihing, D., Jara, M.C., Castilla, J., and Soto, C. (2010). Molecular cross talk between misfolded proteins in animal models of Alzheimer's and prion diseases. *J. Neurosci.* 30**,** 4528-4535.

Morinaga, A., Hasegawa, K., Nomura, R., Ookoshi, T., Ozawa, D., Goto, Y., Yamada, M., and Naiki, H. (2010). Critical role of interfaces and agitation on the nucleation of Aβ amyloid fibrils at low concentrations of Aβ monomers. *Biochim Biophys Acta Proteins Proteom* 1804**,** 986-995.

Murakami, K., and Ono, K. (2022). Interactions of amyloid coaggregates with biomolecules and its relevance to neurodegeneration. *FASEB J.* 36**,** e22493.

Murphy, M.P., and Levine, H., 3rd (2010). Alzheimer's disease and the amyloid-beta peptide. *J Alzheimers Dis* 19**,** 311-323.

Naiki, H., Higuchi, K., Hosokawa, M., and Takeda, T. (1989). Fluorometric determination of amyloid fibrils in vitro using the fluorescent dye, thioflavine T. *Anal. Biochem.* 177**,** 244-249.

Navarro, S., and Ventura, S. (2014). Fluorescent dye ProteoStat to detect and discriminate intracellular amyloid-like aggregates in Escherichia coli. *Biotechnol. J.* 9**,** 1259-1266.

Nelson, R., Sawaya, M.R., Balbirnie, M., Madsen, A.Ø., Riekel, C., Grothe, R., and Eisenberg, D. (2005). Structure of the cross-β spine of amyloid-like fibrils. *Nature* 435**,** 773-778.

Nhan, H.S., Chiang, K., and Koo, E.H. (2015). The multifaceted nature of amyloid precursor protein and its proteolytic fragments: friends and foes. *Acta Neuropathol.* 129**,** 1-19.

Nhu, N.T.K., Phan, M.D., Peters, K.M., Lo, A.W., Forde, B.M., Min Chong, T., Yin, W.F., Chan, K.G., Chromek, M., Brauner, A., Chapman, M.R., Beatson, S.A., and Schembri, M.A. (2018). Discovery of New Genes Involved in Curli Production by a Uropathogenic Escherichia coli Strain from the Highly Virulent O45:K1:H7 Lineage. *mBio* 9.

Nilsson, M.R. (2004). Techniques to study amyloid fibril formation in vitro. *Methods* 34**,** 151-160.

Normark, S., Römling, U., Bian, Z., Hammar, M., and Sierralta, W.D. (1998). Curli Fibers Are Highly Conserved between. *J. Bacteriol* 180**,** 722.

Nyarko, J.N.K., Quartey, M.O., Pennington, P.R., Heistad, R.M., Dea, D., Poirier, J., Baker, G.B., and Mousseau, D.D. (2018). Profiles of β-Amyloid Peptides and Key Secretases in Brain Autopsy Samples Differ with Sex and APOE ε4 Status: Impact for Risk and Progression of Alzheimer Disease. *Neuroscience* 373**,** 20-36.

O'nuallain, B., Williams, A.D., Westermark, P., and Wetzel, R. (2004). Seeding specificity in amyloid growth induced by heterologous fibrils. *J Biol Chem* 279**,** 17490-17499.

Oli, M.W., Otoo, H.N., Crowley, P.J., Heim, K.P., Nascimento, M.M., Ramsook, C.B., Lipke, P.N., and Brady, L.J. (2012). Functional amyloid formation by Streptococcus mutans. *Microbiology (Reading, Engl.)* 158**,** 2903-2916.

Olseán, A., Herwald, H., Wikstro¨M, M., Persson, K., Mattsson, E., and Bjo¨Rck, L. (2002). Identification of Two Protein-binding and Functional Regions of Curli, a Surface Organelle and Virulence Determinant ofEscherichia coli*. *J Biol Chem* 277**,** 34568-34572.

Ono, K., Takahashi, R., Ikeda, T., Mizuguchi, M., Hamaguchi, T., and Yamada, M. (2014). Exogenous amyloidogenic proteins function as seeds in amyloid β-protein aggregation. *Biochim Biophys Acta Mol Basis Dis* 1842**,** 646-653.

Ono, K., Takahashi, R., Ikeda, T., and Yamada, M. (2012). Cross-seeding effects of amyloid β-protein and α-synuclein. *J. Neurochem* 122**,** 883-890.

Otzen, D., and Riek, R. (2019). Functional Amyloids. *Cold Spring Harb. Perspect. Biol.* 11.

Paravastu, A.K., Leapman, R.D., Yau, W.-M., and Tycko, R. (2008a). Molecular structural basis for polymorphism in Alzheimer's β-amyloid fibrils. *Proceedings of the National Academy of Sciences* 105**,** 18349-18354.

Paravastu, A.K., Leapman, R.D., Yau, W.-M., and Tycko, R. (2008b). Molecular structural basis for polymorphism in Alzheimer's β-amyloid fibrils. *Proc. Natl. Acad. Sci. U.S.A.* 105**,** 18349-18354.

Paytubi, S., Cansado, C., Madrid, C., and Balsalobre, C. (2017). Nutrient composition promotes switching between pellicle and bottom biofilm in Salmonella. *Front. Microbiol.* 8**,** 2160.

Perov, S., Lidor, O., Salinas, N., Golan, N., Tayeb- Fligelman, E., Deshmukh, M., Willbold, D., and Landau, M. (2019). Structural Insights into Curli CsgA Cross-β Fibril Architecture Inspire Repurposing of Anti-amyloid Compounds as Anti-biofilm Agents. *PLoS Pathog.* 15**,** e1007978.

Petkova, A.T., Leapman, R.D., Guo, Z., Yau, W.M., Mattson, M.P., and Tycko, R. (2005). Self-propagating, molecular-level polymorphism in Alzheimer's beta-amyloid fibrils. *Science* 307**,** 262-265.

Pike, C.J., Burdick, D., Walencewicz, A.J., Glabe, C.G., and Cotman, C.W. (1993). Neurodegeneration induced by beta-amyloid peptides in vitro: the role of peptide assembly state. *J. Neurosci* 13**,** 1676-1687.

Piscitelli, A., Cicatiello, P., Gravagnuolo, A.M., Sorrentino, I., Pezzella, C., and Giardina, P. (2017). Applications of Functional Amyloids from Fungi: Surface Modification by Class I Hydrophobins. *Biomolecules* 7**,** 45.

Prakash, P., Lantz, T.C., Jethava, K.P., and Chopra, G. (2019). Rapid, Refined, and Robust Method for Expression, Purification, and Characterization of Recombinant Human Amyloid beta 1-42. *Methods Protoc.* 2**,** 48.

Prusiner, S.B. (1996). Molecular biology and pathogenesis of prion diseases. *Trends Biochem. Sci.* 21**,** 482-487.

Prusiner, S.B. (1998). Prions. *Proc. Natl. Acad. Sci. U.S.A.* 95**,** 13363-13383.

Pryor, N.E., Moss, M.A., and Hestekin, C.N. (2012). Unraveling the Early Events of Amyloid-β Protein (Aβ) Aggregation: Techniques for the Determination of Aβ Aggregate Size. *Int. J. Mol. Sci.* 13**,** 3038-3072.

Qian, X.-H., Liu, X.-L., Chen, G., Chen, S.-D., and Tang, H.-D. (2022). Injection of amyloid-β to lateral ventricle induces gut microbiota dysbiosis in association with inhibition of cholinergic anti-inflammatory pathways in Alzheimer's disease. *J. Neuroinflammation* 19**,** 236.

Quartey, M.O., Nyarko, J.N.K., Maley, J.M., Barnes, J.R., Bolanos, M.a.C., Heistad, R.M., Knudsen, K.J., Pennington, P.R., Buttigieg, J., De Carvalho, C.E., Leary, S.C., Parsons, M.P., and Mousseau, D.D. (2021). The Aβ(1-38) peptide is a negative regulator of the Aβ(1-42) peptide implicated in Alzheimer disease progression. *Sci. Rep.* 11**,** 431.

Querfurth, H.W., and Laferla, F.M. (2010). Alzheimer's disease. *NEJM* 362**,** 329-344.

Raber, J., Wong, D., Buttini, M., Orth, M., Bellosta, S., Pitas, R.E., Mahley, R.W., and Mucke, L. (1998). Isoform-specific effects of human apolipoprotein E on brain function revealed in ApoE knockout mice: increased susceptibility of females. *Proc. Natl. Acad. Sci. U.S.A.* 95**,** 10914-10919.

Rajan, K.B., Weuve, J., Barnes, L.L., Mcaninch, E.A., Wilson, R.S., and Evans, D.A. (2021). Population estimate of people with clinical Alzheimer's disease and mild cognitive impairment in the United States (2020–2060). *Alzheimers. Dement.* 17**,** 1966-1975.

Rambaran, R.N., and Serpell, L.C. (2008). Amyloid fibrils: abnormal protein assembly. *Prion* 2**,** 112-117.

Ramsden, M., Henderson, Z., and Pearson, H.A. (2002). Modulation of Ca2+ channel currents in primary cultures of rat cortical neurones by amyloid β protein (1–40) is dependent on solubility status. *Brain Res. J.* 956**,** 254-261.

Raymond, J.J., Robertson, D.M., and Dinsdale, H.B. (1986). Pharmacological modification of bradykinin induced breakdown of the blood-brain barrier. *Can J Neurol Sci* 13**,** 214-220.

Reinke, A.A., and Gestwicki, J.E. (2011). Insight into amyloid structure using chemical probes. *Chem Biol Drug Des* 77**,** 399-411.

Ren, B., Zhang, Y., Zhang, M., Liu, Y., Zhang, D., Gong, X., Feng, Z., Tang, J., Chang, Y., and Zheng, J. (2019). Fundamentals of cross-seeding of amyloid proteins: an introduction. *J. Mater. Chem. B* 7**,** 7267-7282.

Ribarič, S. (2018). Peptides as Potential Therapeutics for Alzheimer's Disease. *Molecules* 23.
Richardson, J.S., and Richardson, D.C. (2002). Natural beta-sheet proteins use negative design to avoid edge-to-edge aggregation. *Proc. Natl. Acad. Sci. U.S.A.* 99**,** 2754-2759.
Rising, A., Gherardi, P., Chen, G., Johansson, J., Oskarsson, M.E., Westermark, G.T., and Westermark, P. (2021). AA amyloid in human food chain is a possible biohazard. *Sci. Rep.* 11**,** 21069.
Robinson, L.S., Ashman, E.M., Hultgren, S.J., and Chapman, M.R. (2006). Secretion of curli fibre subunits is mediated by the outer membrane-localized CsgG protein. *Mol. Microbiol.* 59**,** 870-881.
Rodríguez-Massó, S.R., Erickson, M.A., Banks, W.A., Ulrich, H., and Martins, A.H. (2021). The Bradykinin B2 Receptor Agonist (NG291) Causes Rapid Onset of Transient Blood–Brain Barrier Disruption Without Evidence of Early Brain Injury. *Front. Neurosci.* 15.
Romero, D., Aguilar, C., Losick, R., and Kolter, R. (2010). Amyloid fibers provide structural integrity to Bacillus subtilis biofilms. *PNAS* 107**,** 2230-2234.
Römling, U., Bian, Z., Hammar, M., Sierralta, W.D., and Normark, S. (1998). Curli fibers are highly conserved between Salmonella typhimurium and Escherichia coli with respect to operon structure and regulation. *J. Bacteriol* 180**,** 722-731.
Römling, U., Bokranz, W., Rabsch, W., Zogaj, X., Nimtz, M., and Tschäpe, H. (2003). Occurrence and regulation of the multicellular morphotype in Salmonella serovars important in human disease. *Int. J. Med. Microbiol.* 293**,** 273-285.
Rönicke, R., Klemm, A., Meinhardt, J., Schröder, U.H., Fändrich, M., and Reymann, K.G. (2008). Abeta mediated diminution of MTT reduction--an artefact of single cell culture? *PLoS One* 3**,** e3236.
Roterman, I., Banach, M., and Konieczny, L. (2017). Application of the Fuzzy Oil Drop Model Describes Amyloid as a Ribbonlike Micelle. *Entropy* 19**,** 167.
Ruschak, A.M., and Miranker, A.D. (2007). Fiber-dependent amyloid formation as catalysis of an existing reaction pathway. *Proc. Natl. Acad. Sci. U.S.A.* 104**,** 12341-12346.
Ryan, T.M., Caine, J., Mertens, H.D., Kirby, N., Nigro, J., Breheney, K., Waddington, L.J., Streltsov, V.A., Curtain, C., Masters, C.L., and Roberts, B.R. (2013). Ammonium hydroxide treatment of Aβ produces an aggregate free solution suitable for biophysical and cell culture characterization. *PeerJ* 1**,** e73.
Sampson, T.R., Challis, C., Jain, N., Moiseyenko, A., Ladinsky, M.S., Shastri, G.G., Thron, T., Needham, B.D., Horvath, I., Debelius, J.W., Janssen, S., Knight, R., Wittung-Stafshede, P., Gradinaru, V., Chapman, M., and Mazmanian, S.K. (2020). A gut bacterial amyloid promotes alpha-synuclein aggregation and motor impairment in mice. *Elife* 9.
Sanders, D.W., Kaufman, S.K., Devos, S.L., Sharma, A.M., Mirbaha, H., Li, A., Barker, S.J., Foley, A.C., Thorpe, J.R., Serpell, L.C., Miller, T.M., Grinberg, L.T., Seeley, W.W., and Diamond, M.I. (2014). Distinct tau prion strains propagate in cells and mice and define different tauopathies. *Neuron* 82**,** 1271-1288.
Sardar Sinha, M., Ansell-Schultz, A., Civitelli, L., Hildesjö, C., Larsson, M., Lannfelt, L., Ingelsson, M., and Hallbeck, M. (2018). Alzheimer's disease pathology propagation by exosomes containing toxic amyloid-beta oligomers. *Acta Neuropathol.* 136**,** 41-56.

Sarell, C.J., Syme, C.D., Rigby, S.E.J., and Viles, J.H. (2009). Copper(II) Binding to Amyloid-β Fibrils of Alzheimer's Disease Reveals a Picomolar Affinity: Stoichiometry and Coordination Geometry Are Independent of Aβ Oligomeric Form. *Biochemistry* 48**,** 4388-4402.

Sarroukh, R., Cerf, E., Derclaye, S., Dufrêne, Y.F., Goormaghtigh, E., Ruysschaert, J.-M., and Raussens, V. (2011). Transformation of amyloid β(1–40) oligomers into fibrils is characterized by a major change in secondary structure. *Cell. Mol. Life Sci.* 68**,** 1429-1438.

Sawaya, M.R., Hughes, M.P., Rodriguez, J.A., Riek, R., and Eisenberg, D.S. (2021). The expanding amyloid family: Structure, stability, function, and pathogenesis. *Cell* 184**,** 4857-4873.

Scarmeas, N., Luchsinger, J.A., Schupf, N., Brickman, A.M., Cosentino, S., Tang, M.X., and Stern, Y. (2009). Physical activity, diet, and risk of Alzheimer disease. *JAMA* 302**,** 627-637.

Scherpelz, K.P., Lu, J.X., Tycko, R., and Meredith, S.C. (2016). Preparation of Amyloid Fibrils Seeded from Brain and Meninges. *Methods Mol. Biol.* 1345**,** 299-312.

Schützmann, M.P., Hasecke, F., Bachmann, S., Zielinski, M., Hänsch, S., Schröder, G.F., Zempel, H., and Hoyer, W. (2021). Endo-lysosomal Aβ concentration and pH trigger formation of Aβ oligomers that potently induce Tau missorting. *Nat. Commun.* 12**,** 4634.

Schwartz, K., Syed, A.K., Stephenson, R.E., Rickard, A.H., and Boles, B.R. (2012). Functional amyloids composed of phenol soluble modulins stabilize Staphylococcus aureus biofilms. *PLoS Pathog.* 8**,** e1002744.

Selkoe, D.J. (2008). Soluble oligomers of the amyloid beta-protein impair synaptic plasticity and behavior. *Behav. Brain Res.* 192**,** 106-113.

Sengupta, U., Nilson, A.N., and Kayed, R. (2016). The Role of Amyloid-β Oligomers in Toxicity, Propagation, and Immunotherapy. *EBioMedicine* 6**,** 42-49.

Sevigny, J., Chiao, P., Bussière, T., et al. (2016). The antibody aducanumab reduces Aβ plaques in Alzheimer's disease. *Nature* 537**,** 50-56.

Sewell, L., Stylianou, F., Xu, Y., Taylor, J., Sefer, L., and Matthews, S. (2020). NMR insights into the pre-amyloid ensemble and secretion targeting of the curli subunit CsgA. *Sci. Rep.* 10**,** 7896.

Shahnawaz, M., Bilkis, T., and Park, I.-S. (2021). Amyloid β cytotoxicity is enhanced or reduced depending on formation of amyloid β oligomeric forms. *Biotechnol. Lett.* 43**,** 165-175.

Sharma, D., Misba, L., and Khan, A.U. (2019). Antibiotics versus biofilm: an emerging battleground in microbial communities. *Antimicrob. Resist. Infect. Control.* 8**,** 76.

Sheffield, C., Crippen, T., Andrews, K., Bongaerts, R., and Nisbet, D. (2009). Planktonic and biofilm communities from 7-day-old chicken cecal microflora cultures: characterization and resistance to Salmonella colonization. *J. Food Prot.* 72**,** 1812-1820.

Shen, C.L., and Murphy, R.M. (1995). Solvent effects on self-assembly of beta-amyloid peptide. *Biophys. J.* 69**,** 640-651.

Shewmaker, F., Mcglinchey, R.P., Thurber, K.R., Mcphie, P., Dyda, F., Tycko, R., and Wickner, R.B. (2009). The functional curli amyloid is not based on in-register parallel β-sheet structure. *J Biol Chem* 284**,** 25065-25076.

Sivaranjani, M., Hansen, E., Perera, S., Flores, P., Tükel, Ç., and White, A. (2022). Purification of the Bacterial Amyloid "Curli" from Salmonella enterica serovar Typhimurium and detection of curli from Infected Host Tissues. *Bio-protoc.*

Sjöbring, U., Pohl, G., and Olsén, A. (1994). Plasminogen, absorbed by Escherichia coli expressing curli or by Salmonella enteritidis expressing thin aggregative fimbriae, can be activated by simultaneously captured tissue-type plasminogen activator (t-PA). *Mol. Microbiol.* 14**,** 443-452.

Sleutel, M., Pradhan, B., Volkov, A.N., and Remaut, H. (2023). Structural analysis and architectural principles of the bacterial amyloid curli. *Nat. Commun.* 14**,** 2822.

Snyder, S.W., Ladror, U.S., Wade, W.S., Wang, G.T., Barrett, L.W., Matayoshi, E.D., Huffaker, H.J., Krafft, G.A., and Holzman, T.F. (1994). Amyloid-beta aggregation: selective inhibition of aggregation in mixtures of amyloid with different chain lengths. *Biophys. J.* 67**,** 1216-1228.

Solomon, E.B., Niemira, B.A., Sapers, G.M., and Annous, B.A. (2005). Biofilm formation, cellulose production, and curli biosynthesis by Salmonella originating from produce, animal, and clinical sources. *J. Food Prot.* 68**,** 906-912.

Soto, C. (2003). Unfolding the role of protein misfolding in neurodegenerative diseases. *Nat. Rev. Neurosci.* 4**,** 49-60.

Soto, C. (2012). Transmissible proteins: expanding the prion heresy. *Cell* 149**,** 968-977.

Soto, C., Estrada, L., and Castilla, J. (2006). Amyloids, prions and the inherent infectious nature of misfolded protein aggregates. *Trends Biochem. Sci.* 31**,** 150-155.

Soto, C., and Pritzkow, S. (2018). Protein misfolding, aggregation, and conformational strains in neurodegenerative diseases. *Nat. Neurosci.* 21**,** 1332-1340.

Stefanis, L. (2012). α-Synuclein in Parkinson's disease. *Cold Spring Harb. Perspect. Med.* 2**,** a009399.

Stine, W.B., Dahlgren, K.N., Krafft, G.A., and Ladu, M.J. (2003). In Vitro Characterization of Conditions for Amyloid-β Peptide Oligomerization and Fibrillogenesis*. *Journal of Biological Chemistry* 278**,** 11612-11622.

Stine, W.B., Jungbauer, L., Yu, C., and Ladu, M.J. (2011). Preparing synthetic Aβ in different aggregation states. *Methods Mol. Biol.* 670**,** 13-32.

Stöhr, J., Watts, J.C., Mensinger, Z.L., Oehler, A., Grillo, S.K., Dearmond, S.J., Prusiner, S.B., and Giles, K. (2012). Purified and synthetic Alzheimer's amyloid beta (Aβ) prions. *Proc. Natl. Acad. Sci. U.S.A.* 109**,** 11025-11030.

Subedi, S., Sasidharan, S., Nag, N., Saudagar, P., and Tripathi, T. (2022). Amyloid Cross-Seeding: Mechanism, Implication, and Inhibition. *Molecules* 27.

Sun, Y., Sommerville, N.R., Liu, J.Y.H., Ngan, M.P., Poon, D., Ponomarev, E.D., Lu, Z., Kung, J.S.C., and Rudd, J.A. (2020). Intra-gastrointestinal amyloid-β1-42 oligomers perturb enteric function and induce Alzheimer's disease pathology. *J. Physiol.* 598**,** 4209-4223.

Sunde, M., and Blake, C. (1997). The structure of amyloid fibrils by electron microscopy and X-ray diffraction. *Adv Protein Chem Struct Biol* 50**,** 123-159.

Sunde, M., Serpell, L.C., Bartlam, M., Fraser, P.E., Pepys, M.B., and Blake, C.C. (1997). Common core structure of amyloid fibrils by synchrotron X-ray diffraction. *J Mol Biol* 273**,** 729-739.

Supattapone, S. (2014). Elucidating the role of cofactors in mammalian prion propagation. *Prion* 8**,** 100-105.
Sureshbabu, N., Kirubagaran, R., and Jayakumar, R. (2009). Surfactant-induced conformational transition of amyloid β-peptide. *Eur. Biophys. J* 38**,** 355-367.
Tang, M.K., and Zhang, J.T. (2001). Salvianolic acid B inhibits fibril formation and neurotoxicity of amyloid beta-protein in vitro. *Acta Pharmacol. Sin.* 22**,** 380-384.
Tanzi, R.E. (2012). The genetics of Alzheimer disease. *Cold Spring Harb. Perspect. Med.* 2.
Tatulian, S.A. (2022). Challenges and hopes for Alzheimer's disease. *Drug Discov. Today* 27**,** 1027-1043.
Tavassoly, O., Sade, D., Bera, S., Shaham-Niv, S., Vocadlo, D.J., and Gazit, E. (2018). Quinolinic Acid Amyloid-like Fibrillar Assemblies Seed α-Synuclein Aggregation. *J Mol Biol* 430**,** 3847-3862.
Thakur, G., Micic, M., Yang, Y., Li, W., Movia, D., Giordani, S., Zhang, H., and Leblanc, R.M. (2011). Conjugated Quantum Dots Inhibit the Amyloid β (1–42) Fibrillation Process. *Int. J. Alzheimers Dis.* 2011**,** 502386.
Thies, W., and Bleiler, L. (2012). 2012 Alzheimer's disease facts and figures Alzheimer's Association ∗. *Alzheimers. Dement.* 8**,** 131-168.
Tian, Y., and Viles, J.H. (2022). pH Dependence of Amyloid-β Fibril Assembly Kinetics: Unravelling the Microscopic Molecular Processes. *Angew. Chem., Int. Ed. Engl.* 61**,** e202210675.
Topman, G., Sharabani-Yosef, O., and Gefen, A. (2011). A Method for Quick, Low-Cost Automated Confluency Measurements. *Microsc. Microanal.* 17**,** 915-922.
Tükel, C., Nishimori, J.H., Wilson, R.P., Winter, M.G., Keestra, A.M., Van Putten, J.P., and Bäumler, A.J. (2010). Toll-like receptors 1 and 2 cooperatively mediate immune responses to curli, a common amyloid from enterobacterial biofilms. *Cell. Microbiol.* 12**,** 1495-1505.
Tursi, S.A., and Tükel, Ç. (2018). Curli-Containing Enteric Biofilms Inside and Out: Matrix Composition, Immune Recognition, and Disease Implications. *Microbiol. Mol. Biol.* 82.
Tycko, R. (2015). Amyloid polymorphism: structural basis and neurobiological relevance. *Neuron* 86**,** 632-645.
Vadukul, D.M., Gbajumo, O., Marshall, K.E., and Serpell, L.C. (2017). Amyloidogenicity and toxicity of the reverse and scrambled variants of amyloid-β 1-42. *FEBS Lett.* 591**,** 822-830.
Vadukul, D.M., Maina, M., Franklin, H., Nardecchia, A., Serpell, L.C., and Marshall, K.E. (2020). Internalisation and toxicity of amyloid-β 1-42 are influenced by its conformation and assembly state rather than size. *FEBS Lett.* 594**,** 3490-3503.
Van Cauwenberghe, C., Van Broeckhoven, C., and Sleegers, K. (2016). The genetic landscape of Alzheimer disease: clinical implications and perspectives. *Genet. Med.* 18**,** 421-430.
Van Dyck, C.H., Swanson, C.J., Aisen, P., Bateman, R.J., Chen, C., Gee, M., Kanekiyo, M., Li, D., Reyderman, L., Cohen, S., Froelich, L., Katayama, S., Sabbagh, M., Vellas, B., Watson, D., Dhadda, S., Irizarry, M., Kramer, L.D., and Iwatsubo, T. (2023). Lecanemab in Early Alzheimer's Disease. *N. Engl. J. Med.* 388**,** 9-21.
Van Gerven, N., Klein, R.D., Hultgren, S.J., and Remaut, H. (2015). Bacterial amyloid formation: structural insights into curli biogensis. *Trends Microbiol.* 23**,** 693-706.

Vassar, P.S., and Culling, C.F. (1959). Fluorescent stains, with special reference to amyloid and connective tissues. *Arch. Pathol.* 68**,** 487-498.

Vaz, M., and Silvestre, S. (2020). Alzheimer's disease: Recent treatment strategies. *Eur. J. Pharmacol.* 887**,** 173554.

Vestergaard, M.D., Hamada, T., Saito, M., Yajima, Y., Kudou, M., Tamiya, E., and Takagi, M. (2008). Detection of Alzheimer's amyloid beta aggregation by capturing molecular trails of individual assemblies. *BBRC* 377**,** 725-728.

Vitvitsky, V.M., Garg, S.K., Keep, R.F., Albin, R.L., and Banerjee, R. (2012). Na+ and K+ ion imbalances in Alzheimer's disease. *Biochim Biophys Acta Bioenerg* 1822**,** 1671-1681.

Walker, L.C., and Jucker, M. (2015). Neurodegenerative diseases: expanding the prion concept. *Annu. Rev. Neurosci.* 38**,** 87-103.

Walsh, D.M., and Selkoe, D.J. (2007). A beta oligomers - a decade of discovery. *J. Neurochem.* 101**,** 1172-1184.

Walsh, D.M., Tseng, B.P., Rydel, R.E., Podlisny, M.B., and Selkoe, D.J. (2000). The Oligomerization of Amyloid β-Protein Begins Intracellularly in Cells Derived from Human Brain. *Biochemistry* 39**,** 10831-10839.

Wang, C., Lau, C.Y., Ma, F., and Zheng, C. (2021a). Genome-wide screen identifies curli amyloid fibril as a bacterial component promoting host neurodegeneration. *Proc. Natl. Acad. Sci. U.S.A.* 118.

Wang, H., Duo, L., Hsu, F., Xue, C., Lee, Y.K., and Guo, Z. (2020a). Polymorphic Aβ42 fibrils adopt similar secondary structure but differ in cross-strand side chain stacking interactions within the same β-sheet. *Sci. Rep.* 10**,** 5720.

Wang, H., Wu, J., Sternke-Hoffmann, R., Zheng, W., Mörman, C., and Luo, J. (2022). Multivariate effects of pH, salt, and Zn2+ ions on Aβ40 fibrillation. *Commun. Chem* 5**,** 171.

Wang, H., Yang, J., Schneider, J.A., De Jager, P.L., Bennett, D.A., and Zhang, H.-Y. (2020b). Genome-wide interaction analysis of pathological hallmarks in Alzheimer's disease. *Neurobiol. Aging* 93**,** 61-68.

Wang, L., Bharti, Kumar, R., Pavlov, P.F., and Winblad, B. (2021b). Small molecule therapeutics for tauopathy in Alzheimer's disease: Walking on the path of most resistance. *Eur. J. Med. Chem.* 209**,** 112915.

Wang, X., Smith, D.R., Jones, J.W., and Chapman, M.R. (2007). In vitro polymerization of a functional Escherichia coli amyloid protein. *J Biol Chem* 282**,** 3713-3719.

White, A., Gibson, D., Grassl, G., Kay, W., Finlay, B., Vallance, B., and Surette, M. (2008). Aggregation via the red, dry, and rough morphotype is not a virulence adaptation in Salmonella enterica serovar Typhimurium. *Infect. Immun.* 76**,** 1048-1058.

White-Grindley, E., Li, L., Mohammad Khan, R., Ren, F., Saraf, A., Florens, L., and Si, K. (2014). Contribution of Orb2A stability in regulated amyloid-like oligomerization of Drosophila Orb2. *PLoS Biol.* 12**,** e1001786.

Willey, J.M., Willems, A., Kodani, S., and Nodwell, J.R. (2006). Morphogenetic surfactants and their role in the formation of aerial hyphae in Streptomyces coelicolor. *Mol. Microbiol.* 59**,** 731-742.

Williams, D.R. (2006). Tauopathies: classification and clinical update on neurodegenerative diseases associated with microtubule-associated protein tau. *Intern. Med. J.* 36**,** 652-660.

Wu, C., Biancalana, M., Koide, S., and Shea, J.-E. (2009). Binding Modes of Thioflavin-T to the Single-Layer β-Sheet of the Peptide Self-Assembly Mimics. *J. Mol. Biol.* 394**,** 627-633.

Wu, X., Yang, M., Fang, X., Zhen, S., Zhang, J., Yang, X., Qiao, L., Yang, Y., and Zhang, C. (2018). Expression and regulation of phenol-soluble modulins and enterotoxins in foodborne Staphylococcus aureus. *AMB Express* 8**,** 187.

Xiao, Y., Ma, B., Mcelheny, D., Parthasarathy, S., Long, F., Hoshi, M., Nussinov, R., and Ishii, Y. (2015). Aβ(1-42) fibril structure illuminates self-recognition and replication of amyloid in Alzheimer's disease. *Nat. Struct. Mol. Biol.* 22**,** 499-505.

Xu, W., Tan, L., Wang, H.F., Jiang, T., Tan, M.S., Tan, L., Zhao, Q.F., Li, J.Q., Wang, J., and Yu, J.T. (2015). Meta-analysis of modifiable risk factors for Alzheimer's disease. *J. Neurol. Neurosurg. Psychiatry* 86**,** 1299-1306.

Xue, C., Lin, T.Y., Chang, D., and Guo, Z. (2017). Thioflavin T as an amyloid dye: fibril quantification, optimal concentration and effect on aggregation. *R. Soc. Open Sci.* 4**,** 160696.

Xue, W.-F., Homans, S.W., and Radford, S.E. (2008). Systematic analysis of nucleation-dependent polymerization reveals new insights into the mechanism of amyloid self-assembly. *Proc. Natl. Acad. Sci. U.S.A.* 105**,** 8926-8931.

Yakupova, E.I., Bobyleva, L.G., Vikhlyantsev, I.M., and Bobylev, A.G. (2019). Congo Red and amyloids: history and relationship. *Biosci. Rep.* 39**,** BSR20181415.

Yang-Hartwich, Y., Bingham, J., Garofalo, F., Alvero, A.B., and Mor, G. (2015). Detection of p53 protein aggregation in cancer cell lines and tumor samples. *Apoptosis***,** 75-86.

Yao, J., Petanceska, S.S., Montine, T.J., et al. (2004). Aging, gender and APOE isotype modulate metabolism of Alzheimer's Aβ peptides and F2-isoprostanes in the absence of detectable amyloid deposits. *J. Neurochem.* 90**,** 1011-1018.

Yu, J.T., Xu, W., Tan, C.C., et al. (2020). Evidence-based prevention of Alzheimer's disease: systematic review and meta-analysis of 243 observational prospective studies and 153 randomised controlled trials. *J. Neurol. Neurosurg.* 91**,** 1201-1209.

Zhou, Y., Smith, D.R., Hufnagel, D.A., and Chapman, M.R. (2013). Experimental manipulation of the microbial functional amyloid called curli. *Methods Mol Biol* 966**,** 53-75.

Ziaunys, M., Mikalauskaite, K., Sakalauskas, A., and Smirnovas, V. (2021). Interplay between epigallocatechin-3-gallate and ionic strength during amyloid aggregation. *PeerJ* 9**,** e12381.

Zidar, J., and Merzel, F. (2011). Probing Amyloid-Beta Fibril Stability by Increasing Ionic Strengths. *J. Phys. Chem. B* 115**,** 2075-2081.